Sub-Nyquist Wideband Spectrum Sensing and Sharing

by

Yuan Ma

Doctor of Philosophy

School of Electronic Engineering and Computer Science
Queen Mary University of London
United Kingdom

June 2017

Abstract

The rising popularity of wireless services resulting in spectrum shortage has motivated dynamic spectrum sharing to facilitate efficient usage of the underutilized spectrum. Wideband spectrum sensing is a critical functionality to enable dynamic spectrum access by enhancing the opportunities of exploring spectral holes, but entails a major implementation challenge in compact commodity radios that have limited energy and computation capabilities. The sampling rates specified by the Shannon-Nyquist theorem impose great challenges both on the acquisition hardware and the subsequent storage and digital signal processors. Sub-Nyquist sampling was thus motivated to sample wideband signals at rates far lower than the Nyquist rate, while still retaining the essential information in the underlying signals.

This thesis proposes several algorithms for invoking sub-Nyquist sampling in wideband spectrum sensing. Specifically, a sub-Nyquist wideband spectrum sensing algorithm is proposed that achieves wideband sensing independent of signal sparsity without sampling at full bandwidth by using the low-speed analog-to-digital converters based on sparse Fast Fourier Transform. To lower signal spectrum sparsity while maintaining the channel state information, the received signal is pre-processed through a proposed permutation and filtering algorithm. Additionally, a low-complexity sub-Nyquist wideband spectrum sensing scheme is proposed that locates occupied channels blindly by recovering the signal support, based on the jointly sparse nature of multiband signals. Exploiting the common signal support shared among multiple secondary users, an efficient cooperative spectrum sensing scheme is developed, in which the energy consumption on signal acquisition, processing, and transmission is reduced with the detection performance guarantee. To further reduce the computation complexity of wideband spectrum sensing, a hybrid framework of sub-Nyquist wideband spectrum sensing with geolocation database

is explored. Prior channel information from geolocation database is utilized in the sensing process to reduce the processing requirements on the sensor nodes. The models of the proposed algorithms are derived and verified by numerical analyses and tested on both real-world and simulated TV white space signals.

Acknowledgments

Foremost, I would like to express my sincere gratitude to my supervisor, Dr. Yue Gao, for his continuous support, patience, and guidance throughout my entire PhD. His immense knowledge, enthusiasm, and encouragement provided me a great opportunity to gain expertise in my area of research. I would like to convey my special thanks to him for spending so much time discussing my work in details and helping me improve my work. His valuable feedback helped shape much of the work in this thesis. I am also very grateful for his generous financial support for sending me to various conferences to meet all leading experts in the field, which enriched my whole PhD experience.

I would also like to express my appreciation to Professor Clive G. Parini and Professor Andrea Cavallaro for their valuable advice and insightful comments throughout my research work. I am very grateful for all our discussions on my research and scientific writing. I would also like to thank Professor Shuguang Cui (University of California, Davis), Professor Ying-Chang Liang (University of Electronic Science and Technology of China), and Professor Wei Zhang (University of New South Wales) who gave me lots of constructive comments and suggestions on cognitive radio and compressive sensing.

I would also like to express my appreciation to all the friends in the Queen Mary, including Dr. Nan Wang, Dr. Zhijin Qin, Dr. Yansha Deng, Dr. Lifeng Wang, Dr. Yun Li, Dr. Xiang Li, Dr. Zeng Yang, Dr. Oleksandr Sushko, Qianyun Zhang, Wei Su, Haoran Qi, Shaker Alkaraki, etc. I enjoyed all our discussions every day in the lab. You guys made my life in Queen Mary full of happy and unforgettable moments.

I would also like to thank the committee for my viva defense: Professor Arumugam Nallanathan, and Professor Mike E. Davies, for their encouragement and insightful comments.

Finally, with my love and gratitude, I would like to thank my family, especially my parents and boyfriend, who are always there for me and giving me enormous love, support, and never-ending encouragement. To them I dedicate this thesis.

Table of Contents

Abstract **i**

Acknowledgments **iii**

Table of Contents **v**

List of Figures **ix**

List of Tables **xiii**

List of Abbreviations **xiv**

List of Symbols **xvii**

1 Introduction **2**

1.1 Motivations and Contributions 3

1.1.1 Sparsity independent sub-Nyquist rate wideband spectrum sensing 4

1.1.2 Low-complexity sub-Nyquist sampling and wideband spectrum sensing in cooperative cognitive radio networks 4

1.1.3 Joint sub-Nyquist spectrum sensing scheme with geolocation database 5

1.2 Publication List 6

1.3 Outline of the Thesis 8

2 Background **10**

2.1 Dynamic Spectrum Access 11

2.2 Narrowband Spectrum Sensing . . . 15
2.3 Wideband Spectrum Sensing . . . 16
2.3.1 Nyquist Wideband Spectrum sensing . . . 17
2.3.2 Sub-Nyquist Wideband Spectrum sensing . . . 20
2.4 Cooperative Spectrum Sensing . . . 30
2.4.1 Joint Sparse Recovery . . . 32
2.4.2 Matrix Completion . . . 33
2.5 Summary . . . 34

3 Sparsity Independent Sub-Nyquist Wideband Spectrum Sensing 36
3.1 Introduction . . . 37
3.1.1 Related Work . . . 37
3.1.2 Contributions . . . 38
3.2 System Model . . . 39
3.2.1 Signal Permutation and Filtering . . . 40
3.2.2 Spectrum Estimation . . . 42
3.2.3 Multi-channel Joint Detection . . . 45
3.2.4 Application to Real-world TVWS Signals . . . 47
3.3 Numerical Analysis . . . 50
3.3.1 Experimental Setup . . . 50
3.3.2 Simulated TVWS Signals: analysis . . . 52
3.3.3 Real-world TVWS Signals: analysis . . . 56
3.4 Summary . . . 59

4 Low-Complexity Sub-Nyquist Wideband Spectrum Sensing 60
4.1 Introduction . . . 61
4.1.1 Related Work . . . 61
4.1.2 Contributions . . . 63
4.2 Individual Sub-Nyquist Wideband Spectrum Sensing . . . 64
4.2.1 Blind Sub-Nyquist Wideband Signal Acquisition . . . 66

4.2.2 Reliable Computation Efficient Joint Sparse Recovery 71
4.3 Cooperative Sub-Nyquist Wideband Spectrum Sensing 75
4.4 Numerical Analysis 77
4.4.1 Experimental Setup and Performance Measures 78
4.4.2 Individual Sub-Nyquist Wideband Spectrum Sensing 80
4.4.3 Cooperative Sub-Nyquist Wideband Spectrum Sensing 83
4.4.4 Real-world TVWS Signal Analysis 86
4.5 Summary 89

5 Joint Sub-Nyquist Spectrum Sensing Scheme with Geolocation Database 91
5.1 Introduction 92
5.1.1 Related Work 92
5.1.2 Contributions 93
5.2 System Architecture and Problem Formulation 94
5.2.1 System Architecture 94
5.2.2 Problem Formulation 95
5.3 Joint Sparse Recovery Incorporated with Geolocation Database 98
5.3.1 Subspace-Augmented Joint Sparse Recovery with Prior Information 102
5.3.2 Iterative Reweighted Support Detection with Prior Information . . 103
5.4 Numerical Analysis 106
5.4.1 Spectrum Sensing Performance versus SNR and Sub-Nyquist Sampling Ratio 107
5.4.2 Average Iteration Numbers to Convergence 109
5.4.3 Spectrum Sensing Performance with Partially Incorrect Prior Information 111
5.5 Summary 111

6 Conclusions and future work 114
6.1 Summary 114
6.2 Future work 116

6.2.1 Adaptive Wideband Spectrum Sensing 117
6.2.2 Performance Limits under Practical Imperfections 117
6.2.3 Real-time Compressive Wideband Spectrum Sensing Testbed . . . 117
6.2.4 Short-and Long-Term White Space Measurement Analysis 118
References 119

List of Figures

2.1 The real-time spectrum occupancy recorded at QMUL (51.523021°N 0.041592°W) on March 5th, 2016. The figure shows that the spectrum is sparsely occupied on $\mathcal{F} = [0, 6000]$ MHz. 11

2.2 Cognitive cycle of cognitive radio system. 12

2.3 Schematic illustration of multiband joint detection. 18

2.4 Schematic illustration of wavelet detection. 18

2.5 Schematic illustration of sequential scanning. 19

2.6 Schematic illustration of filter bank algorithm. 20

2.7 Schematic illustration of random demodulator. 24

2.8 Schematic illustration of modulated wideband converter. 25

2.9 Schematic illustration of multicoset sampler. 26

2.10 Schematic illustration of the cooperative spectrum sensing, where each SU transmits its individual observation or decision via control channels to a fusion centre, which makes final decision on the spectral occupancy status. 31

3.1 Block diagram of the proposed sparsity independent sub-Nyquist wideband spectrum sensing scheme. 40

3.2 Flowchart of the proposed signal permutation and filtering algorithm. . . 40

3.3 (left) Input signal spectrum with 3 channels (N = 16). (right) Signal spectrum after permutation. Through the bandpass filter, it can extract the central frequencies in each channel. 42

3.4 The power spectrum density (PSD) of real-time TVWS signal recorded at (51.523021°N 0.041592°W). 48
3.5 Permutation and filtering on real-world TVWS signal under $\beta = 0.25\%$. . 49
3.6 Measurement setup for real-time TVWS signals recording at Queen Mary University of London. 51
3.7 Detection probability P_d vs. SNR under different extraction ratio β with spectrum utilization $\alpha = 50\%$. 52
3.8 Runtime of sFFT and FFT for the permuted and filtered signal under different spectrum utilization α and extraction ratio β. 53
3.9 Detection probability P_d vs. SNR for the proposed sensing scheme and the conventional MJD based on FFT under different extraction ratio β with different spectrum utilization $\alpha = 10\%, 20\%, 50\%$. 55
3.10 ROC curve for the proposed sensing scheme and the conventional MJD based on FFT under different extraction ratio β. 55
3.11 Comparison of the reconstructed and original filtered signal. 57
3.12 Detection probability P_d and false alarm probability P_f of (a) the original real-world signal detection under noise uncertainty η and (b) the reconstructed real-world signal detection with different extraction ratio β under noise uncertainty η. 58

4.1 Centralized cooperative spectrum sensing model in a cognitive radio network. 64
4.2 Wideband spectrum $X(f)$ with $M = 10$ and $\kappa = 4$ active channels, $\boldsymbol{\mathcal{S}} = [1, 2, 5, 8]$. 65
4.3 Examples of two multicoset sampling patterns for $(M, p) = (10, 4)$. (a) $C = \{0, 1, 4, 6\}$; (b) $C = \{1, 3, 6, 8\}$. 66
4.4 The parallel implementation of the multicoset non-uniform sub-Nyquist sampling. 67
4.5 Flow chart to get the multicoset sampling measurements. 68

4.6 Eigenvalues of the sample correlation matrix ordered in decreasing order with $p = 9, \kappa = 4$. 73
4.7 Simulated signal illustration in time and frequency domains, with $M = 40$, $\kappa = 4$ and $\boldsymbol{\mathcal{S}} = [4, 11, 19, 26]$. 78
4.8 Normalized power spectrum density (PSD) of the real-time TVWS signal recorded at QMUL, $\boldsymbol{\mathcal{S}} = [22, 23, 25, 26, 28, 29, 30, 33]$. 79
4.9 Detection Probability P_d vs. varying SNR values under different sub-Nyquist sampling ratios $\Omega = p/M$ with $\kappa = 4$. 81
4.10 Reconstructed signal in the time and frequency domains with $p = 15$. The relative reconstruction MSE compared with the original signal in Fig. 4.7 is 2.7%. 82
4.11 Detection Probability P_d vs. number of cosets p under different SNR values with $\kappa = 4$, $\Omega = p/M$. 82
4.12 Detection Probability P_d vs. varying SNR values for different numbers of active channels κ with $p = 20$ ($\Omega = 50\%$). 83
4.13 Global detection probability P_d vs. varying SNR values. 84
4.14 Global detection probability P_d vs. varying SNR values with different numbers of SUs, $\kappa = 4$ and $p = 10$ ($\Omega = 25\%$). 85
4.15 Global detection probability P_d vs. varying SNR values with different numbers of SUs, $\kappa = 4$ and $p = 5$ ($\Omega = 12.5\%$). 86
4.16 Normalized PSD of the reconstructed real-world TVWS signal under $p = 10$ and $p = 15$ at individual spectrum sensing. 87
4.17 Normalized PSD of the reconstructed real-world TVWS signal under $p = 10$ at cooperative spectrum sensing of $J = 3$ SUs. 88
4.18 Detection probability P_d vs. number of cosets p for the real-world TVWS signal. 88

5.1 System architecture of the proposed hybrid scheme. 95
5.2 Whole flowchart of the proposed joint sub-Nyquist sensing scheme. 99

5.3 Detection probability P_d vs. number of cosets p with $\kappa = 8$ and SNR $= -5$ dB under different number of occupied channels known from geolocation database based on SA-SOMP. 108
5.4 Detection probability P_d vs. number of cosets p with $\kappa = 8$ and SNR $= -5$ dB under different number of occupied channels known from geolocation database based on MFOCUSS. 108
5.5 Detection probability P_d vs. SNR with $\kappa = 8$ and $p = 15$ under different number of occupied channels known from geolocation database based on SA-SOMP. 109
5.6 Detection probability P_d vs. SNR with $\kappa = 8$ and $p = 15$ under different number of occupied channels known from geolocation database based on MFOCUSS. 109
5.7 Average number of iterations based on MFOCUSS to achieve convergence. 110
5.8 Detection probability P_d vs. number of cosets p with $\kappa = 8$ and SNR $= -5$ dB based on SA-SOMP under different number of occupied channels known from geolocation database with partially incorrect prior information. 112
5.9 Detection probability P_d vs. number of cosets p with $\kappa = 8$ and SNR $= -5$ dB based on MFOCUSS under different number of occupied channels known from geolocation database with partially incorrect prior information. 112

List of Tables

2-A Summary of advantages and disadvantages of narrowband and wideband spectrum sensing algorithms. 35

3-A Improvements of sFFT compared with FFT with subsampling rate 4.00% under different extraction ratio β. 56

4-A Comparison of complexity of the proposed cooperative recovery scheme with SOMP and DOMP. 84

List of Abbreviations

ADC	Analog-to-Digital Conversion
APGL	Accelerated Proximal Gradient Line
AWGN	Additive White Gaussian Noise
BP	Basis Pursuit
BPDN	Basis Pursuit Denoising
BPF	Band Pass Filter
CBRS	Citizens Broadband Radio Service
CDF	Complementary Distribution Function
CoSamp	Compressive Sampling Matching Pursuit
CS	Compressive Sensing
CSS	Cooperative Spectrum Sensing
DFT	Discrete Fourier Transform
DSA	Dynamic Spectrum Access
DOMP	Distributed Orthogonal Matching Pursuit
DTT	Digital Terrestrial Television
EFT	Exponential Fitting Test
FCC	Federal Communications Commission
FFT	Fast Fourier Transform
FOCUSS	FOCal Underdetermined System Solver

FPCA	Fixed-Point Continuation with Approximate
GAA	General Authorized Access
IA	Incumbent Access
IHT	Iterative Hard Thresholding
IRLS	Iterative Reweighted Least Squares
LASSO	Least Absolution Shrinkage and Selection Operator
LP	Linear Programming
MDL	Minimum Description Length
MJD	Multi-channel Joint Detection
MMV	Multiple Measurement Vector
MSE	Mean Squared Error
M2M	Machine-to-Machine
MUSIC	MUltiple SIgnal Classification
MWC	Modulated Wideband Converter
NPRM	Notice of Proposed Rule Making
Ofcom	Office of Communications
OFDM	Orthogonal Frequency Division Multiplexing
OMP	Orthogonal Matching Pursuit
PA	Priority Access
PFMJD	Permuted and Filtered Multi-channel Joint Detection
PMSE	Programme Making and Special Events
PSD	Power Spectrum Density
PU	Primary User
QMUL	Queen Mary University of London
RF	Radio Frequency
RIP	Restricted Isometry Property
ROC	Receiver Operating Characteristic

RREVD	Rank-Revealing Eigenvalue Decomposition
SA-SOMP	Subspace-Augmented Simultaneous Orthogonal Matching Pursuit
sFFT	sparse Fast Fourier Transform
SMV	Single Measurement Vector
SNR	Signal to Noise Ratio
SOMP	Simultaneous Orthogonal Matching Pursuit
StOMP	Stagewise OMP
SU	Secondary User
SVT	Singular Value Thresholding
TVWS	TV White Space
UHF	Ultra High Frequency
U-NII	Unlicensed National Information Infrastructure
WSD	White Space Device

List of Symbols

$\mathbf{A}$	Matrix
$\mathbf{a}_i$	i-th column of $\mathbf{A}$
$\mathbf{A}[i]$	i-th row of $\mathbf{A}$
$\mathbf{A}_{ij}$	ij-th entry of $\mathbf{A}$
$\mathbf{A}^T, \mathbf{A}^H$	The transpose and Hermitian transpose of $\mathbf{A}$
$\mathbf{A}^\dagger$	Pseudo-inverse of the matrix $\mathbf{A}$
$\mathbf{A}_{\boldsymbol{\mathcal{S}}}$	The matrix made of the columns of $\mathbf{A}$ with indices from $\boldsymbol{\mathcal{S}}$
$\|\|\mathbf{A}\|\|_{p,q}$	$\ell_{p,q}$ norm of $\mathbf{A}$: $\|\|\mathbf{A}\|\|_{p,q} \triangleq (\sum_{i=1}^{L} \|\|A[i]\|\|_p^q)^{\frac{1}{q}}$
$\mathcal{I}(\mathbf{A})$	Support of $\mathbf{A}$: $\mathcal{I}(\mathbf{A}) = \{i \vert \mathbf{A}[i] \neq 0\}$ indicates the indices of rows containing nonzero entries
$\mathcal{B}$	The whole bandwidth of the spectrum of interest
$\mathcal{B}_0$	Bandwidth of each sub-channel
$\mathcal{C}$	Sampling pattern in the multicoset sampling
f_s	Nyquist sampling rate
H_0	Hypothesis of PU absent
H_1	Hypothesis of PU present
J	Number of secondary users in the cooperative cognitive radio network
k	Number of non-zero dominant frequency components over the spectrum of interest
k_l^m	Lower bin index of the m-th sub-channel
k_u^m	Upper bin index of the m-th sub-channel

L	Number of samples on each sub-channel
M	Number of sub-channels over the spectrum of interest
N	Number of samples over the whole spectrum at Nyquist rate
$n(t)$	White Gaussian noise
P_d	Probability of detection
P_f	Probability of false alarm
p	The number of cosets in the multicoset sampling
$\mathbf{R}$	Correlation matrix of the samples
$\boldsymbol{\mathcal{S}}$	The set of the indices of the occupied channels over the spectrum of interest
$s(t)$	Primary signal in time domain
T_m	Test statistics of the m-th sub-channel
T_s	Sensing duration
$\mathbf{\Lambda}$	Diagonal matrix of eigenvalues
$\mathbf{U}$	Matrix whose columns are the eigenvectors so that $\mathbf{RU} = \mathbf{U\Lambda}$.
$\mathcal{W}$	Noise sets containing the indices of the unoccupied spectral components
$x(t)$	Continuous-time signal with finite energy
$\widehat{\boldsymbol{x}}$, $X(f)$	Fourier transform of $\boldsymbol{x}$
$X_m(f)$	The pieces of the spectrum in the m-th sub-channel
α	Spectrum occupation ratio
β	Extraction ratio in the permutation and filtering scheme
η	Noise uncertainty
κ	Number of occupied sub-channels over the spectrum of interest
λ	Eigenvalue of $\mathbf{R}$
λ_n	Threshold in the spectrum detection
μ	Eigenvector of $\mathbf{R}$
σ_n^2	Noise variance
τ	Time offset
Ω	Sub-Nyquist sampling ratio

Chapter 1

Introduction

The rapid growth of internet of things and mobile services is overwhelming current static spectrum supply, and thus encouraging an urgent need for improved and dynamic spectrum usage to mitigate the spectrum supply-demand gap [1]. There is an increased interest in the promising technique of spectrum sharing to facilitate efficient use of the spectrum driven by the following three factors: first, there is a significant spectrum crunch faced by the commercial mobile broadband users with the compelling need to get additional spectrum for the wireless broadband services [2]; second is the awareness that many licensed frequency bands are underutilized in practice either over time or geography [3–6]; finally, there have been some rapid advances towards the development of dynamic spectrum access through approaches such as geolocation database and cognitive radio [7–9].

The threat of spectrum scarcity has encouraged the governments to take critical steps towards releasing multiple bands for dynamic spectrum sharing, such as TV White Space (TVWS) [10, 11], Citizens Broadband Radio Service (CBRS) in the 3.5 GHz band [12], and the 5 GHz unlicensed bands [13]. Compact and low-power white space devices (WSDs) for rural broadband/WiFi-like accesses and Machine-to-Machine (M2M) communications could operate on these vacant bands without causing interferences to the

primary transmissions [14, 15]. To enable dynamic spectrum access over white spaces, fast and accurate detection of the spectrum is crucial to ensure that there is no harmful interference caused to the surrounding licensed services. To achieve spectrum awareness over a wide frequency range, wideband spectrum sensing is a highly desirable feature in cognitive radio networks [16]. If a primary user (PU) reappears over a certain band, the availability of several other possible vacant channels facilitates the seamless handoff from one spectrum channel to another, which reduces secondary data transmission interruptions. However, for wideband spectrum sensing, a stringent requirement arises from the Nyquist signal acquisition, which is quite expensive, power-consuming, and computation intensive [17]. Due to the energy constraint in compact secondary users (SUs), efficient real-time wideband spectrum sensing emerges as a crucial challenge for dynamic spectrum sharing in cognitive radio networks.

Landau in [18] demonstrated that an arbitrary wideband signal can be perfectly reconstructed if being sampled at a rate no less than the total bandwidth of occupied spectrum. As wireless signals over an open spectrum are typically sparse in the frequency domain, it can be recovered by sampling at a rate far less than the Nyquist rate in practice. Sub-Nyquist sampling techniques were thus introduced to implement wideband sensing using lower-than-Nyquist sampling rates to reduce the requirements of high-speed signal processing. Subsequently, the application of sub-Nyquist sampling on wideband spectrum sensing has attracted much attention [19]. This thesis will present three sub-Nyquist sampling systems that implement wideband spectrum sensing by low-rate analog-to-digital converters (ADCs), aiming to facilitate the efficient usage of the spectrum for dynamic spectrum sharing.

1.1 Motivations and Contributions

The specific motivations and contributions of my Ph.D. research are summarised in the following.

1.1.1 Sparsity independent sub-Nyquist rate wideband spectrum sensing

Sub-Nyquist sampling has attracted significant interests for wideband spectrum sensing, while most of existing algorithms typically assume that the wideband signals are sparse in the frequency domain given the low spectrum utilization. As the secondary market for the spectrum sharing has been opened to public usage [10, 11], multiple SUs compete for the white space spectrum resources to serve a large pool of end-users. Therefore, the wideband signals may no longer be static and sparse, i.e., sparsity level may be time-varying and larger than 30% [4, 5]. Hence a fast wideband spectrum sensing scheme that can subsample the wideband signals regardless of signal sparsity is of great interest.

In this thesis, a sub-Nyquist wideband spectrum sensing algorithm is proposed that achieves wideband spectrum sensing independent of signal sparsity without sampling at full bandwidth by using the low-speed ADCs based on sparse Fast Fourier Transform (sFFT) [20]. To lower signal spectrum sparsity while maintaining the channel state information, the received signal is pre-processed through a proposed permutation and filtering algorithm. The proposed algorithm is derived and verified by numerical analyses and tested on real-time TVWS signals. The experimental results show that the proposed algorithm achieves high detection performance on sparse and non-sparse wideband signals with reduced runtime and implementation complexity.

1.1.2 Low-complexity sub-Nyquist sampling and wideband spectrum sensing in cooperative cognitive radio networks

In a particular geographical region and over a certain time period, some frequency bands may not be used by the PUs and are available for opportunistic spectrum access. Wideband spectrum sensing is thus crucial as the SUs need to detect spectral holes from a wide frequency band to enable dynamic spectrum access, but it entails a major implementation challenge in compact commodity radios that only have limited energy and

computation capabilities. Exploiting the common signal support shared among multiple SUs, a low-complexity cooperative spectrum sensing scheme is developed, in which the energy consumption on wideband signal acquisition, processing, and transmission is reduced with the detection performance guarantee. In contrast to traditional sub-Nyquist approaches where a wideband signal or its power spectrum is first reconstructed from compressed samples [17, 21–23], the proposed sub-Nyquist wideband spectrum sensing scheme locates occupied channels blindly by recovering the signal support, based on the jointly sparse nature of multiband signals. Through subspace decomposition, a low-dimensional measurement matrix, computed at each SU from local sub-Nyquist samples, is deployed to reduce the transmission and computation overhead while maintaining noise robustness. The theoretical analysis of the proposed sub-Nyquist wideband sensing algorithm is derived and verified by numerical analyses and further tested on real-world TVWS signals.

1.1.3 Joint sub-Nyquist spectrum sensing scheme with geolocation database

To further reduce the computation complexity of wideband spectrum sensing, a hybrid framework of sub-Nyquist wideband spectrum sensing with geolocation database is explored in this thesis. Prior channel state information from geolocation database is utilized in the sensing process to reduce the processing requirements on the sensor node. With the assists from geolocation database, part of the complexity of local wideband spectrum sensing is transferred to the core network, thus decreasing the energy consumption and processing complexity required on the spectrum sensing. Two reconstruction algorithms, greedy algorithm and ℓ_p norm minimization, are modified to incorporate the prior information from geolocation database. Theoretical analyses and experimental results show that the proposed joint scheme speeds up the sensing process with enhanced detection performance and smaller required sampling rate, while the updated channel information from local spectrum sensing reduces the risks of SUs interfering with dynamic incumbent users.

1.2 Publication List

Book Chapter

- Y. Gao, and **Y. Ma**, "Spectrum Sensing, Database, and Its Hybrid," published by Springer, 2017.

Journal Paper

- **Y. Ma**, Y. Gao, Y.-C. Liang, and S. Cui, "Reliable and Efficient Sub-Nyquist Wideband Spectrum Sensing in Cooperative Cognitive Radio Networks," *IEEE Journal on Selected Areas in Communications*, vol. 34, no. 10, pp. 2750-2762, Oct. 2016.

- **Y. Ma**, Y. Gao, A. Cavallaro, C. G. Parini, W. Zhang, and Y.-C. Liang, "Sparsity Independent Sub-Nyquist Rate Wideband Spectrum Sensing on Real-time TV White Space," *IEEE Transactions on Vehicular Technology*, Apr. 2017 (Accepted).

- X. Zhang, **Y. Ma**, Y. Gao, and S. Cui, "Real-time Adaptively-Regularized Compressive Sensing in Cognitive Radio Networks," *IEEE Transactions on Vehicular Technology*, 2017 (Accepted).

- **Y. Ma**, X. Zhang, and Y. Gao, "Joint Sub-Nyquist Spectrum Sensing Scheme with Geolocation Database over TV White Space," *IEEE Transactions on Vehicular Technology*, 2017 (Minor Revision).

Conference Paper

- X. Zhang, Y. Ma, and Y. Gao, "Blind Compressive Spectrum Sensing in Cognitive Internet of Things," in Proc. IEEE Global Communication Conference (GLOBECOM'17), Singapore, Dec. 2017 (accepted to appear).

- X. Zhang, Y. Zhang, Y. Ma, and Y. Gao, "Blind Cooperating User Selection for Compressive Spectrum Sensing in Cognitive Radio Networks," in IEEE/CIC

International Conference on Communication in China (ICCC'17), Qingdao, China, Oct. 2017 (accepted to appear).

- Y. Gao, X.Zhang, and Y. Ma, "Hybrid sub-Nyquist Spectrum Sensing with Geolocation Database in M2M Communications", in the IEEE Vehicular Technology Conference, VTC2017-Fall in Toronto, Canada, Sep. 2017 (accepted to appear).

- X. Zhang, Y. Zhang, **Y. Ma**, and Y. Gao, "RealSense: Real-time Compressive Spectrum Sensing Testbed over TV White Space," in *IEEE International Conference on World of Wireless, Mobile and Multimedia Networks (WoWMoM'17)*, Macao, Jun. 2017.

- **Y. Ma**, X. Zhang, and Y. Gao, "An Efficient Joint Sub-Nyquist Spectrum Sensing Scheme with Geolocation Database over TV White Space," in *Proc. IEEE International Conference on Communications (ICC'17)*, Paris, France, May 2017.

- **Y. Ma**, Y. Gao, Y.-C. Liang, and S. Cui, "Efficient Blind Cooperative Wideband Spectrum Sensing based on Joint Sparsity," in *Proc. IEEE Global Communication Conference (GLOBECOM'16)*, Washington, D.C., Dec. 2016.

- X. Zhang, **Y. Ma**, and Y. Gao, "Adaptively Regularized Compressive Spectrum Sensing From Real-time Signals to Real-time Processing," in *Proc. IEEE Global Communication Conference (GLOBECOM'16)*, Washington, D.C., Dec. 2016.

- X. Zhang, **Y. Ma**, and Y. Gao, "Autonomous Compressive Spectrum Sensing Approach for 3.5 GHz Shared Spectrum," in *IEEE Global Conference on Signal and Information Processing (GlobalSIP'16)*, Washington, D.C., Dec. 2016, pp. 1378-1382.

- Y. Gao, **Y. Ma**, W. Zhang, and R. Cepeda, "Data-assisted Sub-Nyquist Spectrum Sensing," in *IEEE International conference on Communication Systems (ICCS'16)*, Shenzhen, Dec. 2016, pp. 1-5.

- **Y. Ma**, X. Zhang, and Y. Gao, "Sub-Nyquist Cooperative Wideband Spectrum Sensing based on Multicoset Sampling for TV White Spaces," in *IEEE/CIC International Conference on Communication in China (ICCC'16)*, Chengdu, 2016.

- **Y. Ma**, Y. Gao, and C. G. Parini, "Sub-Nyquist rate wideband spectrum sensing over TV white space for M2M communications," in *IEEE International Conference on World of Wireless, Mobile and Multimedia Networks (WoWMoM'15)*, Boston, MA, Jun. 2015, pp. 1-6.

- **Y. Ma**, Y. Gao, X. Zhang, and L. Cuthbert, "Optimization of collaborating secondary users in a cooperative sensing under noise uncertainty," in *IEEE International Conference on on Personal Indoor and Mobile Radio Communications (PIMRC'13)*, London, UK, Sep. 2013, pp. 2502-2506.

1.3 Outline of the Thesis

Chapter 2 provides an overview of the background knowledge including dynamic spectrum sharing, narrowband spectrum sensing, Nyquist and sub-Nyquist wideband spectrum sensing, and cooperative spectrum sensing.

Chapter 3 proposes a sparsity independent sub-Nyquist wideband spectrum sensing on TV white space. The numerical analyses of the proposed scheme are presented on both simulated and real-world TVWS signals.

Chapter 4 investigates multicoset sampling based wideband spectrum sensing schemes for both individual and cooperative spectrum sensing cases to reduce energy consumption on wideband signal acquisition, processing, and transmission, with detection performance guarantee by exploiting the joint sparsity of multiband signals.

Chapter 5 presents a hybrid framework of sub-Nyquist wideband spectrum sensing with geolocation database for the efficient use of white spaces within the coexistence of

dynamic incumbent systems.

Chapter 6 draws the conclusion and a plan for the future work.

Chapter 2

Background

With the explosive proliferation of wireless devices and rapid growth of wireless services, spectrum scarcity has become a major bottleneck for wireless industry. The threat of spectrum shortage has encouraged the governments to release multiple frequency bands for dynamic spectrum sharing, motivated by the fact that the actual spectrum is under-utilized in practice [10–12]. To enable dynamic spectrum access, a crucial requirement is fast and accurate detection of the surrounding spectrum that does not cause interferences to primary transmissions. This task is fulfilled by the function of spectrum sensing. To achieve spectrum awareness over a wide frequency range, wideband spectrum sensing is of prime importance to enhance the opportunities of exploring spectral holes.

In this chapter, Section 2.1 introduces the definition of dynamic spectrum access, and its structure and the functionalities. Section 2.2 provides a short survey on narrowband spectrum sensing. Here, the term "narrowband" implies that the frequency range is sufficiently narrow such that the channel frequency response can be considered as flat [19]. A literature review on wideband spectrum sensing is presented in Section 2.3. Wideband spectrum sensing can be broadly categorized into two types: Nyquist wideband spectrum sensing and sub-Nyquist wideband spectrum sensing. The former acquires the signals at or above the Nyquist rate, whereas the latter processes signals lower than

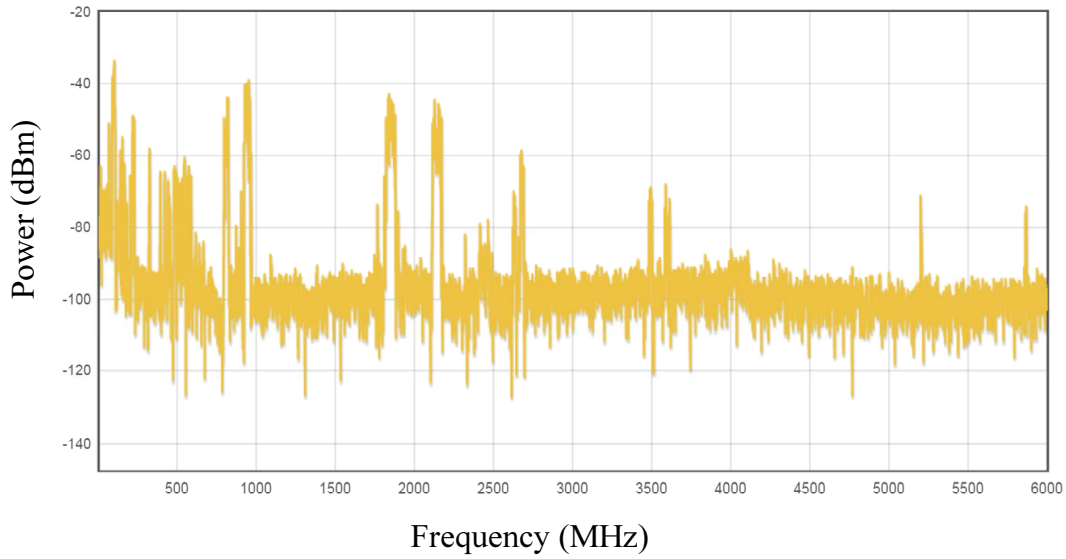

Figure 2.1: The real-time spectrum occupancy recorded at QMUL (51.523021°N 0.041592°W) on March 5th, 2016. The figure shows that the spectrum is sparsely occupied on $\mathcal{F} = [0, 6000]$ MHz.

the Nyquist rate. This section first discusses Nyquist wideband spectrum sensing techniques, i.e., multiband joint detection, wavelet detection, sequential scanning, and filter bank detection in Section 2.3.1. Sub-Nyquist wideband spectrum sensing algorithms are then analysed in Section 2.3.2. Section 2.4 discusses the cooperative spectrum sensing strategies. Section 2.5 concludes this chapter.

2.1 Dynamic Spectrum Access

The evolution of modern wireless communications to cater for higher throughput and higher mobility is challenged by spectrum scarcity in current static spectrum supply. Nevertheless, recent studies reveal that various spectrum bands are underutilized through fixed spectrum assignment [7]. For instance, Fig. 2.1, collected by the RFeye node [24] located at Queen Mary University of London (QMUL) in London, United Kingdom, shows that a large portion of the spectrum remains unused. Dynamic spectrum access is one of the promising approaches to alleviate this problem [25]. Such spectrum access

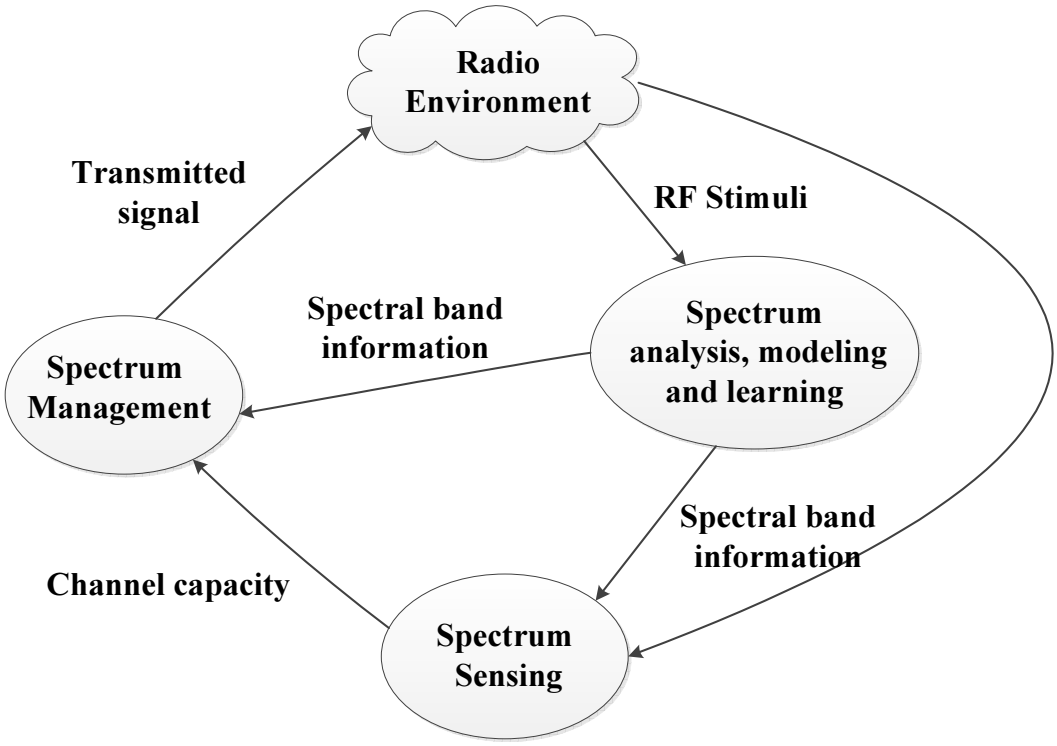

Figure 2.2: Cognitive cycle of cognitive radio system.

methods aims at reusing the unused spectrum bands, called *spectrum holes or white spaces*, while causing no harmful interference to the actual licensees.

Dynamic spectrum access is made possible by recent advances in cognitive radio technology [3, 7]. Cognitive radio can sense the surrounding spectrum environment and accordingly adapt radio parameters such as the centre frequency, bandwidth, transmit power, and waveform to utilize spectrum bands currently not used by primary users (PUs). These tasks can be implemented by a basic cognitive cycle: *spectrum analysis, modelling and learning, spectrum sensing, and spectrum management*, as shown in Fig. 2.2 [26]. In the *spectrum analysis, modelling and learning* step, the secondary user (SU) analyses the spectrum, estimates the PU's transmission parameters, and models the PU's transmission structure through observations over a long time period. This information can then be used to formulate the threshold, noise statistics, etc. in the *spectrum sensing* step. Finally, in the *spectrum management* step, SU adapts itself to transmit in the open bands, potentially changing its carrier frequency, transmit power,

modulation type, and packet length.

The critical need for increasing commercial access to shared spectrum has encouraged the governments to take steps towards releasing multiple bands for spectrum sharing. In September 2010, the Federal Communications Commission (FCC) issued final rules to allow low-power unlicensed devices to operate on the unused channels in the TV broadcast bands (often called the TV white spaces (TVWS)) in the U.S. [27]. Two IEEE standards, namely IEEE 802.22 [8] and IEEE 802.11af [9], were developed to enable communications in the TVWS. In 2012, the FCC has opened up the 3.5 GHz (3550 - 3700 MHz) band to secondary access [12]. This band will be home to the new Citizens Broadband Radio Service (CBRS). The entrant users will share the spectrum among themselves and incumbents through a three-tiered access model composed of the Incumbent Access (IA), Priority Access (PA) and General Authorized Access (GAA) tiers. In 2013, the FCC, in its Notice of Proposed Rule Making (NPRM), announced that it intends to modify rules that govern the operation of Unlicensed National Information Infrastructure (U-NII) devices and make available an additional 195 MHz of spectrum in the 5 GHz band [13]. In the ongoing proceedings for the 5 GHz band, there is a growing contention between unlicensed LTE and Wi-Fi stakeholders for access to the band. Recently, in August 2015, the LTE-U and Wi-Fi stakeholders held a meeting to discuss these coexistence issues.

Regulatory bodies in Europe have also put spectrum-related initiatives in motion. In February 2015, the UK communication regulator, Office of Communications (Ofcom), finalized the licence exempt regulations over TVWS, which allows SUs to access the unused parts of radio spectrum in the 470-790 MHz band through dynamic spectrum sharing [10]. It has since been shown that over 50% of locations in the UK are likely to have more than 150 MHz of unutilized TV spectrum and that even 90% of locations might have around 100 MHz of spectrum available [28]. Hence, making this spectrum available for reuse could bring substantial value to the citizens and consumers [14, 29]. In addition, Ofcom recently issued a *call for inputs*, which tried to gauge interests and

assess the potential for enabling enhanced spectrum sharing in the 3.8 GHz to 4.2 GHz band [30].

The progress on enabling dynamic spectrum access shows promise in advancing increased spectrum sharing in multiple bands. TVWS is the first major instance of spectrum sharing to be considered, which refers to the unused TV channels among the active ones in the ultra-high frequency (UHF) spectrum [31, 32]. The experiences and concepts of utilizing TVWS can also be extended to other white space bands. Compared with traditional Wi-Fi, the superior penetration propagation characteristic over UHF spectrum enables TVWS to have longer communication distance and better penetration through obstacles [33].

To enable dynamic spectrum access over white space, accurate detection of the spectrum is crucial to ensure that there is no harmful interference caused to the surrounding licensed services, including Digital Terrestrial Televisions (DTT), Programme Making and Special Events (PMSE) users, e.g., wireless microphone systems, and other future incumbent users [10]. Two classes of solutions for addressing these challenges are being considered from engineering and regulatory viewpoints:

- *Spectrum Sensing.* The problem of spectrum sensing is to measure signal levels across time and frequency in order to obtain awareness about the spectrum usage as well as potential PUs in a geographical area. Spectrum sensing was an initial ingredient in the standards discussion for the establishment of secondary access to vacated TV channels provided no harmful interference is caused to incumbent services, which requires sensitivity of -120 dBm over 8 MHz for TV channels and -126 dBm over a 200 kHz bandwidth for wireless microphones [28].

- *Geolocation Database.* The other class of solutions is geolocation database, which is a centralized database to store the maximum allowed equivalent isotropic radiated power (EIRP) for each vacant TV channel at a specific location and time [34]. The secondary device, also named as white space device (WSD), determines its loca-

tion and queries the central database that will return a list of available frequency channels and their associated maximum transmit powers at current location. So far, several geo-location database providers, such as Google, Nominet, Spectrum Bridge, etc., have been approved by Ofcom in UK [34].

2.2 Narrowband Spectrum Sensing

As the core component of dynamic spectrum access, spectrum sensing aims to obtain awareness about the spectrum usage and the existence of PU in a certain geographical area at a particular duration of time. It allows the SU to detect spectral holes and opportunistically use these under-utilized frequency bands [3]. According to the bandwidth of the spectrum of interest, spectrum sensing can be categorized into two types, narrowband spectrum sensing and wideband spectrum sensing. The term "narrowband" implies that the bandwidth of interest is less than the coherence bandwidth of the channel such that the channel frequency response can be considered as flat [19]. Many narrowband spectrum sensing algorithms have been studied in the literature [35], including matched filtering, energy detection, and cyclostationary feature detection.

The matched filter detection [36, 37] is the optimal scheme for spectrum sensing as it maximizes the signal-to-noise ratio (SNR) in the presence of additive noise and achieves high sensing reliability within short sensing time. It correlates the received signal with a template to detect the presence of a known signal in the received signal. However, it requires the prior knowledge of PU in order to demodulate the received signal. For various types of signal processing, it also needs different types of filters, leading to increased implementation complexity.

Cyclostationary feature detection [38, 39] detects and distinguishes different types of primary signals by exploiting their cyclostationary features caused by periodical characteristics in the signal or in its statistics like mean and autocorrelation. Cyclostationary detection is robust to noise uncertainty and can distinguish noise from primary sig-

nals [40]. However, the computational cost of such an approach is relatively high and a long sensing period is required.

Among these three approaches of spectrum sensing, energy detection [41, 42] is mostly commonly researched. Energy detection is a non-coherent sensing approach that avoids the needs for prior knowledge of the primary transmission and the complicated receivers required by the matched filter. Based on the binary hypothesis model, each SU makes the decision on the existence of PU by calculating the received signal power or energy. Then it compares the received signal power with a threshold dependent on the noise variance of the environment. Specifically, the decision rule can be formulated as,

$$T(x) = \frac{1}{N}\sum_{n=1}^{N} |x[n]|^2 \underset{H_0}{\overset{H_1}{\gtrless}} \lambda, \tag{2.1}$$

where $T(x)$ is the test statistic and λ is the corresponding test threshold. According to the central limit theorem, when N is large enough, the value of $T(x)$ approximates Gaussian distribution [43],

$$\begin{aligned} T(x) &\sim \mathcal{N}(\sigma_\omega^2, 2\sigma_\omega^4/N), && H_0(c) \\ T(x) &\sim \mathcal{N}((1+\gamma)\sigma_\omega^2, 2(1+\gamma)^2\sigma_\omega^4/N), && H_1(c) \end{aligned} \tag{2.2}$$

where γ is the received SNR at the SU over the sensing channel.

The reliability of the energy detection is susceptible to noise uncertainty or under low SNR, and cannot distinguish the signal types. However, the hardware implementation and computational complexity of energy detection are relatively low.

2.3 Wideband Spectrum Sensing

While traditional narrowband spectrum sensing schemes have focused on exploiting spectral opportunities over narrow frequency range, cognitive radio networks will eventually be required to exploit spectral opportunities over a wide frequency range from

hundreds of megahertz to several gigahertz for achieving higher opportunistic throughput [2, 16, 19]. For instance, to exploit white space in the UHF TV band, wideband spectrum sensing techniques should be employed. Narrowband spectrum sensing approach cannot be directly used for wideband sensing as it make a single binary decision for the whole spectrum and thus cannot identify individual channel occupancy state that lie within the wideband spectrum.

Wideband spectrum sensing can be broadly divided into two types: Nyquist wideband spectrum sensing and sub-Nyquist wideband spectrum sensing. Nyquist wideband sensing processes the received signals sampled at or above the Nyquist rate, which requires the sampling rate to be at least twice the bandwidth of the signal. As technology advances, Nyquist theorem impose severe challenges both on the acquisition hardware and on the subsequent storage and digital signal processors. As sub-Nyquist approach acquires signals using a sampling rate much lower than the Nyquist rate, it attracts more and more attention to achieve a more flexible and faster wideband spectrum sensing.

2.3.1 Nyquist Wideband Spectrum sensing

A simple approach to wideband spectrum sensing is to directly acquire the wideband signal using a standard ADC and then use digital signal processing techniques to detect spectral opportunities.

In [16], Quan *et al.* proposed a multiband joint detection (MJD) algorithm that can sense the primary signal over multiple frequency bands jointly. As shown in Fig. 2.3, the wideband signal is firstly sampled by a high-rate ADC, after which a serial-to-parallel conversion is used to divide sampled data into parallel data sequences. Fast Fourier transform (FFT) is then implemented to convert the received signals into frequency domain. The wideband spectrum is then divided into a series of narrowband spectra $X_f^{(1)}, X_f^{(2)}, ..., X_f^{(M)}$. Finally, spectral occupancy of each narrowband is determined by using the binary hypotheses tests, where H_0 denotes the absence of PUs and H_1 denotes

the presence of PUs.

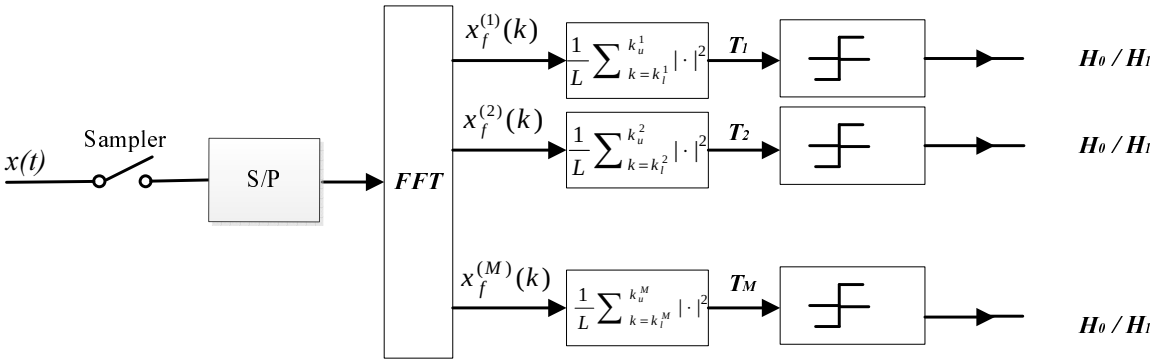

Figure 2.3: Schematic illustration of multiband joint detection.

Furthermore, Tian and Giannakis proposed a wavelet-based wideband spectrum sensing algorithm [44], which formulates the wideband sensing as a spectral edge detection problem and exploits wavelet transform to scan over the wide bandwidth to identify all piecewise smooth subbands. In this algorithm, the power spectral density (PSD) of the wideband spectrum is modelled as a train of consecutive frequency subbands, where the PSD is smooth within each subband but exhibits discontinuities on the border of two subbands. The wavelet transform is then used to characterize the edges exhibited in the wideband PSD.

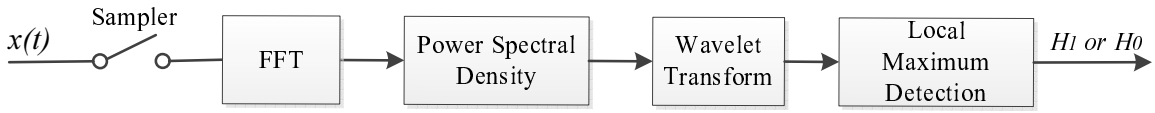

Figure 2.4: Schematic illustration of wavelet detection.

However, in the wideband regime, a major challenge arises from the stringent requirements on the high sampling rate at the ADC to transform the received signals into digital signals by sampling at the Nyquist rate, which presents significant challenges in the high-speed sampling hardware and signal processing algorithms.

A simple approach to relax the high sampling rate requirement for wideband spectrum

sensing is to use a tunable narrowband bandpass filter (BPF) at the RF front-end to scan through all the channels one by one to detect the existence or non-existence of licensed primary transmissions [45–48]. The tuning range of each BPF needs to be pre-selected. The occupancy of each channel is determined by measuring the energy of the signal at the output of each filter. However, the performance of sequential spectrum scanning depends mainly on how fast the device can scan. In the absence of fast scanning, the system can miss short lived signals (e.g., radar). For example, state-of-the-art spectrum monitors like the RFeye [24], which is used in the Microsoft spectrum observatory, has a fast scanning mode of 40 GHz/second and scans in chunks of 20 MHz, so it will take 25 ms to scan 1 GHz, much higher than the fast sensing requirements in the 802.22 ($<$ 1 ms). Thus, for the wideband sensing, the sequential nature of such scheme could introduce a long sensing period. Such delay in the sensing process will cause missed opportunities or interferences to primary transmissions.

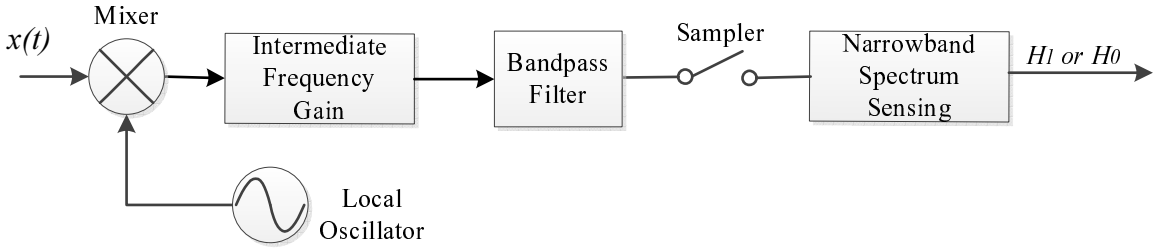

Figure 2.5: Schematic illustration of sequential scanning.

Another solution is the filter bank algorithm [49]. As shown in Fig. 2.6, the wideband signal to be monitored is passed through a bank of filters with different shifted central frequencies, and the output power of each filter is measured as an estimate of the spectral power over the associated subband. This algorithm can therefore capture the dynamic nature of wideband spectrum by using low sampling rates. However, it requires a great number of RF front-end components, e.g., BPFs, ADCs, etc., and therefore significantly increases the implementation costs.

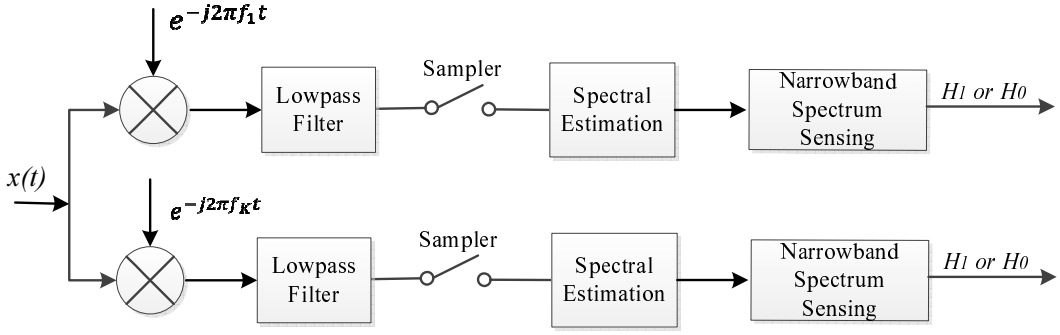

Figure 2.6: Schematic illustration of filter bank algorithm.

2.3.2 Sub-Nyquist Wideband Spectrum sensing

Due to the drawbacks of high sampling rate or high implementation complexity in Nyquist systems, sub-Nyquist approaches are drawing more and more attention for fast, efficient, and in-expensive signal processing algorithms, applications, and devices. Landau in [18] demonstrated that an arbitrary wideband signal can be perfectly reconstructed if being sampled at a rate no less than the total bandwidth of occupied spectrum. As wireless signals over an open spectrum are typically sparse in the frequency domain, it can be recovered by sampling at a rate far less than the Nyquist rate in practice.

Compressive sensing (CS), as a new sampling paradigm, facilitates signal acquisition by reducing the number of samples required for original signal reconstruction, and thus appears to be a promising technique for wideband spectrum sensing [17]. The entire process of CS consists of three parts: signal sparse representation; measurement collection (linear encoding); sparse reconstruction (non-linear decoding). In this following, these three parts will be briefly discussed in this section.

2.3.2.1 Sparse and Compressible Signals

Many signals of interest often have *sparse* representations, which means that the signal can often be well-approximated by a linear combination of only a few elements from a specific basis. The traditional strategy to exploit this sparsity is to first acquire the

signal in a high-dimensional space and then apply a compression method to capture the dominant part in the appropriate basis, such as MP3 for audio signals and JPEG for images. The research area of compressed sensing challenges this strategy by suggesting merging compression and sampling, so that a compact representation can be acquired directly.

The sparsity of a signal is often quantified by the ℓ_0-norm in the CS literature, i.e., the number of nonzero elements in the signal under certain domain [50]. For vectors in $\mathbb{C}^N$, define the ℓ_0 "quasinorm":

$$||\boldsymbol{x}||_0 = |\text{supp}(\boldsymbol{x})| = |\{j : x_j \neq 0\}|. \tag{2.3}$$

We say that a signal $\boldsymbol{x}$ is *k-sparse* when $||\boldsymbol{x}||_0 \leq k$.

Sparse signals are an idealization that we do not encounter in practical applications, but real signals are often *compressible*, which means that their entries decay rapidly when sorted by magnitude in a descending order [51]. As a result, compressible signals are well approximated by sparse signals.

We can also describe signals that are compressible with respect to other orthonormal bases, such as Fourier or wavelet basis. In this case, the sequence of coefficients in the orthogonal expansion decays quickly. Typically, signals we are dealing with in the time domain are not sparse. Suppose $\boldsymbol{x}$ can be expressed as a linear combination of $\boldsymbol{\theta} \in \mathbb{C}^N$ in some orthonormal basis $\boldsymbol{\Psi} \in \mathbb{C}^{N \times N}$, that is $\boldsymbol{x} = \boldsymbol{\Psi\theta}$, we still refer to $\boldsymbol{x}$ as *k-sparse* if $||\boldsymbol{\theta}||_0 \leq k$. We call the set of indices corresponding to the nonzero entries the *support* of $\boldsymbol{\theta}$ and denote it by $\text{supp}(\boldsymbol{\theta})$.

2.3.2.2 Sensing Matrices and Compressive Measurements

The process of collecting compressive measurements can be viewed as the action of a *sampling matrix* $\boldsymbol{\Phi}$ on the target signal. If we take m measurements, or samples, of a

signal in $\mathbb{C}^N$, then the sampling matrix $\mathbf{\Phi}$ has dimensions $m \times N$. A measurement is a linear function applied to the signal. Our goal is to push m as close as possible to the signal sparsity k in order to perform as much signal "compression" during acquisition as possible.

The sampling matrix must not map two different *k-sparse* signals to the same set of samples. One of the important properties of CS sampling matrices is that they must preserve the signal information to enable practical algorithms to accurately and efficiently recover the original signal. A key sampling matrix condition, used to study the general system's robustness, is known as the restricted isometry property (RIP) [51, 52].

Definition 1. *A matrix* $\mathbf{\Phi}$ *satisfies the RIP of order* k *if for all* k*-sparse vectors* $\boldsymbol{x}$ *there exists a constant* $0 < \delta_k < 1$ *such that*

$$(1 - \delta_k)||\boldsymbol{x}||_2^2 \leq ||\mathbf{\Phi}\boldsymbol{x}||_2^2 \leq (1 + \delta_k)||\boldsymbol{x}||_2^2. \tag{2.4}$$

The smallest constant δ_k (*as a function of* k) *for which* (2.4) *holds is defined as the RIP constant.*

Although it is computationally difficult to check the RIP for a given matrix, a striking fact is that many types of random sampling matrices satisfy RIP with high probability, which includes the sampling matrices whose entries following the i.i.d. Gaussian distribution, Bernoulli distribution, and the partial Fourier matrix [50]. For these matrices, the order $2k$ RIP condition is satisfied with overwhelming probability if the number of measurements satisfies the inequality

$$m \geq Ck\log(N/k), \tag{2.5}$$

where C is a constant depending on the specific measurement matrix instance. Therefore, for the above mentioned matrices, there exists a stable algorithm with which the exact sparse signal reconstruction is achievable with overwhelmingly high probability.

An alternative approach to guarantee the stability of CS recovery is to ensure that the sampling matrix $\mathbf{\Phi}$ is incoherent with the sparsifying basis $\mathbf{\Psi}$. More specifically, incoherence property requires that the rows of $\mathbf{\Phi}$ cannot sparsely represent the columns of $\mathbf{\Psi}$ and vice versa. The *mutual coherence* between the sampling matrix $\mathbf{\Phi}$ and the representation basis $\mathbf{\Psi}$ is defined as:

$$\mu(\mathbf{\Phi}, \mathbf{\Psi}) = \sqrt{N} \cdot \max_{1 \leq j,k \leq N} |\langle \phi_j, \psi_k \rangle|. \tag{2.6}$$

The coherence measures the largest correlation between any two elements of $\mathbf{\Phi}$ and $\mathbf{\Psi}$. It follows from linear algebra that $\mu(\mathbf{\Phi}, \mathbf{\Psi}) \in [1, \sqrt{N}]$. Within the CS framework, low coherence between $\mathbf{\Phi}$ and $\mathbf{\Psi}$ leads to fewer samples required for signal reconstruction [53].

As the wideband spectrum is normally under-utilized in reality, the received signal $x(t)$ bears a spectrally sparse property in the frequency domain such that all (or most) of its energy is concentrated in one or more disjoint frequency bands, i.e., its spectral measure is small relative to the overall signal bandwidth. This motivates to apply the idea of sub-Nyquist sampling to wideband spectrum sensing that would bring substantial saving in terms of the sampling rate.

However, compressive sensing has concentrated on finite-length and discrete-time signals. Thus, innovative technologies are required to extend compressive sensing to continuous-time signal acquisition (i.e., implementing compressive sensing in the analog domain).

To realize the analog compressive sensing, Tropp et al. proposed a new type of signal acquisition system, called *random demodulator* [54], constructed from low-power, readily available components, which is a good basis for the translation of compressive sampling from theory into practice. The random demodulator employs structured sensing matrices for the acquisition of periodic multitone analog signals. As shown in Fig. 2.7, random demodulator consists of a pseudo-random number generator, a mixer, an accumulator, and a low-rate sampler. The pseudo-random number generator produces a sign wave-

form that alternates randomly at the Nyquist rate W. Then, the mixer multiplies the continuous-time input signal $x(t)$ by this pseudonoise sequence, which smears the frequency spectrum of the original signal across the entire spectrum. Subsequently, the demodulated signal is intergraded by the accumulator and then sampled using a low-rate sampler for every $1/R$ seconds, where R is the sub-Nyquist sampling rate which is much lower than the Nyquist rate W. The sparse signal can then be reconstructed from the resulting compressive measurements. However, analog signals require a great number of harmonics to approximate them well in the discrete model, which makes the reconstruction computationally infeasible and precludes processing at a low rate.

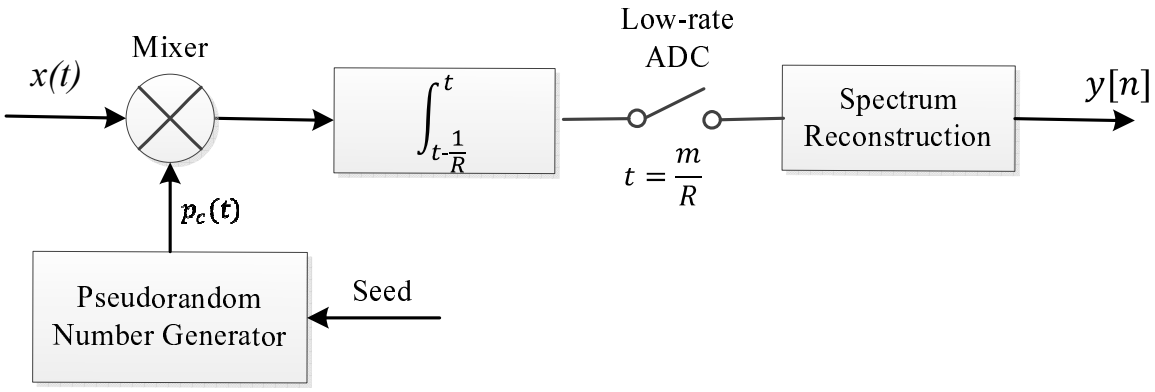

Figure 2.7: Schematic illustration of random demodulator.

In [55], Mishali and Eldar proposed another hardware implementation system, named as modulated wideband converter (MWC). The main difference between MWC and random demodulator is that MWC has multiple sampling channels, with the accumulator in each channel replaced by a general low-pass filter. As shown in Fig. 2.8, the analog signal is firstly multiplied with a bank of periodic waveforms, whose period corresponds to the multiband model parameters. Subsequently, the product is low-pass filtered and sampled uniformly at a low rate. One significant advantage of MWC is that it is robust against the noise and model mismatches. Furthermore, the dimension of the measurement matrix is reduced in the proposed framework, efficiently reducing the computation complexity of the spectral reconstruction. However, the implementation is specifically

designed for MWC, and difficult to extend to make it match well with the other existing compressive sensing algorithms.

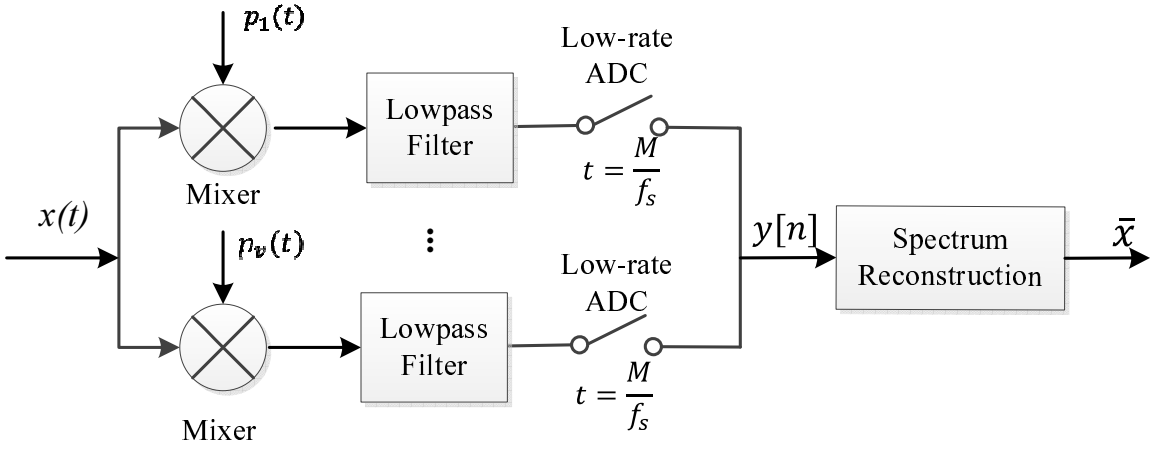

Figure 2.8: Schematic illustration of modulated wideband converter.

An alternative multichannel sub-Nyquist sampling approach is multicoset sampling. Multicoset sampling selects a subset of samples from a uniform grid, which is obtained using a sampling rate f_s at or above the Nyquist rate. The uniform grid is then divided into blocks of M consecutive samples, and in each block only p ($p \leq M$) samples are retained, while the rest are skipped. Multicoset sampling can be implemented by using p sampling channels with sampling rate of f_s/M and different time offsets on each sampling channel, as shown in Fig. 2.9. The advantage of multicoset sampling is that the sampling rate in each channel is M times lower than the Nyquist rate. Furthermore, the number of measurements is only p/M of that in the Nyquist sampling case. In [56], wideband spectrum sensing scheme based on multicoset sampling was proposed. In addition, a low-speed sub-Nyquist multicoset sampling strategy was proposed in [57] for wideband spectrum sensing without the need of analog front-end processing. However, it requires the knowledge of the spectral support to allow for the perfect reconstruction. To estimate the locations of the occupied channels, the MUltiple SIgnal Classification (MUSIC) algorithm, originally proposed for the direction of arrival estimation in the traditional sensor array processing [58], is exploited for the joint support recovery by Feng and

Bresler [56, 59]. However, the detection accuracy based on MUSIC algorithm degrades severely when the SNR decreases [60].

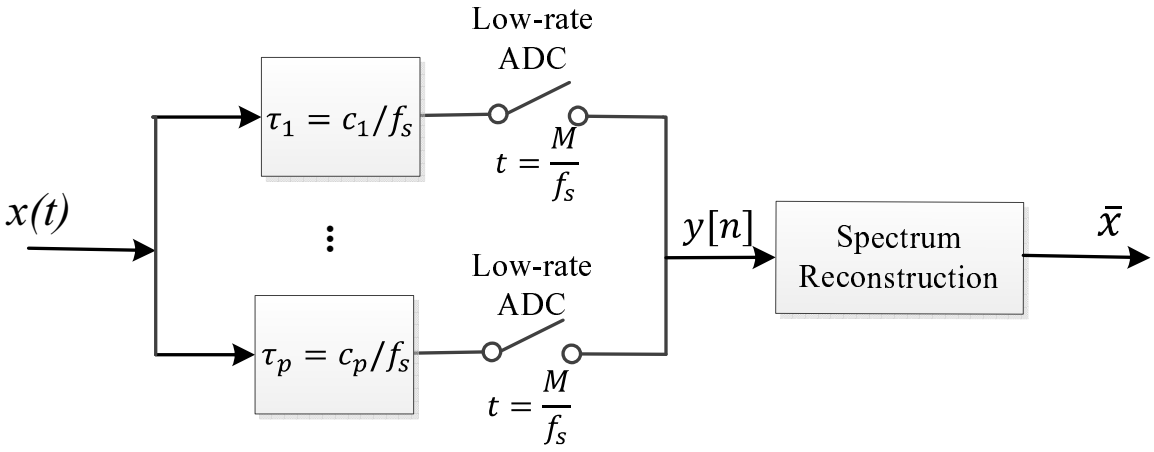

Figure 2.9: Schematic illustration of multicoset sampler.

2.3.2.3 Sparse Reconstruction

The major algorithmic challenge in CS is to recover the sparse or compressible signal from the under-determined linear system: given $\boldsymbol{y}$ and $\boldsymbol{\Phi}$, find a signal $\boldsymbol{x}$ such that $\boldsymbol{y} = \boldsymbol{\Phi x}$ exactly or approximately. There exists a wide variety of approaches to solving this problem. We now briefly review three typical types of methods in the literature.

Convex Relaxation: To retrieve the unknown signal $\boldsymbol{x}$ as well as preserve its sparsity from the compressive measurements, it is intuitive to consider the following optimization problem

$$\min ||\boldsymbol{x}||_0 \quad \text{subject to} \quad \boldsymbol{y} = \boldsymbol{\Phi x}. \tag{2.7}$$

Due to the unavoidable combinatorial search, this algorithm is however NP-hard [61]. Alternatively, a more computationally tractable approach which relaxes the ℓ_0-norm objective to the ℓ_1-norm has been proposed to approximate the target signal [62], which is defined as $||\boldsymbol{x}||_1 = \sum_{j=1}^{N} |x_j|$. This adaption leads to the following minimization

problem, known as *Basis Pursuit (BP)* [63]:

$$\min ||\boldsymbol{x}||_1 \quad \text{subject to} \quad \boldsymbol{y} = \boldsymbol{\Phi x}. \tag{2.8}$$

Since ℓ_1-norm is convex, (2.8) can be seen as a convex relaxation of (2.7), and can be solved by many off-the-shelf linear programming (LP) solvers. Due to the shape of the ℓ_1 ball, ℓ_1 minimization promotes sparsity [64]. In the presence of noise, the optimization (2.8) can be modified to allow for the noise in the measurements $\boldsymbol{y} = \boldsymbol{\Phi x} + \boldsymbol{n}$, which is formulated as

$$\min ||\boldsymbol{x}||_1 \quad \text{subject to} \quad ||\boldsymbol{\Phi x} - \boldsymbol{y}||_2^2 \leq \varepsilon, \tag{2.9}$$

where $\varepsilon \geq ||\boldsymbol{n}||_2$ is an appropriately chosen bound on the noise magnitude. This optimization is known as *Basis Pursuit Denoising (BPDN)* [65], and is a quadratic program with polynomial complexity solvers. This quadratic program can be converted into an alternative unconstrained form by introducing Lagrange multipliers:

$$\min ||\boldsymbol{\Phi x} - \boldsymbol{y}||_2 + \lambda ||\boldsymbol{x}||_1. \tag{2.10}$$

It is known as the *Least Absolution Shrinkage and Selection Operator (LASSO)* [66] problem. With appropriate choice of λ, the solution of LASSO coincides with that of the constraint minimization in (2.9). Several approaches for choosing λ are discussed in [67, 68].

In summary, this class of algorithms solves a convex optimization problem to reconstruct the signal. The number of measurements required for exact reconstruction is small but these methods are computationally complex. So it may not be very efficient for the large-scale problems.

Greedy Algorithm: Another class of CS reconstruction algorithms is the greedy algorithm. These methods are iterative in nature and select columns of $\boldsymbol{\Phi}$ based on their correlation with the measurements $\boldsymbol{y}$ determined by an appropriate inner product. They

solve the reconstruction problem by making locally optimal choices at each step until a convergence criterion is met. Examples include orthogonal matching pursuit (OMP) [69], stagewise OMP (StOMP) [70], compressive sampling matching pursuit (CoSamp) [71], and iterative hard thresholding (IHT) [72]. The major advantages of this algorithm are its high speed of recovery and its ease of implementation. Taking OMP as an example, given the measurement vector $\boldsymbol{y}$ and the measurement matrix $\boldsymbol{\Phi} = [\phi_1, ..., \phi_N]$, the algorithm can be summarized as follows:

- Initialize the residual $\boldsymbol{r}_0 = \boldsymbol{y}$, the index set $\Lambda_0 = \emptyset$, and the iteration counter $t = 1$.
- Find the index λ_t that solves the optimization problem:

$$\lambda_t = \underset{n=1,...,N}{\arg\max} |\langle \boldsymbol{r}_{t-1}, \phi_n \rangle|. \tag{2.11}$$

- Augment the index set and the matrix of chosen atoms: $\Lambda_t = \Lambda_{t-1} \cup \{\lambda_t\}$ and $\boldsymbol{\Phi}_t = [\boldsymbol{\Phi}_{t-1} \quad \phi_{\lambda_t}]$.
- Solve a least square problem to obtain a new signal estimate:

$$\boldsymbol{x}_t = \underset{\boldsymbol{x}}{\arg\max} ||\boldsymbol{y} - \boldsymbol{\Phi}_t \boldsymbol{x}||_2. \tag{2.12}$$

- Calculate the new approximation of the data and the new residual:

$$\boldsymbol{a}_t = \boldsymbol{\Phi}_t \boldsymbol{x}_t, \quad \boldsymbol{r}_t = \boldsymbol{y} - \boldsymbol{a}_t. \tag{2.13}$$

- If the stopping condition is achieved, stop the algorithm. Otherwise, increment t, and return to Step 2.

Non Convex Minimization Algorithm: Another reconstruction approach is to relax the ℓ_0-norm to l_ν-quasinorm ($0 < \nu < 1$), defined as $||\boldsymbol{x}||_\nu = (\sum_{j=1}^{N} |x_j|^\nu)^{1/\nu}$, which is possible to achieve the exact reconstruction with substantially fewer measurements [73]

and could be formulated as

$$\arg\min_{\boldsymbol{x}\in\mathbb{C}^N} ||\boldsymbol{x}||_\nu \quad \text{subject to } ||\boldsymbol{\Phi x}-\boldsymbol{y}||_2^2 \leq \varsigma. \tag{2.14}$$

As the ℓ_ν norm minimization provides a closer approximation to the ℓ_0 norm minimization, it is a more efficient solution to exactly reconstruct the original signals with less requirements on the signal sparsity and the number of measurements. The ℓ_ν norm minimization is nonconvex but could be solved by iteratively reweighted least squares (IRLS) algorithm [74]. Each iteration of the IRLS algorithm corresponds to a weighted least-squares problem which can be efficiently solved by standard convex optimization methods.

Sparse Bayesian framework: Besides the aforementioned convex and non-convex minimization and greedy algorithms, there are a number of computational approaches for solving the original sparse recovery problem. Recently, sparse Bayesian learning framework has been derived to find robust solutions in sparse signal recovery [75]. Sparse Bayesian framework formulates the CS problem via the Bayesian rule, and its close relationship to the non-convex ℓ_v-norm ($0 < v < 1$) minimization problem is derived in [76, 77]. Different from the traditional convex relaxation algorithms [63, 66], whose global minimum is generally not the sparsest solution [64], the global minimum of sparse Bayesian framework is always the sparsest one. More specifically, in sparse Bayesian framework, a prior distribution for the unknown vector is assumed to find the posterior probability $p(\boldsymbol{x}|\boldsymbol{y};\boldsymbol{\theta})$ based on Bayesian algorithm, which have superior recovery performance, especially in the presence of high correlation of rows in the measurement matrix, high noise level, or poor signal sparsity [75]. The more details of sparse Bayesian framework based CS model can be found in [78–80].

2.4 Cooperative Spectrum Sensing

The spectrum sensing results may sometimes be wrongly calculated due to certain undesirable conditions like multipath fading, shadowing, and noise uncertainty over wireless channels. Likewise, the SUs may not be able to sense the multiple channels at once due to the limitations of hardware and computation capabilities. This motivates the idea of cooperative spectrum sensing to improve sensing reliability by exploiting the spatial diversity across multiple SUs [81, 82]. Based on the data fusion criteria, cooperative spectrum sensing can be realized in either a decentralized or centralized manner.

In decentralized cooperation, each SU only communicates with its neighboring SUs within one hop to reduce the transmission power, so that the exchanged information spreads over the network through multiple rounds to reach the global convergence. Upon convergence, all SUs will have the fused sensing results without the implementation of a fusion centre. Several decentralized cooperative schemes [23, 83–85] have been developed in combination with consensus averaging techniques [86] to reach global fusion and consensus on the estimated spectrum. This scheme requires a periodic update on the spectrum information, hence requires more storage and computations. The convergence speed of decentralized cooperative spectrum sensing is also an issue in large scale networks.

In the centralized implementation, all samples collected at individual SUs, or their local decisions are sent to a fusion centre to make a high-resolution global decision on the spectrum occupancy. As shown in Fig. 2.10, each SU observes the RF spectrum individually, and then forwards its measured/processed data, or local decisions to the fusion centre via a common control channel. The common control channel is responsible for transferring sensing and control information between SUs and the fusion centre. The fusion centre then fuses all sensing data or decisions, makes the final sensing decision, and informs the SUs about the spectrum information. Generally, the final decision at the fusion centre can be made through two methods: *data fusion* and *decision fusion* [25]:

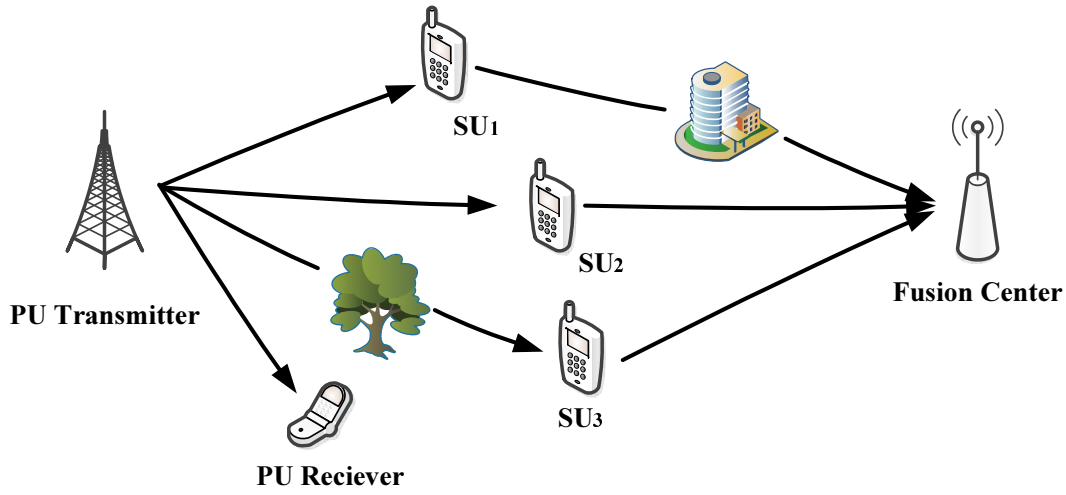

Figure 2.10: Schematic illustration of the cooperative spectrum sensing, where each SU transmits its individual observation or decision via control channels to a fusion centre, which makes final decision on the spectral occupancy status.

- Data Fusion: Each SU sends its original or processed sensing measurements to the fusion centre. The fusion centre processes the measurements from all SUs jointly and then makes the global sensing decision with enhanced accuracy;

- Decision Fusion: Each SU performs local spectrum sensing and feeds back its own binary decision result to the fusion centre, where the decisions are fused and a final decision is made about the spectrum occupancy status.

In comparison to data fusion, the one-bit decision fusion scheme needs a low bandwidth for sharing the spectrum sensing results, as well as saving transmission energy. However, the detection performance is suboptimal due to the loss of information. Soft combination is shown to have the cooperative spectrum sensing performance improvement over hard combination, but suffers from the disadvantage of large transmission overheads and high computation complexity [41]. Sub-Nyquist sampling based cooperative spectrum sensing schemes are therefore proposed to reduce the transmission and computation overhead without degrading the detection accuracy. As the sparse property of received signals can be transformed into low-rank property of the matrix constructed in the cooperative networks, recent advances on *joint sparsity recovery* and *matrix com-*

pletion can be adapted to the collaborative spectrum sensing to allow for the exact recovery from incomplete sensing measurements [87].

2.4.1 Joint Sparse Recovery

In practice, the common sparse support among the SUs enables an efficient reconstruction algorithm to recover all of the signals *jointly*. Specifically, multiple SUs acquire the same primary signal but with different phase shifts or attenuations caused by different signal propagations. Thus the primary signals received at all SUs share a common sparse support with different amplitudes, known as *joint sparsity* [88].

Suppose that J ($J > 1$) SUs are performing sub-Nyquist sampling individually to collect their low-rate measurements $\boldsymbol{y}^{(j)}$, which can be expressed as $\boldsymbol{y}^{(j)} = \boldsymbol{\Phi}^{(j)}\boldsymbol{x}^{(j)}$. The vector model has been extended to a finite set of sparse vectors sharing a common sparsity pattern. The SUs share their compressive measurements, rather than original Nyquist samples to reduce communication overhead, with a fusion centre that will recover the underlying joint support. The overhead in delay and energy caused by cooperative sensing is mitigated by processing sub-Nyquist samples. In this setting, rather than trying to recover a single sparse vector $\boldsymbol{x}$ seperately, the goal is to jointly recover a set of vectors $\boldsymbol{x}(j),\ j = 1, ..., J$ that share a common support. Stacking these vectors into the columns of a matrix $\boldsymbol{X}$, there will be at most k non-zero rows in $\boldsymbol{X}$. The support of $\boldsymbol{X}$ denotes the union of the supports of the columns of $\boldsymbol{X}$, or equivalently, the set of indices of non-zero rows. This class of algorithm is known as the *multiple measurement vectors* (MMVs) problem [89].

In order to determine the support of $\boldsymbol{x}(j),\ j = 1, ..., J$, joint sparse property in the frequency domain is exploited. There are existing algorithms for recovering jointly sparse signals in the literature [90–92]. In [93], Tropp and Gilbert have proposed an iterative algorithm, called Simultaneous Orthogonal Matching Pursuit (SOMP), which can be readily applied in this joint sparse recovery framework. To adapt the SOMP

algorithm to the cooperative spectrum sensing setting, it is first extended to cover a different sampling matrix $\mathbf{\Phi}^{(j)}$ for each received signal $\boldsymbol{x}^{(j)}$ at the SU. Then, in each iteration, the column index $n \in \{1, 2, ..., N\}$ is selected that accounts for the greatest amount of residual energy across all SUs [94, 95]:

$$\lambda_t = \underset{n=1,...,N}{\arg\max} \sum_{j=1}^{J} |\langle \boldsymbol{r}_{t-1}^{(j)}, \phi_n^{(j)} \rangle|. \tag{2.15}$$

It's important to notice that joint spectrum recovery requires much less samples for each SU comparing with separate recovery scheme, which further reduces power and bandwidth for communication and memory size for storage.

2.4.2 Matrix Completion

Another approach of low-rank matrix completion [96–98] can also be implemented to recover the signals in the cooperative cognitive radio networks. In many practical problems, one wants to recover a matrix from a sampling of its entries, in which some of the observations are missed or corrupted by malicious errors and noise. Normally, the matrix to be recovered is structured in the sense that it is *low-rank* or approximately low-rank, e.g. matrix with I rows and J columns has rank K if its rows or columns span a K-dimensional space. Different from compressive sensing, which exploits the sparsity property of signals under certain basis, matrix completion utilises the matrix's low rank property.

In [87], instead of scanning all channels and sending each channel's status to the fusion centre, each SU, equipped with a frequency selective filter, senses a linear combination of multiple channels. The filter coefficients are designed to be random numbers to mix different channel information. The support of the wideband signals then is recovered at the fusion centre from the incomplete samples sent by the SUs. In previous research on matrix completion [96–98], it was proved that under suitable conditions, a

low-rank matrix can be recovered from a random, yet small subset of its entries by nuclear norm minimization. So far, numerous matrix completion solvers have been developed, including the singular value thresholding (SVT) algorithm [99], the fixed point continuation with approximate (FPCA) algorithm [100], and accelerated proximal gradient line (APGL) search method [101].

2.5 Summary

This chapter presents current development on dynamic spectrum access, narrowband spectrum sensing, and wideband spectrum sensing, as well as the fundamental concepts of compressive sensing. The advantages and disadvantages of these algorithms are summarized in Table 2-A. In addition, the literature review on cooperative spectrum sensing is presented.

Table 2-A: Summary of advantages and disadvantages of narrowband and wideband spectrum sensing algorithms.

		Algorithm	***Advantages***	***Disadvantages***	***Ref.***
Narrowband Spectrum Sensing		Matched filtering	Optimal performance	Require prior information of PUs	[36, 37]
		Energy detection	No need for prior information; Low computation cost	Poor performance under low SNR; Cannot differentiate PUs	[41, 42]
		Cyclostationary feature detection	Valid under low SNR; Can differentiate PUs	High computational cost	[38–40]
Wideband Spectrum Sensing	Nyquist Rate	Multiband Joint Detection	Simple structure	High sampling rate	[16, 102]
		Sequential Scanning	Low sampling rate	Long sensing time	[45–48]
		Filter Bank Algorithm	Low sampling rate	High implementation complexity	[49]
	Sub-Nyquist Rate	Compressive Sensing	Low sampling rate	High sampling complexity; Signal sparsity requirements	[17, 23, 103–108]
		Multichannel Sub-Nyquist sampling	Low sampling rate	Requires multiple sampling channels; Sensitive to noise conditions	[55–57, 59]

Chapter 3

Sparsity Independent Sub-Nyquist Wideband Spectrum Sensing

Wideband spectrum sensing based on sub-Nyquist sampling has attracted much attention in recent research, while most of existing algorithms can only work with a sparse spectrum. In this chapter, a sub-Nyquist wideband spectrum sensing algorithm is proposed that achieves wideband sensing independent of signal sparsity without sampling at full bandwidth by using the low-speed ADCs based on sparse Fast Fourier Transform (sFFT). Specifically, the related work on sub-Nyquist wideband spectrum sensing, and main contributions of this chapter are firstly reviewed in Section 3.1. In Section 3.2, each block of the proposed wideband spectrum sensing is presented. The simulations for the performance evaluation of the proposed sensing scheme are presented in Section 3.3 on the simulated and real-world TVWS signals. Finally, Section 3.4 concludes this chapter.

3.1 Introduction

3.1.1 Related Work

Sub-Nyquist sampling techniques implement wideband spectrum sensing using lower-than-Nyquist sampling rates to reduce the requirements of high-speed signal processing [19]. In [17], compressed sensing were introduced to implement wideband sensing by exploiting the sparseness of the wideband signals in the frequency domain. Compressed sensing based wideband spectrum sensing has attracted considerable attention for wideband signal acquisition because it uses fewer measurements [23, 103–108]. However, compressed sensing based approaches require random sub-Nyquist projections of the wideband signals [51], which cannot be done simply by using the standard low-rate ADCs. Therefore, custom ADCs with complex hardware that can perform analog mixing [54, 55] or analog matrix multiplication [51, 105] at Nyquist rate are needed in compressive wideband spectrum sensing schemes. Moreover, most compressed sensing based spectrum sensing algorithms typically assume that the wideband signals are sparse in the frequency domain given the low spectrum utilizations, e.g., 3% in [105], 8% in [106], 10% in [107], 25% in [108], and 30% in [17]. As the secondary market for the spectrum sharing has been opened to public usage, multiple SUs compete for the TVWS spectrum resources to serve a large pool of end-users [10]. Since the usage patterns may change from day-to-day or even from hour-to-hour, there is a wide range of variations in the spectrum occupancy due to the secondary signals vacating or coming into existence [109, 110]. Therefore, the wideband signal may no longer be static and sparse over TVWS, i.e., sparsity level may be time-varying and larger than 30% [4, 5].

The sFFT algorithm estimates the spectrum of a sparse signal directly from the time-domain sub-Nyquist samples [20]. Compared with DFT, sFFT reports only the positions and amplitudes of the large magnitude frequency components of the input signal in the time proportional to the sparsity of the signal spectrum, as opposed to the signal size. As spectrum sensing focuses on clarifying the positions of the occupied frequency bands,

it can benefit from the advances of sFFT, which permit signals whose frequency domain representation is sparse to be recovered using only a small subset of samples [20].

However, the performance of the sFFT has strict requirements on the input signal sparsity, which limits its application to only very sparse signals. sFFT outperforms FFT only when the number of non-zero dominant frequency components k is less than $O(N/\log N)$, where N is the number of frequency bins. For example, when signal size equals to $N = 2^{22}$, the signal sparsity level k/N should be less than 0.048% [20]. However, the PU's spectrum utilization is about 20% to 30% [28], and will be higher when the secondary market is opening for the spectrum sharing to the mobile devices [4]. In [111], a wideband spectrum sensing scheme is proposed for the spectrum that is not sparse, where its goal is to identify the changes in the spectrum occupancy, based on the assumption that although the spectrum is densely occupied, its changes are sparse. However, it can only detect the spectrum changes, not the occupancy states over the whole spectrum, and has strict requirement on the percentage of the spectrum changes, up to 1%. Hence a flexible and fast wideband spectrum sensing scheme that can subsample the wideband signal regardless of signal sparsity is of great interest.

3.1.2 Contributions

In this chapter, a sub-Nyquist wideband spectrum sensing algorithm is proposed based on sFFT [20]. To lower signal spectrum sparsity while maintaining the channel state information, a permutation and filtering algorithm is proposed to pre-process the received signal. The proposed algorithm works for both sparse and non-sparse spectrum without sampling at full bandwidth through the use of low-speed ADCs. Based on the proposed permutation and filtering algorithm, sub-Nyquist wideband sensing can be implemented even when the signal is highly occupied by the PUs. Unlike existing sub-Nyquist approaches [17, 106], the proposed algorithm sub-samples the wideband signal independent of signal sparsity and detects the channel occupancy state based on the estimated spectrum. The mathematical model of the proposed spectrum sensing algorithm

is derived and verified by numerical analyses. Moreover, the proposed algorithm is tested on real-world TVWS signals. This validation shows reduced runtime and implementation complexity as well as high detection performance compared with the conventional wideband sensing algorithms.

3.2 System Model

Without loss of generality, the wideband signal to be monitored is bandlimited with M non-overlapping channels, each of them with bandwidth $\mathcal{B}_0$. The whole bandwidth is $\mathcal{B} = M\mathcal{B}_0$. The channels are indexed from 1 to M. Suppose there are $\kappa \leq M$ active channels occupied by PUs during the sensing period with $\boldsymbol{\mathcal{S}}$ denoting the set containing the indices of the occupied channels. Thus the spectrum utilization ratio of the primary transmission can be expressed as $\alpha = \kappa/M$.

If the input signal x is sampled at the Nyquist rate f_s in the observed time T_s, the signal can be discretized as a vector $\boldsymbol{x} \in \mathbb{C}^N$, where N denotes the number of Nyquist samples and can be written as $N = f_s T_s$. Let s be the wideband primary signal expressed as $s = \sum_{m=1}^{M} s_m$, where s_m is the primary signal in the channel m. The received signal x at the cognitive radio front-end can be expressed as:

$$x = s + n, \tag{3.1}$$

where n represents white Gaussian noise with zero mean and variance σ_n^2. If we denote with k the frequency bin index ($k = 0, 1, ..., N-1$), the Fourier spectrum of $\boldsymbol{x}$, $\widehat{\boldsymbol{x}}$, can be computed by DFT as

$$\widehat{x}_k = \frac{1}{\sqrt{N}} \sum_{i=0}^{N-1} x_i e^{-j2\pi ik/N}. \tag{3.2}$$

Since the bins of DFT are uniformly distributed across the total bandwidth, ignoring the zero frequency, each channel can be represented by the same number of frequency

bins $L = (N-1)/M = k_u^m - k_l^m + 1$, where k_u^m and k_l^m are the upper and lower bin indices of channel m.

The proposed scheme of sparsity independent sub-Nyquist rate wideband spectrum sensing is composed of three main blocks: signal permutation and filtering; spectrum estimation; multi-channel joint detection (MJD) (Fig. 3.1).

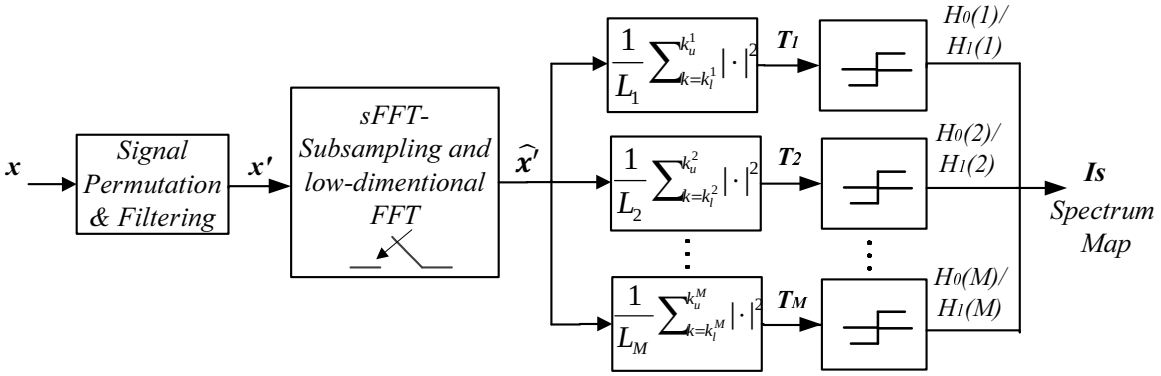

Figure 3.1: Block diagram of the proposed sparsity independent sub-Nyquist wideband spectrum sensing scheme.

3.2.1 Signal Permutation and Filtering

As sFFT has strict requirements on input signal sparsity, a permutation and filtering algorithm is proposed to pre-process the received signal to reduce the spectrum sparsity lower than the sparsity bound of sFFT while maintaining the channel state information. The proposed permutation and filtering algorithm is composed of three main steps, namely permutation, filtering and un-permutation (Fig. 3.2).

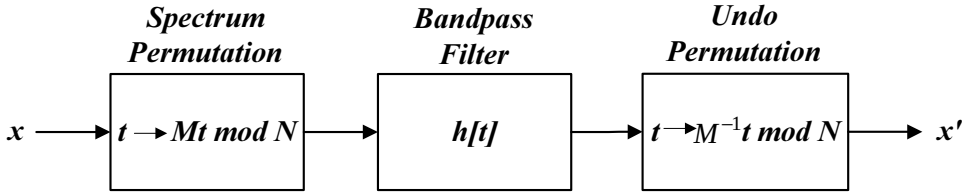

Figure 3.2: Flowchart of the proposed signal permutation and filtering algorithm.

Define the extraction ratio be β, which is the fraction of the channel spectrum that is going to be used to estimate the occupancy, so the number of samples taken on each channel is $L_m = \lfloor \beta L \rfloor$. Given the spectrum utilization ratio α, the sparsity of the input signal $k = SL = \alpha ML$ is reduced to $k' = SL_m = \alpha ML_m \approx \alpha\beta N$. Therefore, the available range of the extraction ratio to retain faster runtime of sFFT than FFT is $\beta \leq \beta_{\max} = \frac{L_m}{L} = \frac{k_{\max}/\alpha M}{N/M} = \frac{k_{\max}}{\alpha N}$, where $k_{\max} = O(N/\log N)$ is the sFFT's sparsity bound for the input signal size N.

Based on the input spectrum utilization α, the extraction ratio β can be chosen to reduce signal sparsity lower than the sFFT's sparsity bound. sFFT can then be applied to reduce the runtime and computational complexity. However, for the M-channel wideband signal, it needs M bandpass filters to extract the subset of central samples from each channel.

To implement the extraction process with low complexity, the signal is permuted through time dilation $t \longmapsto Mt \bmod N$ at first. Assuming that the input signal size N and the number of channels M are coprime, i.e., $N = ML+1$, M is *invertible modulo* N. In the frequency domain, this translates to the frequency mapping $f \longmapsto M^{-1}f \bmod N$, where $MM^{-1} \bmod N = 1$. The inverse of M under mod-N equals to $M^{-1} = N - L$.

Proof. Suppose there exists an integer M^{-1}, $MM^{-1} \bmod N = 1$. There must exist an integer $a \in \mathbb{Z}$, such that $MM^{-1} = aN + 1 = a(ML+1)+1 \overset{a=M-1}{=} (M-1)ML + M$. So $M^{-1} = (M-1)L + 1 = ML + 1 - L = N - L \in \mathbb{Z}$. Hence M is *invertible modulo* N and its *inverse* is $M^{-1} = N - L$.

As shown in Fig. 3.3, the l-th frequencies from each of the M channels $(M-m)L + l$, $m = 1, ..., M$, are moved to $(l-1)M+m$, $l = 1, ..., L$ in the permuted signal. Therefore, the signal components from different channels are uniformly interleaved with each other in the frequency domain after the permutation.

Proof. $[(l-1)M + m] \cdot K^{-1} \bmod N$

$= [(l-1)M + m] \cdot [N - L] \bmod N$

$$
\begin{aligned}
&= N \cdot [(l-1)M + m] - MLl + [M-m]L \bmod N \\
&= N \cdot [(l-1)M + m] - l[ML+1] + [M-m]L + l \bmod N \\
&= N \cdot [(l-1)M + m - l] + [M-m]L + l \bmod N \\
&= [M-m]L + l
\end{aligned}
$$

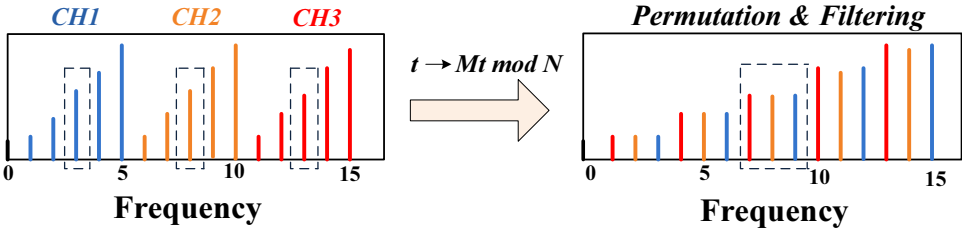

Figure 3.3: (left) Input signal spectrum with 3 channels (N = 16). (right) Signal spectrum after permutation. Through the bandpass filter, it can extract the central frequencies in each channel.

Thus, the permuted signal can pass through one bandpass filter to extract L_m central frequencies from each channel. The bandwidth of the filter is $B_{\text{filter}} = \beta B$. Finally, the frequencies in the filter output are restored to their original spectral locations by carrying out a reverse time dilation $t \longmapsto M^{-1}t \bmod N$.

After the signal permutation and filtering, the sparsity of input signal has been lowered so that its frequency representation $\widehat{\boldsymbol{x}}'$ can then be estimated through sFFT.

3.2.2 Spectrum Estimation

The permuted and filtered signal x' is then subsampled, and its spectrum $\widehat{x}'$ is estimated based on sFFT [20].

The key idea behind sFFT is to identify the positions and amplitudes of the large magnitude frequency components based on the partial measurements from its subsampling process. For $\boldsymbol{x}' \in \mathbb{C}^N$ with a k'-sparse spectrum, it runs two kinds of loops to estimate the spectrum $\widehat{\boldsymbol{x}}'$: location loops (to find positions of k' largest frequencies) and estimation loops (to estimate their magnitudes).

The purpose of the location loops is to generate a list of candidate coordinates $I_J \subset [N]$ which are likely to contain large magnitude frequency coefficients. Given the set I_J, estimation loops are used to determine the magnitude of the frequency coefficients. The steps below are performed in location and estimation loops :

3.2.2.1 Random Permutation

Randomly choose an integer σ that is *invertible modulo* N, i.e. $gcd(\sigma, N) = 1$, and $\tau \in [N]$. Permute the vector $\boldsymbol{x}'$ with the permutation $P_{\sigma,\tau}$ as

$$(P_{\sigma,\tau}x')_i = x'_{\sigma i+\tau}. \tag{3.3}$$

The purpose of this permutation is to rearrange signal's spectrum by modifying its time-domain permutation.

3.2.2.2 Apply Window

Using a flat window function F, obtained from convolving a standard window function G with a "box car" window function H, i.e., $\widehat{F} = \widehat{G} * H$, the filtered vector can be computed as

$$\boldsymbol{y} = F \cdot (P_{\sigma,\tau}\boldsymbol{x}'). \tag{3.4}$$

It allows a subset of signal with size $\omega = |supp(F)|$ to be extracted for computation without touching all the elements to achieve sub-linear runtime. In the frequency domain, the multiplication is equivalent to a convolution of $\widehat{F}$ and $\widehat{P_{\sigma,\tau}\boldsymbol{x}'}$. Random time-domain permutation in the first step changes the set of coefficients binned into the filter in this step.

3.2.2.3 Subsampling and low-dimensional FFT

Based on a parameter B dividing N, a low-dimensional spectrum vector $\widehat{\boldsymbol{z}}$ is computed to estimate the original spectrum, where $\widehat{\boldsymbol{z}}$ is the rate B subsampling of $\widehat{\boldsymbol{y}}$, i.e., $\widehat{z}_j = \widehat{y}_{j\cdot(N/B)}$.

Based on the basic property of the Fourier transform: sub-sampling in the frequency domain causes aliasing in the time domain [112], $\widehat{\boldsymbol{z}}$ is the DFT of $z_i = \Sigma_{j=0}^{\omega/B-1} y_{i+Bj}$. Therefore, $\widehat{\boldsymbol{z}}$ can be obtained through subsampling the filtered signal $\boldsymbol{y}$ via B low-speed ADCs with a decimated sampling rate f_s/B, summing it up, and then computing the B-dimensional DFT.

Define the "hash function" $h_\sigma : [N] \to [B]$ that maps each of the orignal signal coordinates to one of the B "bins" in $\widehat{\boldsymbol{z}}$ as $h_\sigma(j) = \text{round}(\sigma j B/N)$, and the corresponding offset $O_\sigma : [N] \to [-N/(2B), N/(2B)]$ to be $O_\sigma(j) = \sigma j - h_\sigma(j)(N/B)$.

3.2.2.4 Location Loops

Only select the top $d \cdot k'$ coordinates $h_\sigma(j) \in [B]$ of maximum magnitude in $\widehat{\boldsymbol{z}}$ that are likely to contain large coefficients. All elements of $\widehat{\boldsymbol{y}}$ that are closest to those chosen coordinates in $\widehat{\boldsymbol{z}}$ will be selected for estimation and kept as the set J, which has the size of dkN/B. Reverse the coordinates in J to their original positions in $\widehat{\boldsymbol{x}}'$ and output this set as I_J, i.e.,

$$I_J = \{j \in [N] | h_\sigma(j) \in J\}. \tag{3.5}$$

3.2.2.5 Estimation Loops

After running $\mathcal{L} = O(logN)$ iterations of the *location loops*, the number of occurrences of each found coordinate j is counted, and only the coordinates which occurred in at least half of the location loops are kept as set I'_J. For $j \in I'_J$, $\mathcal{L}$ *estimation loops* are run

to estimate each frequency coefficient $\widehat{x}'_j$ as

$$\widehat{x}'_j = \widehat{z}_{h_\sigma(j)} \omega^{\tau j} / \widehat{F}_{O_\sigma(j)}. \tag{3.6}$$

Finally, all frequencies are estimated by taking the median value of $\widehat{x}'_j$ on multiple estimation loops.

To balance the cost of the coordinate selection and estimation step, the dimension of $\widehat{\boldsymbol{z}}$ should be selected somewhat larger than $O(k')$ [20]. Specifically, B is chosen as $B \approx \sqrt{Nk'}$ to achieve the sublinear runtime $O(logN\sqrt{Nk'logN})$, faster than FFT to compute the spectrum for current signal sparsity k' up to $O(N/logN)$.

3.2.3 Multi-channel Joint Detection

The wideband spectrum $\widehat{\boldsymbol{x}}'$ is then divided into a series of narrowband spectra $\{\widehat{\boldsymbol{x}}'[1], ..., \widehat{\boldsymbol{x}}'[M]\}$. The received signal levels over multiple frequency channels are then jointly detected, which is to determine the presence or absence of the PU in each channel.

To perform binary hypothesis testing on each channel, the signal in each channel is decoupled based on the estimated spectrum $\widehat{\boldsymbol{x}}'$. According to Parseval's Theorem [113], the signal power can be calculated by adding the squared FFT bins. Thus, the test statistics T_m of channel m is computed as

$$T_m = \frac{1}{L_m} \sum_{k=k_l^m}^{k_u^m} |\widehat{x}'_k|^2 \underset{H_0}{\overset{H_1}{\gtrless}} \lambda_n, \qquad m = 1, ..., M, \tag{3.7}$$

where L_m is the number of extracted samples taken on each channel after permutation and filtering, H_0 and H_1 denote the hypothesis PU absent and PU present respectively and λ is the threshold above which H_1 is declared.

Based on Central Limit Theorem, the test statistic T_m of channel m approximately

follows the Gaussian Distribution [43]:

$$\begin{aligned} T_m &\sim \mathcal{N}(\sigma_n^2, 2\sigma_n^4/L_m), && H_0(m) \\ T_m &\sim \mathcal{N}((1+\gamma)\sigma_n^2, 2(1+\gamma)^2\sigma_n^4/L_m), && H_1(m), \end{aligned} \tag{3.8}$$

where the channel index $m = 1, ..., M$ and γ is the received SNR at the SU.

The performance of the detection scheme can be evaluated by two metrics: probability of detection P_d and probability of false alarm P_f. P_d is the probability of correctly detecting the existence of PU on the sensing sub-channel when it is truly present and thus can be formulated as

$$P_d = P(T_m > \lambda | H_1) = Q\left(\frac{\lambda_n - \sigma_n^2(\gamma+1)}{\sigma_n^2(\gamma+1)\sqrt{\frac{2}{L_m}}}\right). \tag{3.9}$$

P_f is the probability of falsely testing that the considered channel is occupied by PU when it is actually not, and can be computed as

$$P_f = P(T_m > \lambda | H_0) = Q\left(\frac{\lambda_n - \sigma_n^2}{\sigma_n^2\sqrt{\frac{2}{L_m}}}\right), \tag{3.10}$$

where $Q(x)$ is the standard Gaussian Complementary Distribution Function (CDF).

To achieve the predefined false alarm probability P_f, the threshold λ_n in each channel is set as

$$\lambda_n = \left[\sqrt{\frac{2}{L_m}}Q^{-1}(P_f) + 1\right] \cdot \sigma_n^2, \tag{3.11}$$

where $Q^{-1}(\cdot)$ denotes the inverse complementary distribution function of the standard normal distribution.

3.2.4 Application to Real-world TVWS Signals

The proposed wideband spectrum sensing scheme is further extended to real-world TVWS signal detection, which is collected by the RFeye node located at Queen Mary University of London (QMUL) (51.523021°N 0.041592°W). The TVWS ranges from 470 to 698 MHz in North America and the bandwidth of each channel is 6 MHz, while it ranges from 470 to 790 MHz and the channel bandwidth is 8 MHz in Europe. The setting is consistent with the current bandwidth used in TV broadcasting. For a signal with a certain total bandwidth and extraction ratio, its signal size N and sparsity after the proposed permutation and filtering scheme $\kappa' = \alpha\beta N$ are constant in different channel bandwidth settings, where the available range of the extraction ratio β is determined by the signal size N and the spectrum utilization ratio α. Therefore, the proposed scheme can switch among different bandwidth settings.

In the chapter, the proposed scheme is tested in the real-world TV signals collected by the RFeye node located at Queen Mary University of London (51.523021°N 0.041592°W. As observed in Fig. 3.4, the number of channels M in TVWS is 40 and strong DVB-T signal is received at channel $\{22, 23, 25, 26, 28, 29, 30, 33\}$ in the recorded power spectrum. Thus the PU's spectrum utilization ratio is $\alpha = 20\%$.

To obtain each channel occupancy information, the proposed permutation and filtering algorithm is implemented to lower the sparsity level of the received signal before spectrum estimation via sFFT.

The time domain permutation $t \longmapsto Mt \bmod N$ is firstly applied to the input signal, which corresponds to the spectrum permutation $f \longmapsto M^{-1}f \bmod N$ in the frequency domain. The frequency components from different channels are uniformly interleaved with each other in the frequency domain after the permutation.

The signal size N equals to 819199 in Fig. 3.4. The nearest $NFFT = 2^{20} = 1,048,576$ is taken in the power of 2 to get its spectrum in sFFT. The empirical sparsity bounds

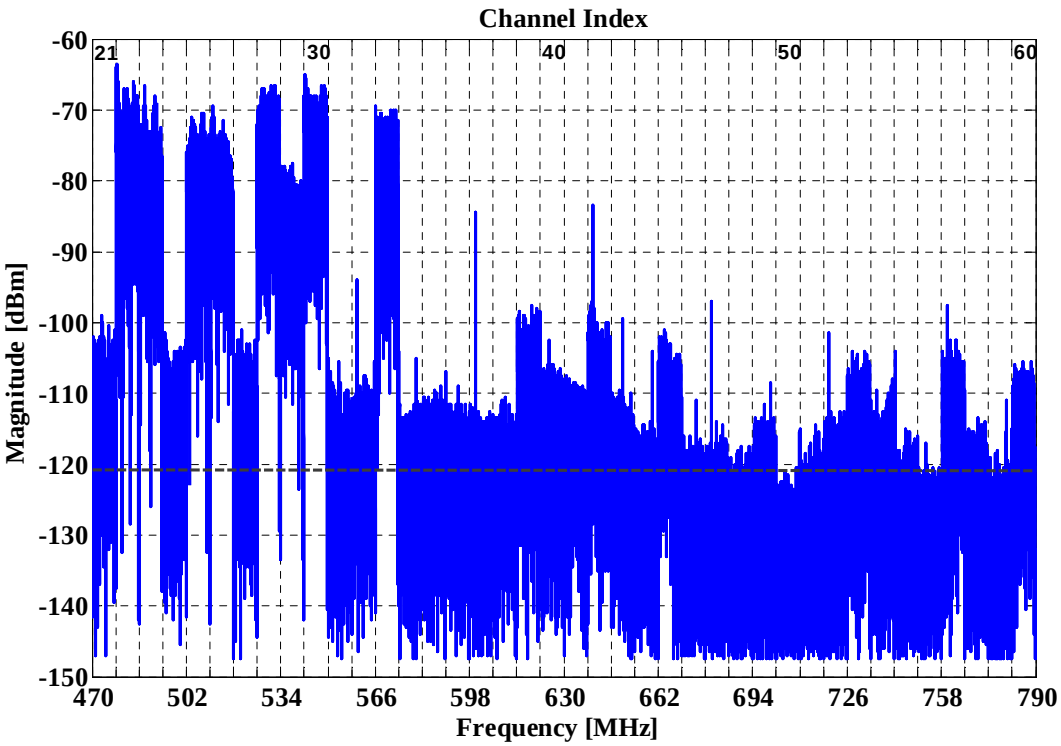

Figure 3.4: The power spectrum density (PSD) of real-time TVWS signal recorded at (51.523021°N 0.041592°W).

.

k of sFFT under 2^{20} is around 420. Thus the range of the extraction ratio β to retain faster runtime of sFFT than FFT is $\beta \leq \beta_{\max} = 0.256\%$.

Multi-channel filtering is then performed through one bandpass filter with bandwidth $B_{\text{filter}} = \beta B$ to extract the desired number of central frequencies from each channel.

Finally, the frequencies in the filter output are restored to their original places by carrying out a reverse time dilation $t \longmapsto M^{-1}t \bmod N$. The corresponding permutation and filtering in the signal spectrum under the extraction ratio $\beta = 0.25\%$ is illustrated in Fig. 3.5.

Signal spectrum is then estimated through sFFT based on its subsampling strategy with faster runtime and low hardware complexity. Based on the estimated spectrum, the presence or absence of PUs is jointly decided on multiple channels. To distinguish a channel occupied by PU signal from a spectrum hole that contains noise only signal,

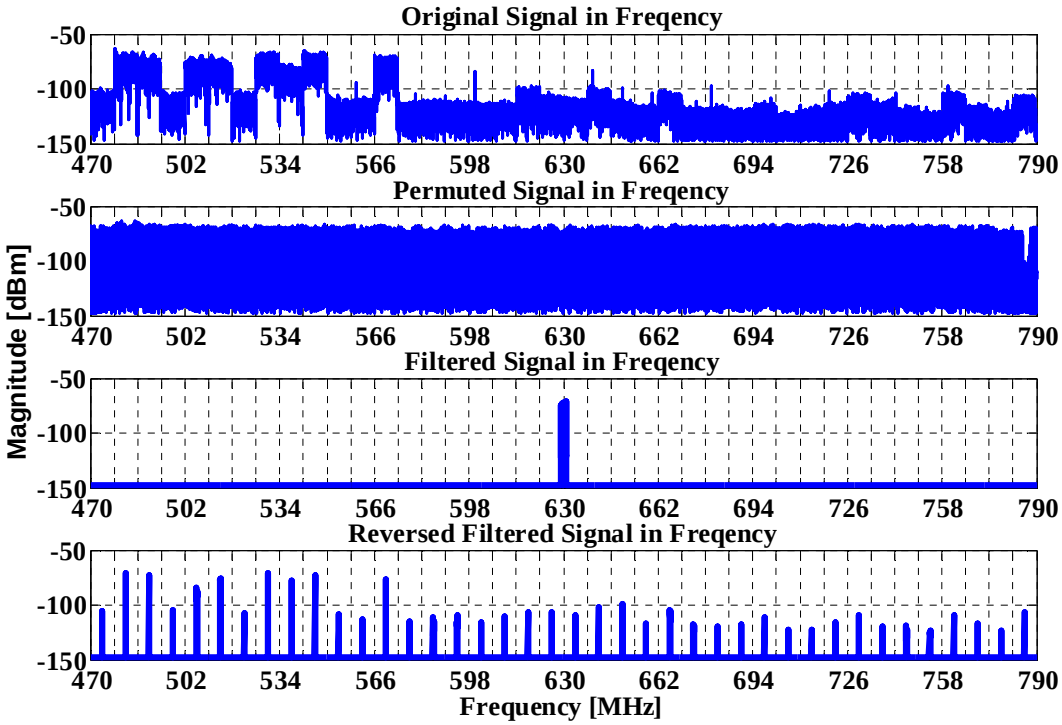

Figure 3.5: Permutation and filtering on real-world TVWS signal under $\beta = 0.25\%$.

the received signal power on each channel is computed and compared with the threshold dependent on the noise variance of the environment.

If the noise spectrum is assumed to be white, the average noise power can be estimated as

$$S_n = \frac{1}{|\mathcal{W}|} \sum_{k \in \mathcal{W}} (\widehat{x}_k)^2, \tag{3.12}$$

where $\mathcal{W}$ represent the classified noise sets containing the indices of the unoccupied spectral components. As the grey dash line in Fig. 3.4 shows, the average noise power S_n in the recorded real-time signal is -121 dBm.

However, in practice, real-time noise magnitude fluctuates with time and radio environment as the noise power is susceptible to the interference from other channels or systems and influenced by environmental factors, such as temperature. These *noise uncertainties* impose fundamental limitations on detection performance. To address this

issue, the detection threshold λ_n is set as

$$\lambda_n = S_n + \eta, \tag{3.13}$$

where η is the noise uncertainty value that reflects the upper bound for the noise power that can be reached above its estimated value S_n. Based on the historical data on the noise energy variation range in Fig. 3.4, the noise uncertainty η varies from 0 to 27 dB.

Before real-time spectrum sensing, secondary devices estimate the instantaneous noise variance through a learning process and averages the history statistics to set up the threshold. If the calculated average power of the channel of interest exceeds the corresponding threshold, a PU signal is declared to be present in that channel.

3.3 Numerical Analysis

In this section, the proposed wideband spectrum sensing scheme is evaluated using both simulated TVWS signals as well as real-time TVWS signals. The performance evaluation measures used in the comparison is also discussed.

3.3.1 Experimental Setup

Consider the incumbent PU signal that is OFDM simulated, which is used in the DVB-T signal over TVWS. The observed wideband signal ranges from 470 MHz to 790 MHz and has $M = 40$ channels in total. Each channel is 8 MHz. The spectrum utilization of the input signal is α and $S = \alpha M$ channels are occupied by PUs. The simulations intend to determine each channel occupancy status, (i.e., occupied or vacant) and to find the positions of the occupied channels.

The real-time TVWS signals are recorded by an RFeye node, an intelligent spectrum monitoring system that can provide real-time 24/7 monitoring of the radio spectrum [24].

To reduce the shadowing of the signal, the RFeye node is located on the top of the Engineering building at Queen Mary University of London (51.523021°N 0.041592°W). The view from the roof of this building, whose height is about 15 meters above ground, is unobstructed as the average clutter height of surrounding buildings is around 10 meters, as shown in Fig. 3.6. There are 40 channels (indexed as Channel 21 - Channel 60) in the recorded TVWS signal, containing either noise only or PU signal with noise on each channel, as shown in Fig. 3.4.

(a). Measurement setup at Queen Mary University of London

(b). RFeye sensing node

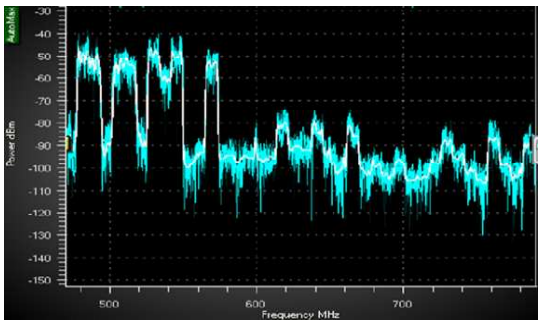

(c). Real-time TVWS signal observed by RFeye sensing node

Figure 3.6: Measurement setup for real-time TVWS signals recording at Queen Mary University of London.

The detection performance is quantified by the *detection probability* P_d, the fraction of occupied channels correctly being reported as occupied; and the *false alarm probability* P_f, the fraction of vacant channels incorrectly being reported as occupied. The target performance requirements for the sensing algorithms are $P_d \geq 90\%$ and $P_f \leq 10\%$ [114].

For spectrum estimation speed evaluation, the runtime of the sFFT is computed and compared with FFT to see the runtime reduction on different extraction ratios. The average $\mathcal{L}_1$ error is also used to compare the difference between the estimated spectrum

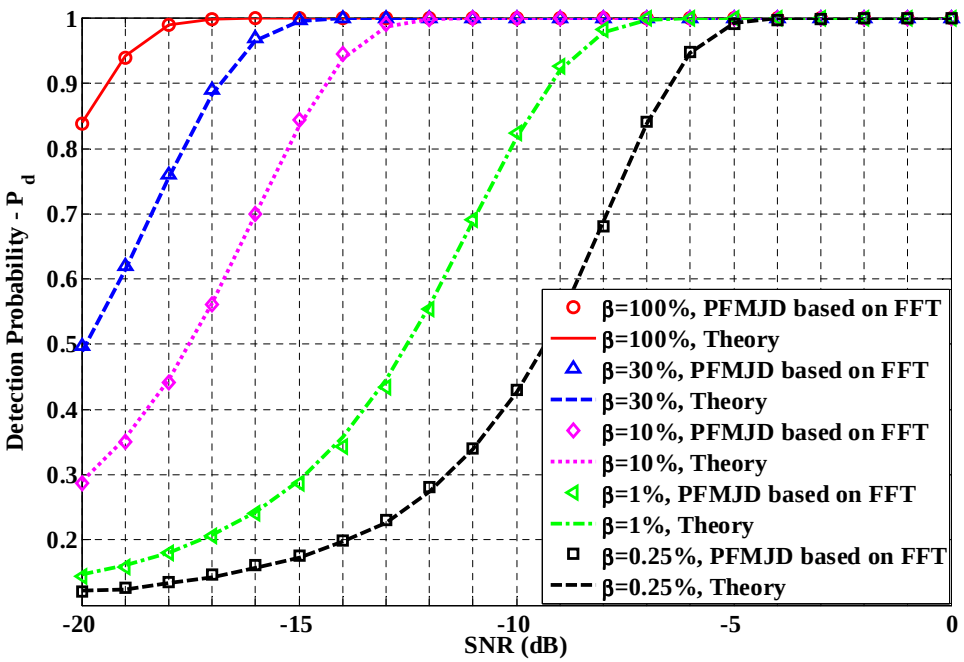

Figure 3.7: Detection probability P_d vs. SNR under different extraction ratio β with spectrum utilization $\alpha = 50\%$.

magnitudes and the original ones for evaluation of spectrum estimation accuracy.

3.3.2 Simulated TVWS Signals: analysis

Fig. 3.7 shows the detection probability P_d under different extraction ratios β with received SNR distributing from -20 dB to 0 dB. The spectrum utilization ratio α is assumed to be 50%, so 20 out of 40 channels are randomly chosen to be occupied. The input signal is processed through the proposed permutation and filtering scheme and then the conventional multiband joint detection scheme (PFMJD) based on FFT is implemented to detect each channel occupancy state. The curves in Fig. 3.7 are well matched to the theoretical results derived from (3.9), which supports the theoretical analysis of the proposed permutation and filtering design for multi-channel wideband spectrum sensing. The extraction ratio $\beta = 100\%$ corresponds to the original signal without permutation and filtering. Since the number of samples taken on each channel L_m decreases with β, the detection performance is degraded in the low SNR region, e.g.,

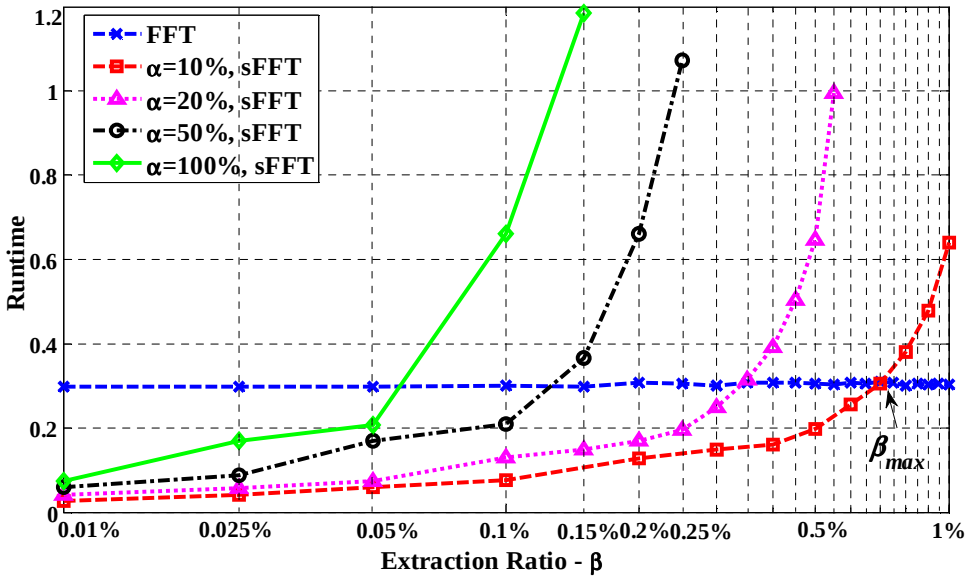

Figure 3.8: Runtime of sFFT and FFT for the permuted and filtered signal under different spectrum utilization α and extraction ratio β.

less than -5 dB.

Next, sFFT is implemented to estimate the spectrum of the permuted and filtered signal for its sub-Nyquist sampling rate and reduced runtime. To evaluate the spectrum computation speed of the proposed wideband sensing scheme based on sFFT, the conventional approach based on FFT is taken for comparison [115]. After feeding the input signal into the proposed permutation and filtering algorithm, the runtime of FFT is compared with that of sFFT. The signal size is fixed as $N = 2^{22}$, but its spectrum utilization α and extraction ratio β are varied in the simulation, thus current signal sparsity $k' = \alpha\beta N$ changes correspondingly.

Through the low extraction ratio β, sFFT can compute signal spectrum with varying spectrum utilization α. Even if the spectrum is highly occupied by PUs, i.e., high α up to 100%, the proposed algorithm can get its spectrum occupancy state using the sub-Nyquist sampling of sFFT based on the proposed permutation and filtering method. As Fig. 3.8 shows, the runtime of the proposed scheme based on sFFT is sublinear with the spectrum utilization α and extraction ratio β, while the runtime of FFT is almost constant as α or β varies. This is because the runtime of FFT is $O(N \cdot logN)$,

independent of the signal sparsity. Thus, it is more efficient to implement wideband sensing through sFFT based on the proposed permutation and filtering algorithm to achieve faster runtime. However, for a given α, as extraction ratio β increases, the number of samples taken from each channel increases. Therefore, the runtime of sFFT exceeds FFT finally as signal sparsity k' increases over sFFT sparsity bound.

Then, the detection probability P_d the proposed wideband sensing scheme based on sFFT achieved is evaluated under different SNR and P_f. Firstly, the false alarm probability P_f is fixed to 0.1 and the received SNR at the SU is varied from -20 dB to 5 dB. The spectrum utilization ratio α is set to $10\%, 20\%$ and 50%. The extraction ratio β is set to $0.15\%, 0.20\%, 0.25\%, 0.3\%, 0.35\%$. As Fig. 3.9 presents, the detection probability P_d increases as received SNR and extraction ratio β increases. For the same extraction ratio β, the proposed wideband sensing scheme based on sFFT under the proposed permutation and filtering scheme can detect the TVWS signal at comparable performance to the conventional PFMJD scheme. Moreover, the detection performance for different spectrum utilization α is almost the same under same extraction ratio β. This is because the detection probability P_d is only related to the number of samples extracted on each channel $L_m = \lfloor \beta L \rfloor$ as (3.9) shows. Comparing the results from Fig. 3.8 and Fig. 3.9, the detection performance of the proposed scheme is independent of spectrum utilization α of the input signal but the available range of $\beta_{\max}$ to retain faster runtime of sFFT shrinks as α increases.

Fig. 3.10 shows the Receiver Operating Characteristic (ROC) curve of the proposed wideband sensing scheme and the PFMJD scheme under the spectrum utilization of $\alpha = 20\%$. The SNR of the SU is set to be -5 dB and the false alarm probability P_f is varied from 0.01 to 1. As Fig. 3.10 shows, as the false alarm probability P_f increases, the detection probability P_d increases as well. The experiment result shows that the proposed wideband sensing algorithm performs almost the same as the conventional MJD scheme based on FFT under the same extraction ratio β.

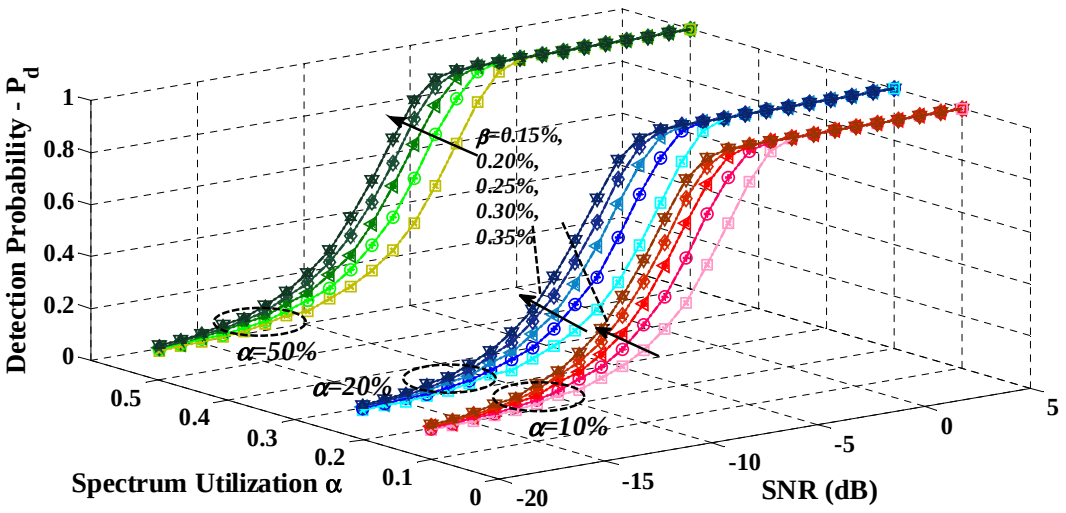

Figure 3.9: Detection probability P_d vs. SNR for the proposed sensing scheme and the conventional MJD based on FFT under different extraction ratio β with different spectrum utilization $\alpha = 10\%, 20\%, 50\%$.

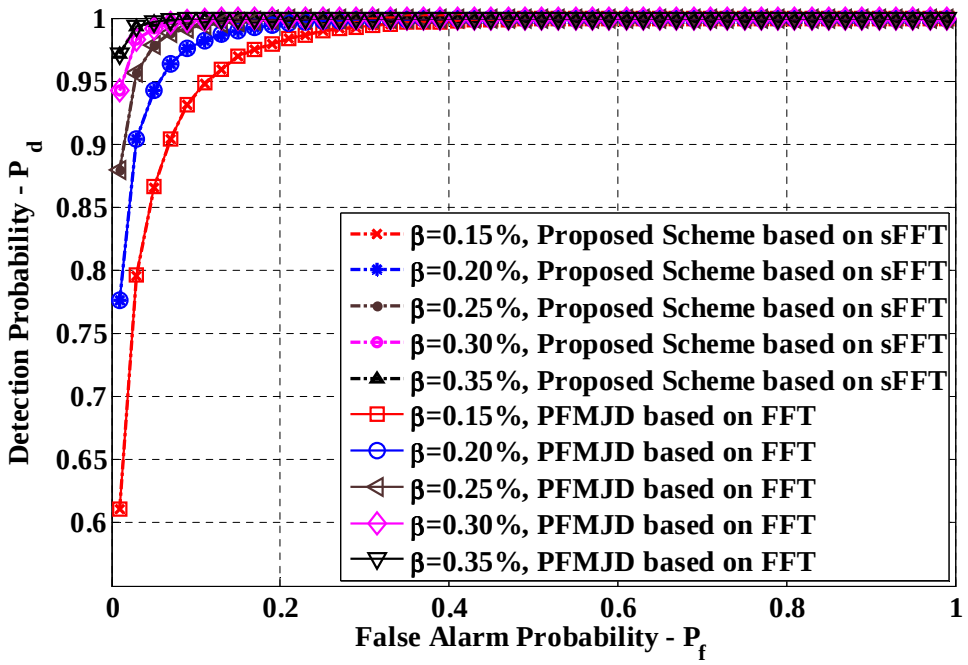

Figure 3.10: ROC curve for the proposed sensing scheme and the conventional MJD based on FFT under different extraction ratio β.

3.3.3 Real-world TVWS Signals: analysis

After the robust performance of the proposed wideband spectrum sensing scheme has been validated with simulated DVB-T signals, it is further tested on real-world TVWS signals recorded by the RFeye node, as shown in Fig. 3.4. The spectrum estimation preformation of the proposed scheme based on sFFT is compared with the original recorded real-world TVWS signals and the impact of threshold setting in (3.13) is also analysed under noise uncertainty.

The sFFT is implemented to estimate the spectrum of the input signal after the proposed permutation and filtering scheme. The difference between the estimated and original spectrum magnitude is shown with the reconstruction error of the sFFT (the average $\mathcal{L}_1$ error of the amplitude estimation). Table 3-A shows the runtime reduction from FFT and $\mathcal{L}_1$ error per large magnitude frequency estimation under different extraction ratio β when the subsampling rate is reduced to 4% of the Nyquist sampling. When extraction ratio β increases to 0.30%, the runtime of sFFT exceeds FFT as signal sparsity k' increases over sFFT's sparsity bounds.

Table 3-A: Improvements of sFFT compared with FFT with subsampling rate 4.00% under different extraction ratio β.

Extraction Ratio β	***Runtime Reduction***	$\mathcal{L}_1$ ***Error***
0.15%	34.85%	0.033
0.20%	16.67%	0.032
0.25%	6.067%	0.034
0.30%	-4.55%	0.032
0.35%	-22.73%	0.032

The comparison of the estimated and the original signal spectrum with $\beta = 0.25\%$ (Fig. 3.11) shows that the proposed scheme based on sFFT can accurately locate the positions of the high magnitude frequencies.

To evaluate the impact of threshold setting in (3.13) for the recorded real-world TVWS signals under noise uncertainty, the signal power in each channel is calculated and compared with the threshold. The noise uncertainty is varied from 0 to 27 dB, based on the historical data on the noise energy variation range. The corresponding P_d and

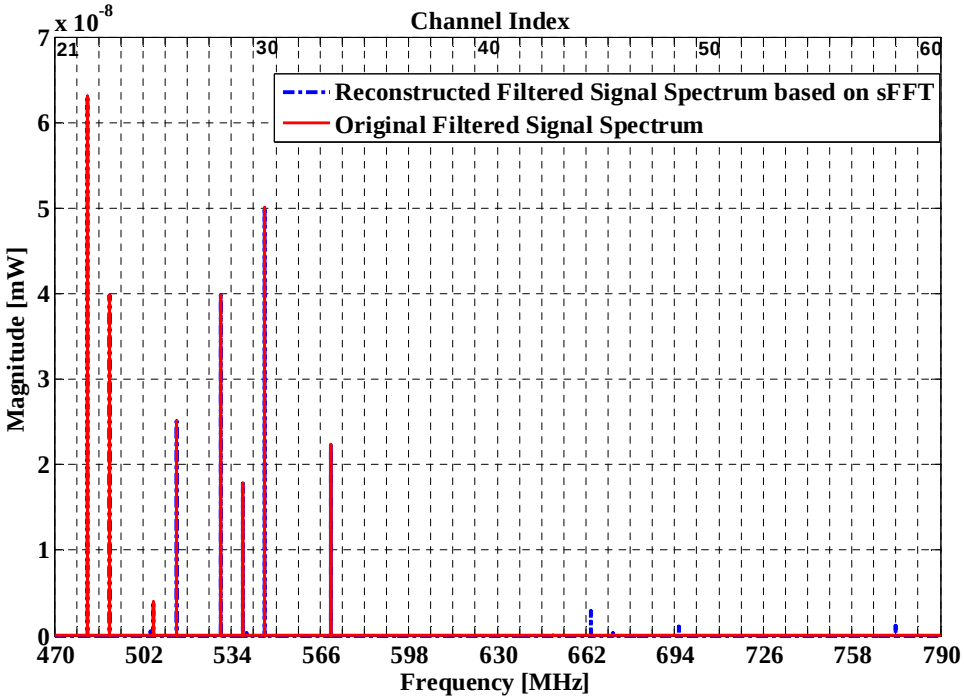

Figure 3.11: Comparison of the reconstructed and original filtered signal.

P_f are computed by comparing the experimental results with the measurement results (Fig. 3.12).

Fig. 3.12 (a) shows the detection probability P_d and false alarm probability P_f of the original real-world signal detection under noise uncertainty η. The signal power in each channel is computed based on its original spectrum without permutation and filtering and sFFT implementation. The false alarm probability P_f decreases with the increase of the noise uncertainty η (Fig. 3.12 (a)), because the narrower the margin assumed for the noise to vary over, the higher the probability that a fluctuation in the noise only signal will be falsely interpreted as a PU signal. As noise uncertainty increases, the floating range of noise increases as well. The detection performance P_d is expected to degrade with the increase of the noise uncertainty η. Since the magnitude of real-world PU signal is higher than the upper bound of the instantaneous noise power that can be reached over, P_d is constant at 100% in Fig. 3.12 (a). The predefined threshold should be larger than -112 dBm, i.e., $\eta > 9$ dB for the recorded TVWS signal to retain the target false

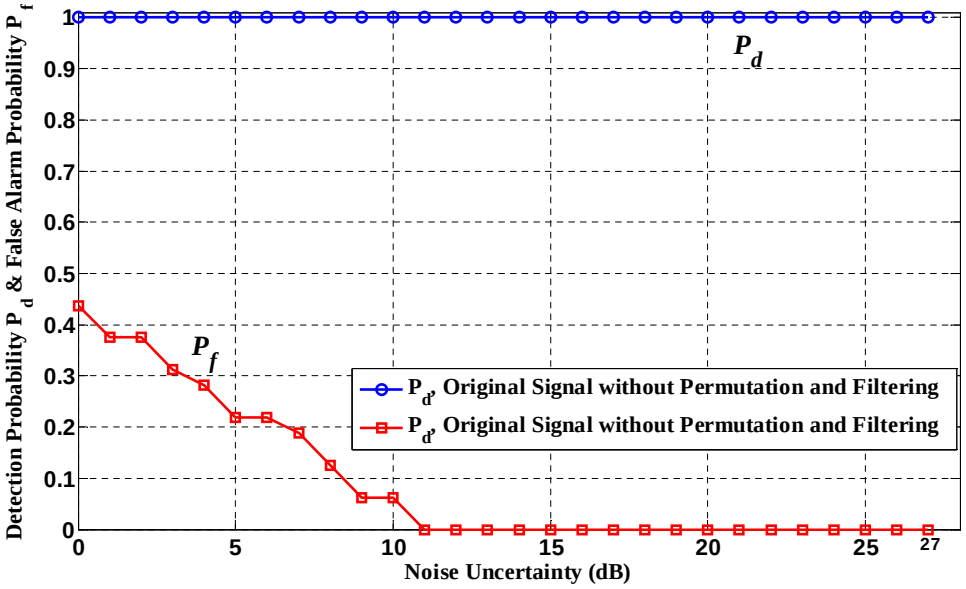

(a)

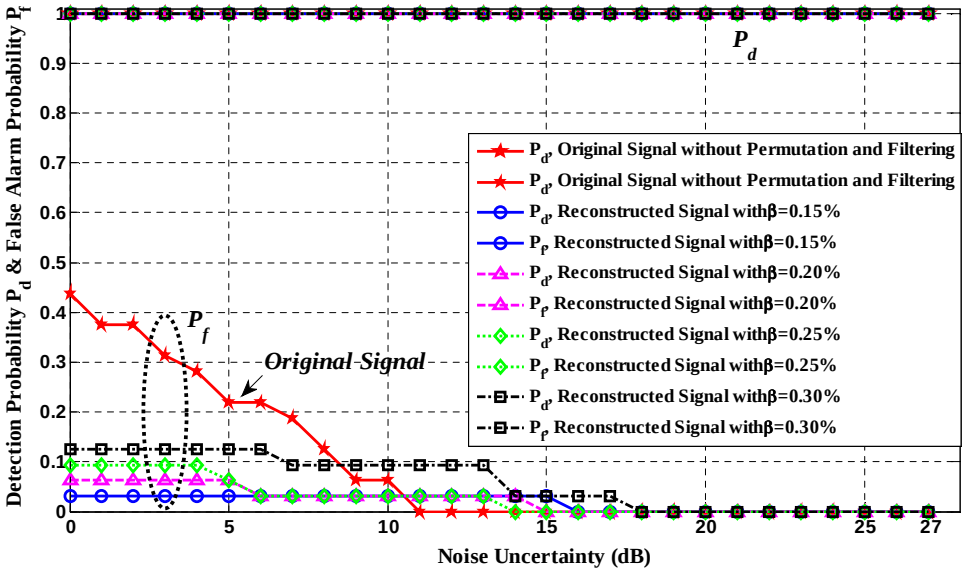

(b)

Figure 3.12: Detection probability P_d and false alarm probability P_f of (a) the original real-world signal detection under noise uncertainty η and (b) the reconstructed real-world signal detection with different extraction ratio β under noise uncertainty η.

alarm probability P_f to be less than 10%.

The detection performance of the proposed spectrum sensing scheme for the real-world signal is then evaluated under different extraction ratios β. Fig. 3.12 (b) shows the

detection probability P_d and false alarm probability P_f for the estimated signal spectrum based on sFFT with different extraction ratios β. As the number of samples retained on each channel is reduced to $L_m = \lfloor \beta L \rfloor$, the probability that the noise fluctuation exceeds the predefined threshed will decrease with such reduced number of samples. Therefore, when the noise uncertainty is less than 8 dB, the reconstructed signal under different extraction ratios achieves smaller P_f than that of the original signal. Since signal magnitudes vary randomly in each channel, the power of the extracted subset of the signal is varied randomly as well, thus influencing the corresponding detection performance. When the noise increases to 11 dB, P_f of original signal is decreased to 0%, but P_f of reconstructed spectrum is larger than original signal and will decrease to 0% until $\eta = 18$ dB. As the desired requirements of P_f should be less than 10%, the threshold setting in the original signal ($\eta > 9$ dB) is suitable to the reconstructed spectrum under different extraction ratio β.

3.4 Summary

In this chapter, an approach for wideband spectrum sensing is presented over TVWS. Based on the prior information on the number of channels and input spectrum utilization, the received signal is pre-processed through a permutation and filtering scheme that reduces signal sparsity to implement sFFT on wideband spectrum sensing. As over TVWS the power spectral density is almost flat within each channel, the extracted subset of frequency samples near the central frequency retains the corresponding channel occupancy state in each channel. The proposed scheme achieves (i) sub-Nyquist wideband sensing through permutation and filtering even when the signal is highly occupied by PUs; (ii) faster runtime and low hardware complexity; (iii) high spectrum estimation accuracy with the adopted subsampling strategy to achieve considerable detection performance as the conventional MJD scheme based on FFT at the same extraction ratio.

Chapter 4

Low-Complexity Sub-Nyquist Wideband Spectrum Sensing

In traditional sub-Nyquist wideband spectrum sensing schemes, a wideband signal or its power spectrum is first reconstructed from compressed samples, and then spectrum sensing will be performed on the reconstructed signal. In contrast to traditional sub-Nyquist approaches, this chapter proposes a sub-Nyquist wideband spectrum sensing scheme that locates occupied channels blindly by recovering the signal support, based on the jointly sparse nature of multiband signals. Exploiting the common signal support shared among multiple SUs, a cooperative spectrum sensing scheme is developed, in which the energy consumption on wideband signal acquisition, processing, and transmission is reduced with detection performance guarantee. Specifically, the related work and main contributions are firstly introduced in Section 4.1. Section 4.2 describes the proposed individual sub-Nyquist wideband spectrum sensing scheme. Based on it, Section 4.3 develops the centralized cooperative spectrum sensing scheme. Section 4.4 analyses and validates the proposed individual and cooperative schemes, over both simulated and real-world TVWS signals. Finally, Section 4.5 concludes this chapter.

4.1 Introduction

4.1.1 Related Work

Sub-Nyquist wideband spectrum sensing is a critical functionality to enable dynamic spectrum access by enhancing the opportunities of exploring spectral holes at a sampling rate lower than the Nyquist rate. Although the energy consumption at the wideband signal sampling part is reduced, random sub-Nyquist projections are hard to implement in practice. Custom ADCs with complex hardware that can perform analog mixing [54, 55] or analog matrix multiplication [51, 105] at high frequency are needed, which do not work well with low-power commodity hardware. Moreover, traditional wideband spectrum sensing based on sub-Nyquist sampling usually consists of two stages [17, 21, 23, 104, 116, 117]. That is, the wideband signal is firstly reconstructed using the sub-Nyquist samples and then spectrum sensing will be performed on the reconstructed signal. Estimating the wideband spectrum from its compressed samples is usually achieved by solving an optimization problem, which requires high computation complexity and thus still entails a major implementation challenge in compact commodity radios that only have limited energy and computation capabilities.

In [56], a multicoset sampling based wideband spectrum sensing scheme was developed, which is a nonuniform sub-Nyquist sampling technique and can be realised using an efficient multi-channel architecture. In [118], based on the particular form of the linear system of equations that describe multicoset sampling, a finite-resolution power spectral density (PSD) estimator is proposed for sub-Nyquist sampled wide-sense stationary random signals. In addition, a low-speed sub-Nyquist multicoset sampling strategy was proposed in [57] for wideband spectrum sensing. However, the knowledge of the frequency support is needed for the perfect reconstruction at the minimal sampling rate provided by the Landau's theorem [18]. To estimate the locations of the occupied channels, Feng and Bresler showed its similarity to the direction of arrival estimation in the traditional sensor array processing, and proposed to use the MUltiple SIgnal Classification (MUSIC)

algorithm for signal detection [56, 58]. However, the detection accuracy based on MUSIC algorithm degrades severely when the SNR decreases. In [119], Mishali and Eldar proposed a spectrum-blind sensing system based on multicoset sampling, which does not require knowledge of the frequency support in the sampling and recovery stages. However, the recovery performance is only analysed in the noise-free case, and the presence of wideband noise is not considered.

To overcome the SNR degeneration due to multipath fading, shadowing, and noise uncertainty over wireless channels, cooperative spectrum sensing was proposed to improve sensing reliability by exploiting the spatial diversity across multiple SUs [16], where as PUs typically transmit at much higher power levels, a common sparse spectrum support is usually perceived by all the surrounding SUs. To minimize the communication overhead for collaboration, distributed orthogonal matching pursuit (DOMP) was proposed in [120], where each SU estimates the common signal support independently based on its local compressed samples via orthogonal matching pursuit (OMP) and then the estimated supports are fused through a majority voting rule to get the final decision. Although the scheme in [120] is efficient to reduce the transmission overhead, it suffers from the disadvantage of requiring a local detector at each SU and losing certain information due to the non-optimal decision fusion. In [83], Tian proposed a distributed cooperative sensing algorithm based on compressive sensing, in which sampling statistics rather than sensing decisions are exchanged to reach a reliable global fusion. However, it increases the transmission cost and the local l_1 optimization introduces a high computation complexity. In [21], each SU implements a wideband channel division scheme to sense K out of L channels and then matrix completion is performed at a fusion centre to reconstruct the original spectrum for decision making. As SUs do not sense the whole spectrum, spatial diversity among SUs is not fully exploited and a threshold needs to be predefined to obtain the final decision.

4.1.2 Contributions

Motivated by the above challenges, this chapter first proposes an individual (working at each individual SU node) sub-Nyquist wideband spectrum sensing scheme that can locate active channels blindly, without knowing a priori spectral support of the signal before sampling and processing. The prior information required is an upper bound κ on the possible number of active channels, the maximum bandwidth $\mathcal{B}$, and the bandwidth of each channel $\mathcal{B}_0$. Thus there are up to κ out of $M = \mathcal{B}/\mathcal{B}_0$ channels occupied. Following the individual wideband spectrum sensing scheme, an efficient cooperative scheme is then proposed to reduce energy consumption on signal acquisition, processing, and transmission, with certain detection performance guarantee. The major contributions of the proposed scheme are summarized as follows:

- As compact SUs have limited energy and computational capabilities, no signal reconstruction is performed at the SUs to reduce the computation load. Each SU simply implements a multicoset sampler to subsample the wideband signal in the goal of reducing energy consumed on signal sampling. Then a low-dimensional measurement matrix is computed based on subspace decomposition to estimate the active channel locations by recovering the joint signal support of the multiband signal. Compared with the original sub-Nyquist samples, the constructed measurement matrix improves the computation efficiency. As noise distortion is reduced in the constructed measurement matrix, the detection performance is improved in the low SNR regime in comparison with the one solved by the traditional MUSIC algorithm.

- By exploiting the common signal support perceived at all SUs, simultaneous-orthogonal matching pursuit (SOMP) [93] is extended to recover the signal support by jointly fusing measurements shared among the SUs. The index that accounts for the largest residual norm among all SUs is selected in each iteration to achieve accurate detection performance. Different sampling patterns are assigned to dif-

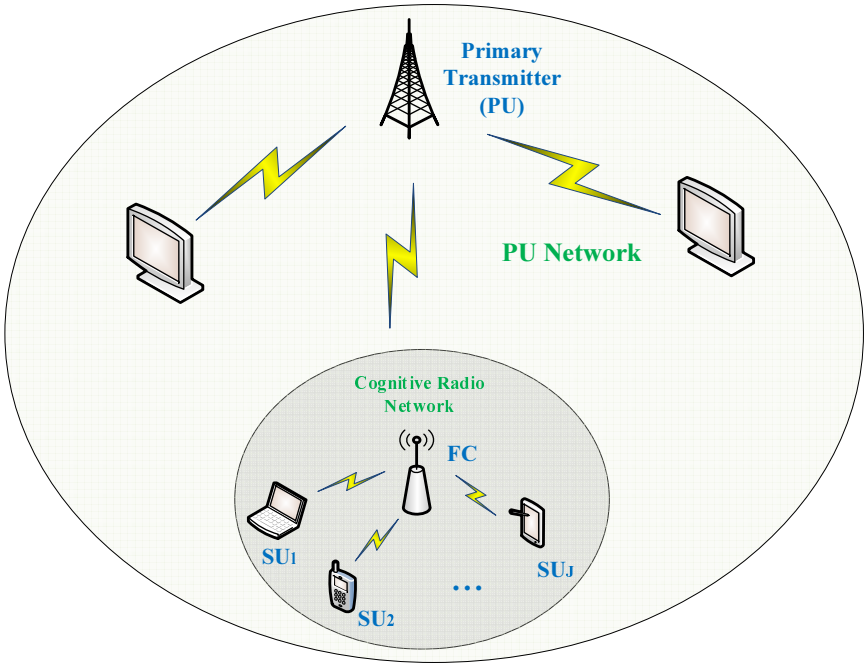

Figure 4.1: Centralized cooperative spectrum sensing model in a cognitive radio network.

ferent SUs for measurement diversity, with cooperation among SUs reducing the required number of cosets close to the active channel number, where reliable cooperative spectrum sensing is achieved at the minimal sampling rate specified by the Landau's theorem [18].

4.2 Individual Sub-Nyquist Wideband Spectrum Sensing

As shown in Fig. 4.1, this chapter investigate both the individual ($J = 1$) and cooperative ($J > 1$) wideband spectrum sensing in a cognitive radio network with a fusion centre and J SUs, which share the same spectral with a PU network. To reduce the energy consumption in high frequency signal processing, compressive multicoset sampling is applied to reduce the signal sampling and acquisition costs by exploiting the sparsity in the wireless wideband signal given the low spectrum utilization. With no prior information assumed on the band locations, blind sub-Nyquist sampling and support recovery are implemented at each individual SU to estimate the active channel locations. To fur-

ther improve the detection performance in low SNR regimes, a centralized cooperative spectrum sensing scheme will be later developed, in which soft fusion is adopted, i.e., SUs send their sampling statistics to the fusion centre, where a high-resolution global sensing decision is made. However, traditional soft fusion rules suffer from the disadvantage of large transmission overheads and high computation complexity. Thus, this chapter further aims to reduce the transmission and computation overhead by adopting a new fusion rule, without degrading the detection accuracy with cooperative spectrum sensing.

Without loss of generality, the wideband sparse spectrum to be monitored in the cognitive radio network is $\mathcal{F} = [0,\ \mathcal{B}]$, which is evenly segmented into M narrowbands, each of them with bandwidth $\mathcal{B}_0$, as illustrated in Fig. 4.2. The channels are indexed from 0 to $M-1$. Suppose there are up to κ active channels occupied by PUs during the sensing period with $\boldsymbol{\mathcal{S}} = [\mathcal{S}_1, \mathcal{S}_2, ..., \mathcal{S}_\kappa]$ denoting the set containing the indices of the occupied channels. Given the prior information on $\mathcal{B}$, $\mathcal{B}_0$, and κ, the task of wideband spectrum sensing is to find the presence and locations of the PU signals or equivalently locating the active channel set $\boldsymbol{\mathcal{S}}$.

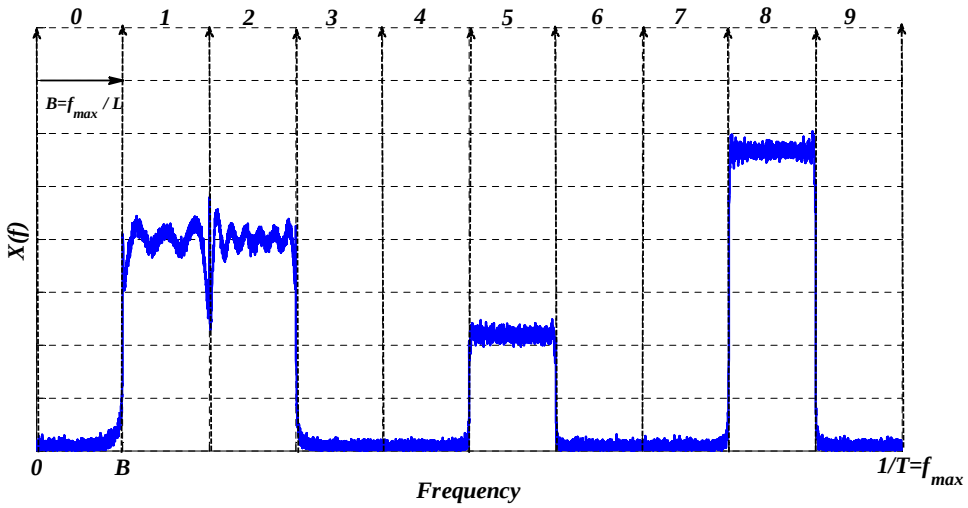

Figure 4.2: Wideband spectrum $X(f)$ with $M = 10$ and $\kappa = 4$ active channels, $\boldsymbol{\mathcal{S}} = [1, 2, 5, 8]$.

In this section, the non-cooperative blind sub-Nyquist wideband spectrum sensing

at each individual SU is first considered, i.e., $J = 1$. For convenience, the index j is dropped in this section.

4.2.1 Blind Sub-Nyquist Wideband Signal Acquisition

Given the prior information on the number of narrowband channels M, multicoset sampling is first executed at each SU by taking non-uniform samples at the time instants $t = (mM + c_i)T$, where $i = 1, ..., p,\ m \in \mathbb{Z}$, and $1/T = f_s$ is the Nyquist sampling rate. The set $\mathcal{C} = \{c_i\}_{i=1}^{p}$, which comprises of p distinct integers chosen from $\{0, 1, ..., M-1\}$, is referred as a (M, p) sampling pattern. Fig. 4.3 presents two multicoset sampling patterns for $(M, p) = (10, 4)$.

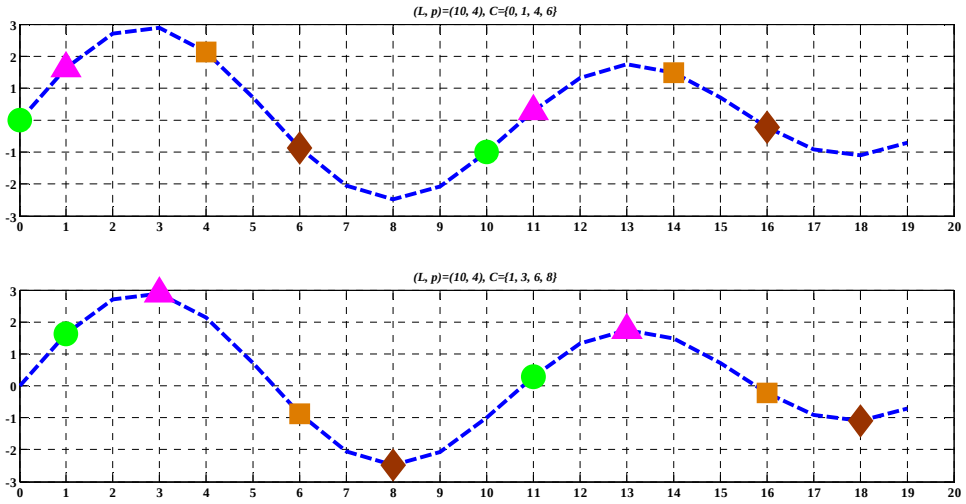

Figure 4.3: Examples of two multicoset sampling patterns for $(M, p) = (10, 4)$. (a) $C = \{0, 1, 4, 6\}$; (b) $C = \{1, 3, 6, 8\}$.

To implement the periodic non-uniform sampling, a multicoset sampler can be realized by p parallel cosets, each of which takes uniform samples at time instants $\{mMT + c_iT\},\ m \in \mathbb{Z}$, via a decimated sampling rate $\frac{1}{MT} = f_s/M$ with a sampling time offset of $\{c_iT\},\ i = 1, ..., p$, as shown in Fig. 4.4.

From the practical standpoint, the non-uniform sub-Nyquist sampling can be realized by a time-interleaved ADC, in which only a subset of channels are used. In [121, 122],

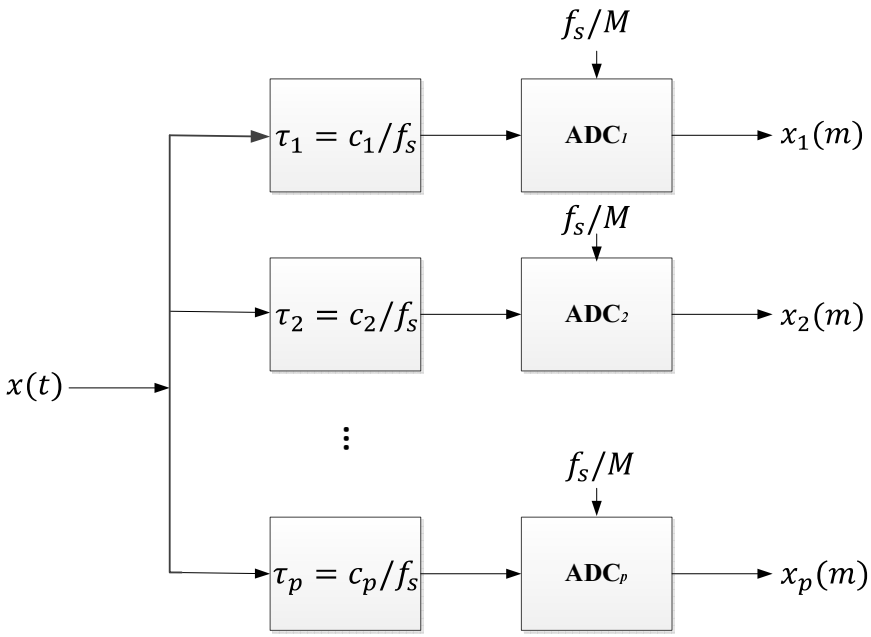

Figure 4.4: The parallel implementation of the multicoset non-uniform sub-Nyquist sampling.

efficient fabrications of time-interleaved ADC implemented as a single integrated circuit are proposed. As multicoset sampler only needs fewer channels than the time-interleaved ADC ($p \leq M$), the hardware implementation would be simpler and less power-consuming. In addition, the time offsets can be realized by connecting the antenna to different ADCs using different delay lines.

The measurement sequence of the i-th coset is defined as

$$x_{c_i}[n] = \begin{cases} x(nT), & n = mM + c_i, m \in \mathbb{Z} \\ 0, & \text{otherwise.} \end{cases} \tag{4.1}$$

In practice, the ADCs of the parallel cosets provide p sample sequences, given by

$$x_i[m] = x[(mM + c_i)T],\ m \in \mathbb{Z},\ i = 1, 2, ..., p. \tag{4.2}$$

In (4.1), each sequence $x_{c_i}[n],\ i = 1, ..., p$, contains $M - 1$ zeros in between the down-

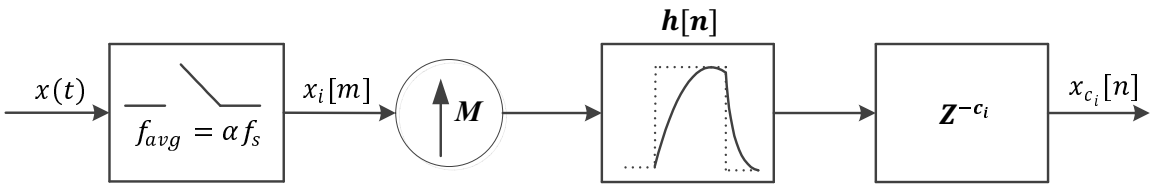

Figure 4.5: Flow chart to get the multicoset sampling measurements.

sampled signals. To get $x_{c_i}[n]$, each $x_i[m]$ is upsampled by a factor of M:

$$x_{u_i}[n] = \begin{cases} x_i[\frac{n}{M}], & n = mM,\ m \in \mathbb{Z} \\ 0, & \text{otherwise,} \end{cases} \tag{4.3}$$

and then filtered to get $x_{h_i}[n] = x_{u_i}[n] * h[n]$, where $h[n]$ is an interpolation filter with the frequency response:

$$H(f) = \begin{cases} 1, & f \in [0, \mathcal{B}_0] \\ 0, & \text{otherwise.} \end{cases} \tag{4.4}$$

The filtered sequence is then delayed with c_i samples to obtain $x_{c_i}[n]$ as

$$x_{c_i}[n] = x_{h_i}[n - c_i]. \tag{4.5}$$

The whole process to obtain the compressed measurements in multicoset sampling can be implemented as shown in Fig. 4.5 [56].

The average sampling rate of each (M, p) multicoset sampling pattern is

$$\frac{1}{T_{avg}} = \frac{p}{MT}, \tag{4.6}$$

where $\Omega = p/M$ is termed as the sub-Nyquist sampling ratio. According to the Landau's theorem [18], Ω is lower-bounded by the maximum possible spectrum occupancy ratio. However, an average sampling rate above the Landau's rate, which equals the total bandwidth of the occupied spectrum, may not be sufficient for individual blind spectrum recovery, and the number of cosets $p \geq 2\kappa$ is needed when the band locations

are unknown [119].

Applying Fourier transform to $x_{c_i}[n]$ gives the link between its spectrum $X_{c_i}(e^{j2\pi fT})$ and the unknown Fourier Transform of $x(t)$ [56]:

$$\begin{aligned} X_{c_i}(e^{j2\pi fT}) &= \textstyle\sum_{n=-\infty}^{+\infty} x_{c_i}[n] e^{-j2\pi fnT} \\ &= \tfrac{1}{MT} \textstyle\sum_{m=0}^{M-1} \underbrace{X(f + \dfrac{m}{MT})}_{X_m(f)} e^{j\frac{2\pi}{M} c_i m} \\ &= \tfrac{1}{MT} \textstyle\sum_{m=0}^{M-1} X_m(f) e^{j\frac{2\pi}{M} c_i m} \qquad \forall f \in [0, \mathcal{B}_0], \end{aligned} \tag{4.7}$$

for every $1 \leq i \leq p$, where $X_m(f),\ m = 0, ..., M-1$, corresponds to the pieces of the original spectrum $X(f)$ in the channel m, which is shifted to the left by $\frac{m}{MT}$ units such that all M channels are folded into the first narrowband $[0, \mathcal{B}_0]$.

Assume that the observed signal is given by $x(t) = s(t) + n(t)$, where $s(t)$ is the primary signal and $n(t)$ is the additive white Gaussian noise with zero mean and variance σ_n^2. The corresponding Fourier transform is given by $X(f) = S(f) + N(f)$. Define $S_m(f) = S(f + \frac{m}{MT}),\ m = 0, ..., M-1$, and $\mathbf{S}(f) = [S_0(f), S_1(f), ..., S_{M-1}(f)]^T$. Similarly we define $N_m(f)$ and $\mathbf{N}(f)$. We can rewrite (4.7) into the matrix form as

$$\begin{aligned}\underbrace{\begin{bmatrix} X_{c_1}(e^{j2\pi fT}) \\ X_{c_2}(e^{j2\pi fT}) \\ \vdots \\ X_{c_p}(e^{j2\pi fT}) \end{bmatrix}}_{\mathbf{Y}(f)} &= \underbrace{\frac{1}{MT}\begin{bmatrix} e^{\frac{j2\pi c_1 0}{M}} & e^{\frac{j2\pi c_1 1}{M}} & \cdots & e^{\frac{j2\pi c_1 (M-1)}{M}} \\ e^{\frac{j2\pi c_2 0}{M}} & e^{\frac{j2\pi c_2 1}{M}} & \cdots & e^{\frac{j2\pi c_2 (M-1)}{M}} \\ \vdots & \vdots & \vdots & \vdots \\ e^{\frac{j2\pi c_p 0}{M}} & e^{\frac{j2\pi c_p 1}{M}} & \cdots & e^{\frac{j2\pi c_p (M-1)}{M}} \end{bmatrix}}_{\mathbf{A}} \\ &\times \underbrace{\begin{bmatrix} X_0(f) \\ X_1(f) \\ \vdots \\ X_{M-1}(f) \end{bmatrix}}_{\mathbf{X}(f)} = \mathbf{A}[\mathbf{S}(f) + \mathbf{N}(f)], \quad \forall f \in [0, \mathcal{B}_0],\end{aligned} \tag{4.8}$$

where $\mathbf{Y}(f)$ is a vector of length p whose i-th element is $X_{c_i}(e^{j2\pi fT})$, $\mathbf{X}(f)$ is the unknown spectrum vectors of $x(t)$ in the M channels, i.e., $\mathbf{X}(f) = [X_0(f), X_1(f), ..., X_{M-1}(f)]^T$, and $\mathbf{A} \in \mathbb{C}^{p \times M}$ is a matrix with (i, j)-th element given by

$$\mathbf{A}_{i,j} = \frac{1}{MT} e^{j\frac{2\pi}{M} c_i (j-1)}. \tag{4.9}$$

As the parameter M in the adopted multicoset sampler is set according to the number of channels in the original spectrum, the support of the original spectrum $supp(\mathbf{S}(f))$ in (4.8) is equivalent to the active channel index set $\boldsymbol{\mathcal{S}}$. Thus in the proposed wideband spectrum sensing scheme, signal reconstruction is unnecessary and only the support of the spectrum is of interest.

4.2.2 Reliable Computation Efficient Joint Sparse Recovery

With multicoset samplers, each SU gets p sample sequences denoted as $\mathbf{Y}(f) \in \mathbb{C}^{p\times N}$, where N is the number of samples in each coset. The correlation matrix of the sampled sequence $\mathbf{Y}(f)$ is defined as

$$\mathbf{R} \triangleq \int_{f\in[0,\mathcal{B}_0]} \mathbf{Y}(f)\mathbf{Y}^H(f)\mathrm{d}f, \tag{4.10}$$

where the superscript $()^H$ denotes the Hermitian transpose. Since there is no correlation between the signal and the noise, it follows that

$$\mathbf{R} = \mathbf{A}[\mathbf{R}_s + \sigma_n^2\mathbf{I}]\mathbf{A}^H, \tag{4.11}$$

where $\mathbf{R}_s \triangleq \int_{f\in[0,\mathcal{B}_0]} \mathbf{S}(f)\mathbf{S}^H(f)\mathrm{d}f$ is the primary signal correlation matrix. Note that $\mathbf{A}$ is a sub-matrix of the complex conjugate of the $M \times M$ discrete Fourier Transform matrix (consisting of p rows indexed by the sampling pattern $\mathcal{C}$) multiplied by a factor of $\frac{1}{MT}$. It is shown that for a larger M, the randomly selected sampling pattern $\mathcal{C}$ enables the matrix $\mathbf{A}$ to have almost orthogonal rows, i.e., $< \mathbf{A}[i], \mathbf{A}[j] >= 0$ for $i \neq j$, and $< \mathbf{A}[i], \mathbf{A}[j] >= \frac{1}{MT^2}$ for $i = j$ with a high probability [50, 123]. Therefore, $\mathbf{R}$ can be derived as:

$$\mathbf{R} \approxeq \mathbf{A}\mathbf{R}_s\mathbf{A}^H + \frac{\sigma_n^2}{MT^2}\mathbf{I}, \tag{4.12}$$

From Parseval's identity [113], the correlation matrix $\hat{\mathbf{R}}$ can be computed directly from the sampled sequence $x_{c_i}[n]$ in the time domain, where $\hat{\mathbf{R}}_{ij} = \frac{1}{N}\sum_{n=1}^{N} x_{c_i}[n]x_{c_j}^H[n]$ [124]. It is shown in [125, 126] that when the number of measurement samples N is much larger than the observation dimension p, $\hat{\mathbf{R}}$ is an accurate estimator of the true correlation matrix.

Assuming the spectral bands are uncorrelated, $\mathbf{R}_s$ is a diagonal matrix whose main diagonal elements represent the power in the M spectral segments of $x(t)$, and whose off-diagonal elements are zero. Since $\mathbf{S}(f)$ is piecewise continuous in f, $[\mathbf{R}_s]_{i,i} = 0$ if and only

if $\mathbf{S}_i(f) = 0, f \in [0, \mathcal{B}_0]$. There are up to κ active channels occupied during the sensing period, thus $|I(\mathbf{R}_s)| = \kappa$. In addition, as the sampling pattern $\mathcal{C}$ is drawn uniformly at random from $\{0, 1, ..., M-1\}$, it yields a full column rank $\mathbf{A}$ with high probability [123]. Thus it follows that the rank of $\mathbf{A}\mathbf{R}_s\mathbf{A}^H$ is κ [119]. Denoting $\lambda_1 \geq \lambda_2 \geq ... \geq \lambda_p$ and $\mu_1, \mu_2, ..., \mu_p$ as the eigenvalues and corresponding eigenvectors of $\mathbf{R}$, respectively, i.e.,

$$\mathbf{R}\mu_i = \lambda_i \mu_i, \ i = 1, ..., p. \tag{4.13}$$

It then has

$$\begin{aligned} &[\mathbf{A}\mathbf{R}_s\mathbf{A}^H + \tfrac{\sigma_n^2}{MT^2}\mathbf{I}][\mu_1, ..., \mu_p] \\ &\qquad = [\mu_1, ..., \mu_p] \begin{bmatrix} \lambda_1 & & & 0 \\ & \lambda_2 & & \\ & & \ddots & \\ 0 & & & \lambda_p, \end{bmatrix}, \end{aligned} \tag{4.14}$$

i.e.,

$$\begin{aligned} &[\mathbf{A}\mathbf{R}_s\mathbf{A}^H][\mu_1, ..., \mu_p] \\ &= [\mu_1, ..., \mu_p] \begin{bmatrix} \lambda_1 - \frac{\sigma_n^2}{MT^2} & & & 0 \\ & \lambda_2 - \frac{\sigma_n^2}{MT^2} & & \\ & & \ddots & \\ 0 & & & \lambda_p - \frac{\sigma_n^2}{MT^2}, \end{bmatrix}. \end{aligned} \tag{4.15}$$

Since $\mathbf{A}\mathbf{R}_s\mathbf{A}^H$ has a rank of κ, there must be $p - \kappa$ λ_i's equal to $\frac{\sigma_n^2}{MT^2}$. As $\mathbf{A}\mathbf{R}_s\mathbf{A}^H$ is positive semidefinite, the λ_i's with values equal to $\frac{\sigma_n^2}{MT^2}$ must be the smallest ones of λ_i's. Therefore, it has

$$\lambda_{\kappa+1} = \lambda_{\kappa+2} = ... = \lambda_p = \frac{\sigma_n^2}{MT^2}. \tag{4.16}$$

As $N \to \infty$, it follows that except for the κ largest, the eigenvalues of $\mathbf{R}$ are related to the noise variance σ_n^2, as shown in Fig. 4.6.

Thus $\mathbf{R}$ can be decomposed via the rank-revealing eigenvalue decomposition (RREVD)

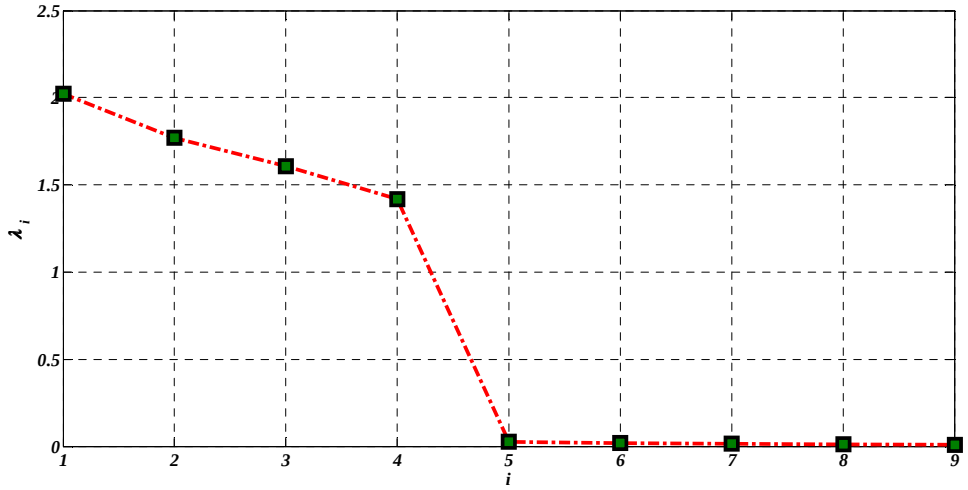

Figure 4.6: Eigenvalues of the sample correlation matrix ordered in decreasing order with $p = 9, \kappa = 4$.

as

$$\mathbf{R} = \mathbf{U}\mathbf{\Lambda}\mathbf{U}^H = \mathbf{U}_s\mathbf{\Lambda}_s\mathbf{U}_s^H + \frac{\sigma_n^2}{MT^2}\mathbf{U}_n\mathbf{U}_n^H, \tag{4.17}$$

where $\mathbf{U} = [\mathbf{U}_s, \mathbf{U}_n]$, $\mathbf{\Lambda}_s = \text{diag}\{\lambda_1, ..., \lambda_\kappa\}$ contains the κ non-increasing principal eigenvalues and $\mathbf{U}_s$ contains the corresponding eigenvectors, while $\mathbf{U}_n$ contains the corresponding eigenvectors associated with the smallest $p - \kappa$ eigenvalues $\frac{\sigma_n^2}{MT^2}$. As the noise term only perturbs the eigenvalues, the range of $\mathbf{R}$ spanned by $\mathbf{U}_s$, coincides with the signal subspace spanned by $\mathbf{AS}(f)$, and its orthogonal complement spanned by $\mathbf{U}_n$ is the noise subspace. Therefore, the κ largest eigenvalues $\mathbf{\Lambda}_s$ and the corresponding eigenvectors $\mathbf{U}_s$ are chosen to construct the measurement matrix as $\boldsymbol{\chi}_s = \mathbf{U}_s\sqrt{\mathbf{\Lambda}_s}$; so it can define the following linear system

$$\boldsymbol{\chi}_s = \mathbf{A}\boldsymbol{\nu}_s, \tag{4.18}$$

where the support of the sparest solution to (4.18) converges to the original primary signal, i.e., $supp(\boldsymbol{\nu}_s) = supp(\mathbf{S}(f))$. Moreover, using $\boldsymbol{\chi}_s \in \mathbb{C}^{p\times\kappa}$ for support recovery instead of $\mathbf{Y}(f) \in \mathbb{C}^{p\times N}$ reduces the transmission overhead and enhances the computational efficiency.

The separation between the signal and noise eigenvalues needs a threshold. Depending on the noise variance and the number of samples, the threshold could vary. To avoid

Algorithm 1 Joint sparse recovery in SA-SOMP

Require: $\mathbf{R} \in \mathbb{C}^{p\times p}$, $\hat{\kappa}$, $\mathbf{A} = [\mathbf{a}_1, ..., \mathbf{a}_M] \in \mathbb{C}^{p\times M}$
Ensure: $\boldsymbol{\mathcal{S}}$
1: $[\mathbf{U}_s, \boldsymbol{\Lambda}_s] \leftarrow \text{RREVD}(\mathbf{R}, \hat{\kappa})$, $\boldsymbol{\chi}_s = \mathbf{U}_s\sqrt{\boldsymbol{\Lambda}_s}$
2: $t = 0$, $\mathbf{R}_0 = \boldsymbol{\chi}_s$, $\boldsymbol{\nu}_0 = \varnothing$, $\boldsymbol{\mathcal{S}} = \varnothing$
3: **while** $t \leq \hat{\kappa}$ **do**
4: $t \leftarrow t + 1$
5: $m_t = \arg\max_m \parallel \mathbf{a}_m^{\mathbf{H}}\mathbf{R}_{t-1} \parallel_2$, $m \in 1, ..., M$
6: $\boldsymbol{\mathcal{S}} \leftarrow \boldsymbol{\mathcal{S}} \cup m_t$, $\boldsymbol{\nu}_t = \mathbf{A}_{\boldsymbol{\mathcal{S}}}^{\dagger}\boldsymbol{\chi}_s$
7: $\mathbf{R}_t \leftarrow \boldsymbol{\chi}_s - \mathbf{A}_{\boldsymbol{\mathcal{S}}}\boldsymbol{\nu}_t$
8: **end while**
9: **return** $\boldsymbol{\mathcal{S}}$=$\boldsymbol{\mathcal{S}}$-1

the tricky threshold setting, some information theoretic criteria for the model order selection, such as exponential fitting test (EFT) can be applied for the estimation of the signal support dimension $\hat{\kappa}$ [127].

As only κ active channels assumed to be occupied by primary transmissions, $\boldsymbol{\nu}_s$ can be approximated to be jointly κ-sparse as it contains no more than κ significant rows. Reconstruction of the unknown matrix $\boldsymbol{\nu}_s$ with jointly sparse columns in (4.18) is referred to as the multiple measurement vectors (MMV) problem, which aims to estimate the support of $\boldsymbol{\nu}_s$ from the measurement matrix $\boldsymbol{\chi}_s$. Some existing greedy algorithms for the sparse recovery problem could be extended to this joint sparse problem, such as SOMP [93]. To improve the detection robustness against noise interference and reduce the computation complexity, SOMP is applied to the constructed low-dimensional measurement matrix $\boldsymbol{\chi}_s$, denoted as subspace-augmented SOMP (SA-SOMP) in this paper. The detailed procedure of the joint sparse recovery in the proposed individual wideband spectrum sensing is summarized in Algorithm 1. In [92], Davies and Eldar analyzed "rank aware" greedy algorithms for the MMV problem, called rank-aware orthogonal matching pursuit (RA-OMP), which posses a clear advantage by exploiting the signal subspace information. The difference between RA-OMP and SA-SOMP is that RA-OMP incorporate an orthogonalization of the column space of the residual in each iteration.

4.3 Cooperative Sub-Nyquist Wideband Spectrum Sensing

As sub-Nyquist measurements are quite vulnerable to channel degradations, cooperation among multiple SUs is necessary in sub-Nyquist wideband sensing. Assume that there are J co-existing SUs within the local region that cooperatively sense the wideband to locate the active channel set $\boldsymbol{\mathcal{S}}$. The received signals at the SUs are from the same primary transmissions but affected differently by fading and shadowing from the common PU transmitter to each SU. Thus all SUs share a common sparse support with different amplitudes.

The proposed cooperative spectrum sensing scheme can be formulated into a three-step framework:

1. Each SU implements a multicoset sampler that independently samples the signal with a different sampling pattern $\mathcal{C}^{(j)}$ from the others, e.g., randomly chosen to allow for more sampling diversity.

2. Measurement matrix $\boldsymbol{\chi}_s^{(j)}$ is constructed at each SU from its sub-Nyquist samples based on subspace decomposition. Then the local matrix $\boldsymbol{\chi}_s^{(j)}$ with the sampling pattern $\mathcal{C}^{(j)}$ is transmitted to the fusion centre.

3. The fusion centre locates the active channels by jointly fusing measurements shared among the SUs to reach a global sensing decision with enhanced accuracy.

Based on the measurement matrix $\boldsymbol{\chi}_s^{(j)}$ and the sampling pattern $\mathcal{C}^{(j)}$ sent from each SU, the fusion centre computes the corresponding reconstruction matrix $\mathbf{A}^{(j)}$ and then locates the active channels by exploiting the common signal support shared by $\boldsymbol{\nu}_s^{(j)}, j = 1, \cdots, J$, across all SUs. At each SU, the following relationship holds:

$$\boldsymbol{\chi}_s^{(j)} = \mathbf{A}^{(j)} \boldsymbol{\nu}_s^{(j)},\ 1 \leq j \leq J. \tag{4.19}$$

Exploiting the common sparse support shared by the J SUs, the fusion centre fuses measurements sent from all SUs to locate the original active channels. Grouping the rows of $\boldsymbol{\nu}_s^{(j)},\ j = 1, ..., J$, with the same indices, forms the matrix $\boldsymbol{\zeta}_s$ as

$$\boldsymbol{\zeta}_s = \left[\underbrace{\boldsymbol{\nu}_s^{(1)}[1]^T \cdots \boldsymbol{\nu}_s^{(J)}[1]^T}_{\boldsymbol{\nu}_s[1]^T} \cdots \underbrace{\boldsymbol{\nu}_s^{(1)}[M]^T \cdots \boldsymbol{\nu}_s^{(J)}[M]^T}_{\boldsymbol{\nu}_s[M]^T} \right]^T, \tag{4.20}$$

where $\boldsymbol{\nu}_s^{(j)}[i]$ denotes the i-th row of $\boldsymbol{\nu}_s^{(j)}$ at the j-th SU. Furthermore, $\boldsymbol{\zeta}_s$ can be partitioned as a concatenation of blocks $\boldsymbol{\nu}_s[m]^T,\ m = 1, ..., M$, and the block size is equal to the number of SUs J. As there are at most κ channels occupied, $\boldsymbol{\zeta}_s$ can be modelled as a block κ-sparse matrix. Thus, in each iteration, the block index that accounts for the largest residual norm among all SUs is selected, i.e.,

$$m_t = \arg\max_m \sum_{j=1}^{J} \parallel \mathbf{a}_m^{(j)\mathbf{H}} \mathbf{R}_{t-1}^{(j)} \parallel_2,\ m \in 1, ..., M, \tag{4.21}$$

where $\mathbf{R}_{t-1}^{(j)}$ is the residue at the $(t-1)$-th iteration at the j-th SU, $\mathbf{a}_m^{(j)}$ is the m-th column in $\mathbf{A}^{(j)}$, and m_t is the selected index. The detailed algorithm for the proposed joint support recovery at the fusion centre is described in Algorithm 2, where each SU implements EFT to estimate the signal sparsity $\hat{\kappa}^{(j)}$, and then the fusion centre takes the average $\hat{\kappa}$, i.e.,

$$\hat{\kappa} = \frac{1}{J} \sum_{j=1}^{J} \hat{\kappa}^{(j)}, \tag{4.22}$$

for the number of iterations at the joint support recovery in Algorithm 2.

Based on the measurements shared among the SUs, the detection performance is improved in low SNR regimes. Moreover, thanks to the measurement diversity across multiple SUs given the different sampling patterns, the fusion centre could obtain an accurate estimate of the occupied channel locations at the sampling rate approaching the Landau's rate as the number of SUs increases, as shown in Fig. 4.15. This is due to

Algorithm 2 Measurement fusion in the proposed centralized cooperative spectrum sensing scheme

Require: $\boldsymbol{\chi}_s^{(j)} \in \mathbb{C}^{p\times\hat{\kappa}^{(j)}}$, $\hat{\kappa}^{(j)}$, $\mathbf{A}^{(j)} = [\mathbf{a}_1^{(j)}, ..., \mathbf{a}_M^{(j)}] \in \mathbb{C}^{p\times M}$
Ensure: $\boldsymbol{\mathcal{S}}$
1: $\hat{\kappa} = \frac{1}{J}\sum_{j=1}^{J}\hat{\kappa}^{(j)}$
2: $t = 0$, $\mathbf{R}_0^{(j)} = \boldsymbol{\chi}_s^{(j)}$, $\boldsymbol{\nu}_0^{(j)} = \varnothing$, $\boldsymbol{\mathcal{S}} = \varnothing$
3: **while** $t \leq \hat{\kappa}$ **do**
4: $t \leftarrow t + 1$
5: $m_t = \arg\max_{m} \sum_{j=1}^{J} \parallel \mathbf{a}_m^{(j)\mathbf{H}}\mathbf{R}_{t-1}^{(j)} \parallel_2,\ m \in 1, ..., M$
6: $\boldsymbol{\mathcal{S}} \leftarrow \boldsymbol{\mathcal{S}} \cup m_t$, $\boldsymbol{\nu}_t^{(j)} = \mathbf{A}_{\boldsymbol{\mathcal{S}}}^{(j)\dagger}\boldsymbol{\chi}_s^{(j)}$
7: $\mathbf{R}_t^{(j)} \leftarrow \boldsymbol{\chi}_s^{(j)} - \mathbf{A}_{\boldsymbol{\mathcal{S}}}^{(j)}\boldsymbol{\nu}_t^{(j)}$
8: **end while**
9: **return** $\boldsymbol{\mathcal{S}} = \boldsymbol{\mathcal{S}} - 1$

the fact that the sub-coherence within the block,

$$\mu = \max_{1\leq m\leq M}\Big(\max_{1\leq i\neq j\leq J} ||a_m^{(i)H}a_m^{(j)}||\Big), \tag{4.23}$$

is substantially smaller than the conventional coherence in the equivalent reconstruction matrix $\mathbf{A}$ [128]. Reconstruction of the block sparse signal in the cooperative sensing scheme therefore can be guaranteed with an eased requirement comparing to the reconstruction in the individual scheme. Therefore, a small number of cosets p proportional to the signal sparsity κ is sufficient for cooperative spectrum sensing. The computation complexity of support recovery at the fusion centre could be expressed as $O(\kappa^3 MJ)$.

4.4 Numerical Analysis

This section provides simulation results to evaluate the proposed wideband spectrum sensing scheme using both simulated signals and real-world TVWS signals. The simulation setup and relevant performance evaluation measures are firstly described, and then the obtained results are analysed and discussed.

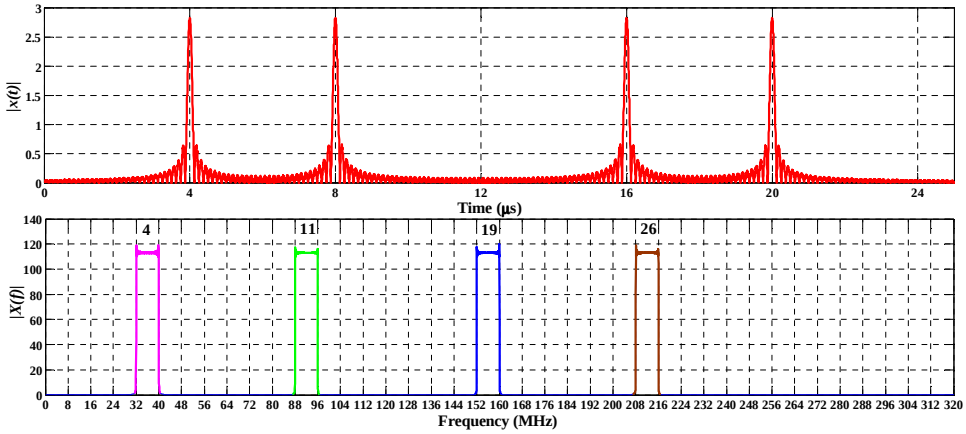

Figure 4.7: Simulated signal illustration in time and frequency domains, with $M = 40$, $\kappa = 4$ and $\boldsymbol{\mathcal{S}} = [4, 11, 19, 26]$.

4.4.1 Experimental Setup and Performance Measures

Consider the received signal $x(t) \in \mathcal{F} = [0, 320]$ MHz containing $M = 40$ channels of equal bandwidth $\mathcal{B}_0 = 8$ MHz and up to $\kappa \leq M$ active channels. The simulated signal is generated as

$$x(t) = \sum_{i=1}^{\kappa} \sqrt{E_i \mathcal{B}_0} \text{sinc}(\mathcal{B}_0(t - t_i)) e^{j2\pi f_i t} + n(t), \tag{4.24}$$

where $\text{sinc}(x) = \sin(\pi x)/(\pi x)$, E_i, t_i, and f_i define the energy, time offset, and carrier frequency respectively, on each active channel, and $n(t) \sim \mathcal{N}(0, \sigma_n^2)$ is the additive white Gaussian noise. Thus the spectrum occupancy ratio of primary transmissions can be expressed as $\alpha = \kappa/M$. The signal is observed on a time frame of $T = 25.6$ μs starting at $t = 0$, which corresponds to $T \cdot 320 \cdot 10^6 = 8192$ Nyquist rate samples. Fig. 4.7 depicts one example of the signal with $\kappa = 4$ active channels, i.e., $\alpha = 10\%$. In this example, $E_i = \{1, 1, 1, 1\}$, $t_i = \{4, 8, 16, 20\}$ μs and the spectrum support is centred at $f_i = \{36, 92, 156, 212\}$ MHz. Thus the active channel set is $\boldsymbol{\mathcal{S}} = [4, 11, 19, 26]$.

The real-time TVWS signals are recorded by an RFeye node, an intelligent spectrum monitoring system that can provide real-time 24/7 monitoring of the radio spectrum [24]. The RFeye node is located at (51.523021°N, 0.041592°W), and the height is about 15 meters above the ground, as shown in Fig. 3.6. There are 40 channels (indexed as

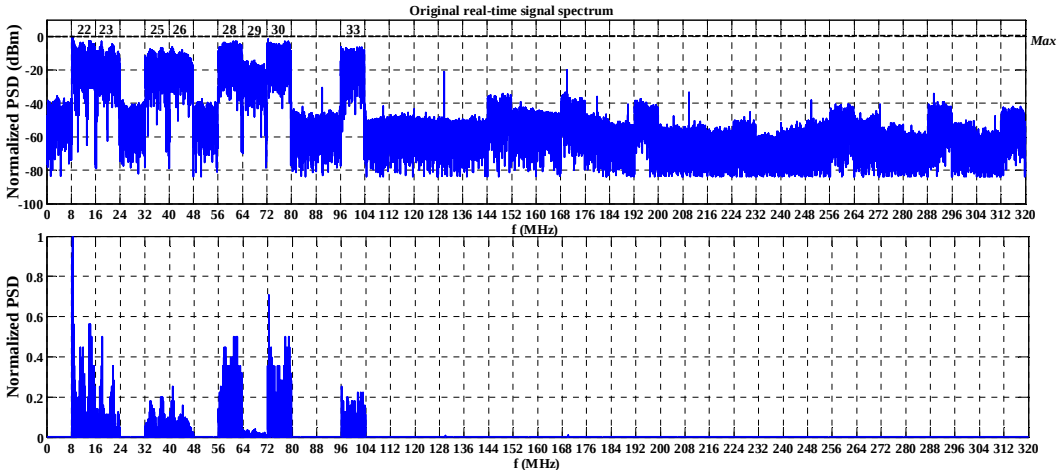

Figure 4.8: Normalized power spectrum density (PSD) of the real-time TVWS signal recorded at QMUL, $\boldsymbol{\mathcal{S}} = [22, 23, 25, 26, 28, 29, 30, 33]$.

Channel 21 - Channel 60) in the recorded TVWS signal, ranging from 470 to 790 MHz and each channel contains either noise only or PU signal with noise. Fig. 4.8 shows the normalized downconverted TVWS signal in the baseband $\mathcal{F} = [0, 320]$ MHz. Strong DVB-T signal reception at channel set $\boldsymbol{\mathcal{S}} = [22, 23, 25, 26, 28, 29, 30, 33]$ can be observed in the recorded spectrum. Thus the spectrum occupancy ratio is $\alpha = 20\%$.

To quantify the detection performance, the detection probability P_d, i.e., the fraction of occupied channels correctly being reported as occupied, is computed. The estimated active channel set $\hat{\boldsymbol{\mathcal{S}}}$ is compared against the original signal support $\boldsymbol{\mathcal{S}}$ to calculate the detection probability under 2000 trials.

Once the signal support is recovered, reconstruction of the sparse signal has a closed-form solution. Based on the estimated signal support $\hat{\boldsymbol{\mathcal{S}}}$ and the sample sequence $x_{c_i}[n]$, the reconstruction formula can be expressed as

$$x_r[n] = \sum_{q=1}^{\hat{\kappa}} \sum_{i=1}^{p} [\mathbf{A}^{\dagger}_{\hat{\boldsymbol{\mathcal{S}}}+1}]_{i,q} x_{c_i}[n] e^{\frac{j2\pi \hat{\mathcal{S}}_q n}{M}}, \tag{4.25}$$

where $x_r[n]$ is the reconstruction signal and $\hat{\kappa}$ is the estimated signal sparsity. The accuracy of the reconstructed signal is evaluated by the relative reconstruction mean

squared error (MSE) compared with the original signal, which is defined as

$$MSE = \frac{||x_r[n] - x[n]||}{||x[n]||}. \tag{4.26}$$

4.4.2 Individual Sub-Nyquist Wideband Spectrum Sensing

To reduce the computation complexity with good noise robustness, subspace decomposition is applied at each SU to derive the measurement matrix $\boldsymbol{\chi}_s$ based on the local sub-Nyquist samples. In this section, the detection performance of the proposed scheme based on SA-SOMP is compared with the one with the MUSIC algorithm, which was proposed in [56] for sparse support recovery with multicoset sampling. The location of the active channels is recovered according to MUSIC algorithm as

$$P_{MU}(m) = \frac{1}{||\mathbf{a}_m \mathbf{U}_n||^2}, 0 \leq m \leq M-1. \tag{4.27}$$

If m is an active channel index, $P_{MU}(m)$ is significant in that point. The estimated active channel set $\hat{\boldsymbol{\mathcal{S}}}$ is determined by choosing the position of the first κ largest values.

The impact of system parameters, such as the SNR, the sub-Nyquist sampling ratio, and the channel occupancy ratio, are also investigated in this section.

4.4.2.1 Spectrum Sensing Performance versus SNR

Fig. 4.9 shows the detection probability P_d with respect to received SNR ranging from -5 dB to 20 dB. The channel occupancy ratio α is assumed to be 10%, such that 4 out of 40 channels are randomly chosen to be occupied. Multicoset samplers with $p = 10, 15, 20$ are used to sample the received signal, corresponding to the sub-Nyquist sampling ratios of $\Omega = p/M = 25\%, 37.5\%, 50\%$. The p integers of each sampling pattern $\mathcal{C}$ are selected randomly out of M. It is shown in Fig. 4.9 that the performance of the proposed SA-SOMP scheme is superior to that with the MUSIC algorithm, and improves

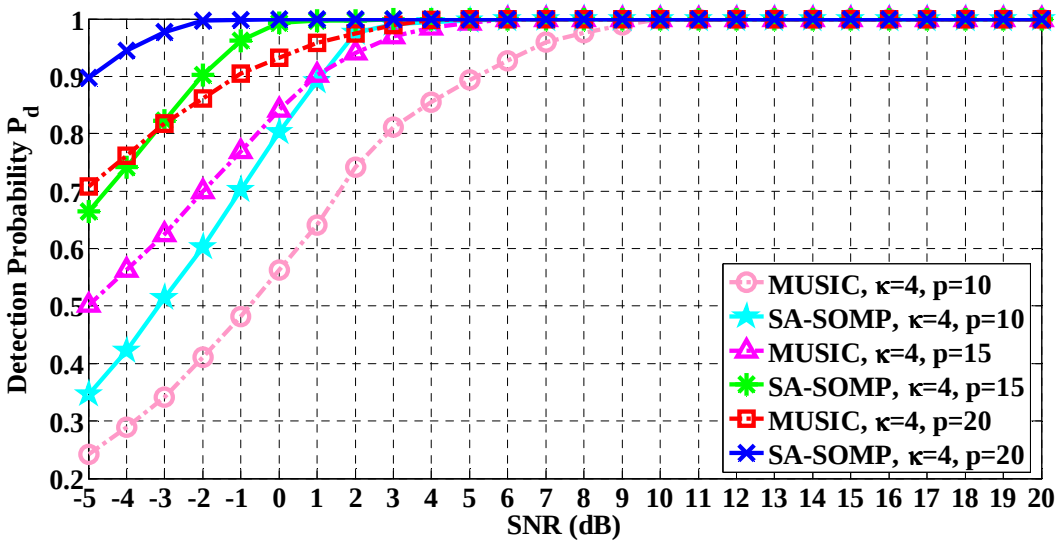

Figure 4.9: Detection Probability P_d vs. varying SNR values under different sub-Nyquist sampling ratios $\Omega = p/M$ with $\kappa = 4$.

monotonically as SNR increases.

4.4.2.2 Spectrum Sensing Performance versus sub-Nyquist Sampling Ratio

Fig. 4.10 depicts the reconstructed signal in time and frequency with $p = 15$. Thus the sub-Nyquist sampling ratio is $\Omega = p/M = 37.5\%$. Compared with original signal shown in Fig. 4.7, the reconstruction MSE is computed to be 2.7%.

To show the relationship between the detection performance and the sub-Nyquist sampling ratio Ω, P_d is plotted against p in Fig. 4.11. The channel occupancy ratio α is still assumed to be 10% ($\kappa = 4$). When the number of cosets p is greater than the number of occupied channels κ only by one, i.e., $\Omega = 12.5\%$, it yields a poor support recovery at individual SUs, thus resulting in a low detection probability. As the number of cosets increases to $p \geq 2\kappa$, better detection performance is achieved, increasing P_d close to 1 under SNR = 5 dB when $p = 10$ for the proposed scheme and outperforming that with the MUSIC algorithm. At SNR = -5 dB, a high detection probability ($P_d \geq 0.9$) is achieved when p increases above 20 ($\Omega = 50\%$) in the proposed scheme, while MUSIC needs more cosets at $p = 30$ ($\Omega = 75\%$).

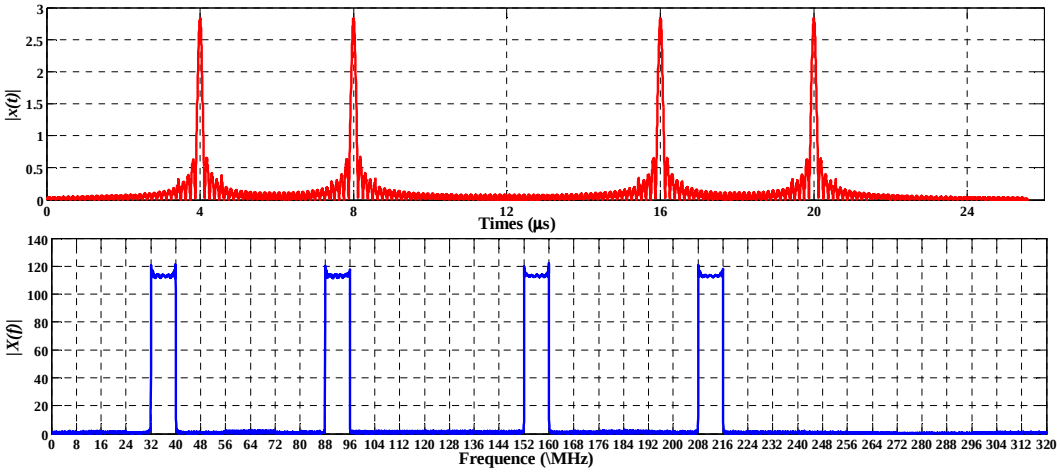

Figure 4.10: Reconstructed signal in the time and frequency domains with $p = 15$. The relative reconstruction MSE compared with the original signal in Fig. 4.7 is 2.7%.

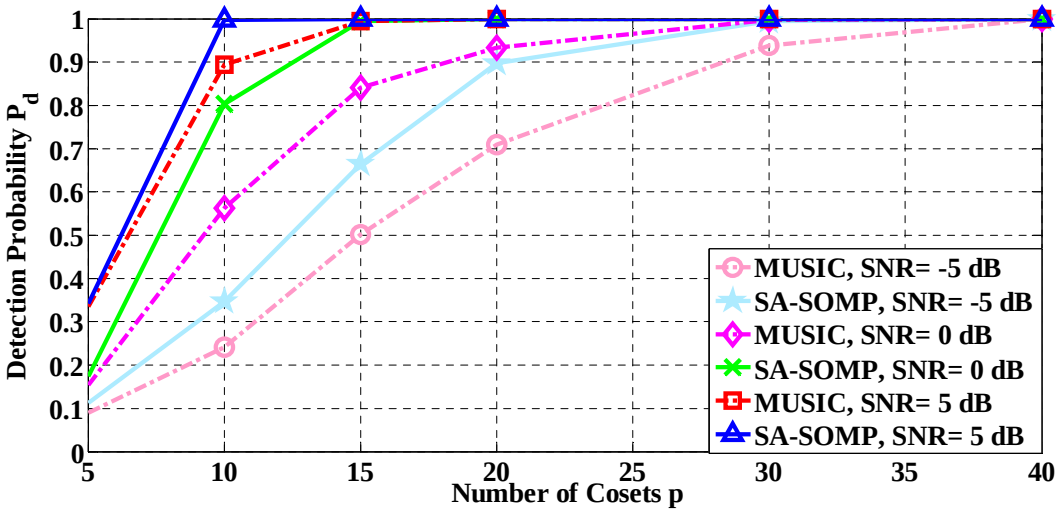

Figure 4.11: Detection Probability P_d vs. number of cosets p under different SNR values with $\kappa = 4$, $\Omega = p/M$.

4.4.2.3 Spectrum Sensing Performance versus Spectrum Occupancy Ratio

Fig. 4.12 shows the detection performance of the proposed spectrum sensing scheme with different numbers of active channels κ. A multicoset sampler with $p = 20$ is used, such that the sub-Nyquist sampling ratio is $\Omega = 50\%$. The number of active channels κ varies from 4, 8 to 12 and their positions are randomly selected out of $M = 40$ channels. As Fig. 4.12 shows, the detection performance degrades as the number of active channels

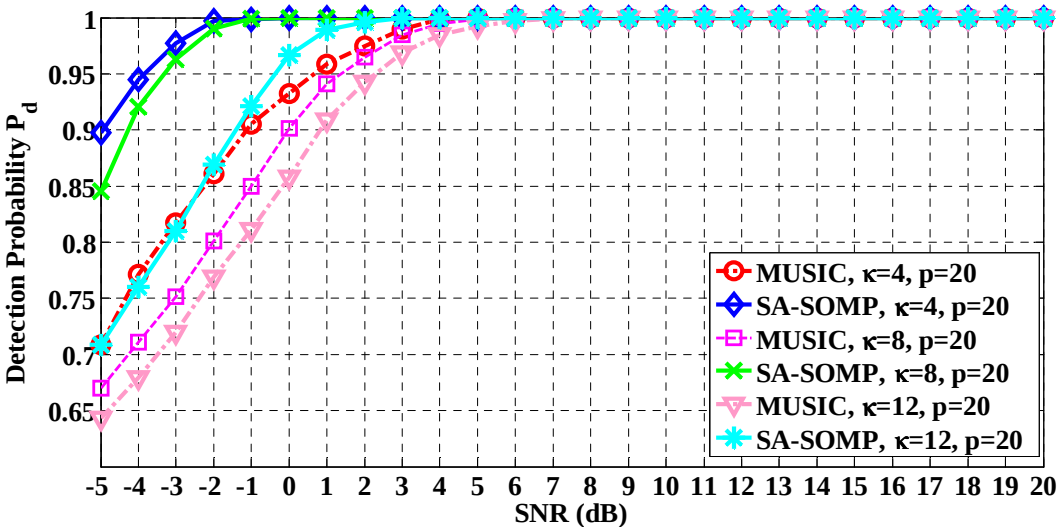

Figure 4.12: Detection Probability P_d vs. varying SNR values for different numbers of active channels κ with $p = 20$ ($\Omega = 50\%$).

increases, which indicates that more samples should be collected for signal reconstruction to ensure that the detection performance is not degraded as the channel occupancy ratio α increases.

4.4.3 Cooperative Sub-Nyquist Wideband Spectrum Sensing

In this section, the performance of the proposed cooperative wideband spectrum sensing scheme is compared with several other cooperative schemes in terms of transmission and computation complexity and detection accuracy. The impacts of the sub-Nyquist sampling ratio and the number of cooperative SUs on cooperative spectrum sensing are also analysed.

4.4.3.1 Performance Comparison against SOMP and DOMP

To analyse the efficiency of the proposed scheme in terms of transmission overhead and local/fusion computation complexity, the proposed algorithm is compared with two extreme cases: performing OMP at each SU independently and then fusing the estimated supports via majority rule (termed DOMP), and transmitting the original sub-Nyquist

Table 4-A: Comparison of complexity of the proposed cooperative recovery scheme with SOMP and DOMP.

Approach	*Transmission Overhead*	*Local Computation Complexity*	*Global Computation Complexity*
SA-SOMP	$O(\kappa^2)$	$O(\kappa^2 N + \kappa^3)$	$O(\kappa^3 MJ)$
SOMP	$O(\kappa N)$	–	$O(\kappa^2 NMJ)$
DOMP	$O(\kappa)$	$O(\kappa^2 NM)$	$O(\kappa J log J)$

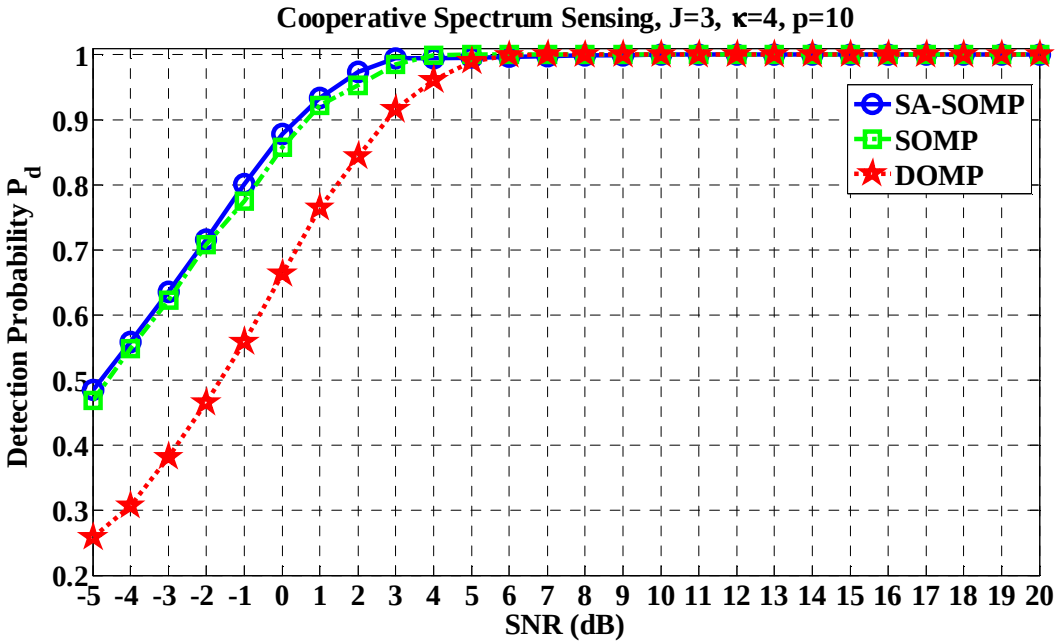

Figure 4.13: Global detection probability P_d vs. varying SNR values.

samples and then jointly recovering signal support based on SOMP (termed SOMP), as shown in Table 4-A. Fig. 4.13 presents the detection performance of the three schemes. Although DOMP has the minimum transmission overhead, its detection performance is the worst. Compared with SOMP, the proposed scheme achieves comparable detection performance with lower transmission overhead and computation complexity, due to the subspace decomposition.

4.4.3.2 Spectrum Sensing Performance versus Number of SUs and Sub-Nyquist Sampling Ratio

Fig. 4.14 shows the global detection probability P_d of the proposed cooperative spectrum sensing scheme with different numbers of SUs. It is observed that the detection

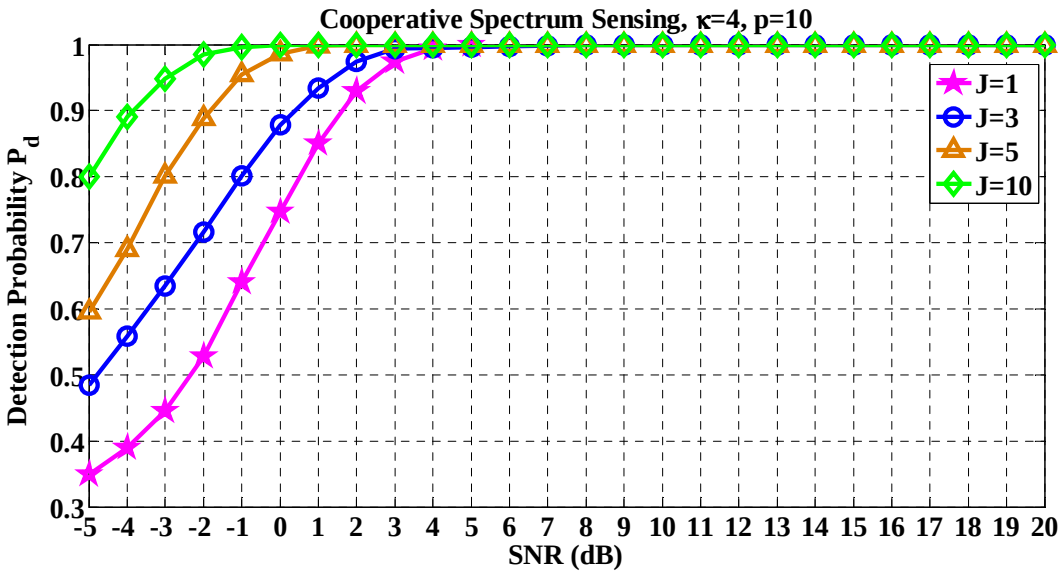

Figure 4.14: Global detection probability P_d vs. varying SNR values with different numbers of SUs, $\kappa = 4$ and $p = 10$ ($\Omega = 25\%$).

performance is improved as the number of cooperative SUs increases. This is because as more SUs joints, measurements shared among SUs make the wideband sensing more accurate. By incorporating the observations from multiple SUs, it is possible to achieve the desired detection performance even at low SNR levels. For the desired detection performance, e.g., $P_d \geq 0.9$, individual spectrum sensing ($J = 1$) requires SNR = 2 dB under sub-Nyquist sampling ratio $\Omega = 25\%$ ($p = 10$), while the collaboration of 10 SUs can achieve it at SNR = -4 dB.

For the same wideband signal, Fig. 4.15 shows the global detection performance when the number of cosets at each SU reduces to $p = 5$. As p is greater than the number of occupied channels κ only by one, individual sensing ($J = 1$) yields poor detection performance even in the high SNR region. Based on measurements fusion among multiple SUs, cooperative spectrum sensing can improve the detection performance as the number of joint SUs J increases. As the value of SNR increases, SU cooperation could achieve highly reliable detection at the minimal sampling rate provided by the Landau's theorem [18], such that a lower number of cosets p is required at each SU.

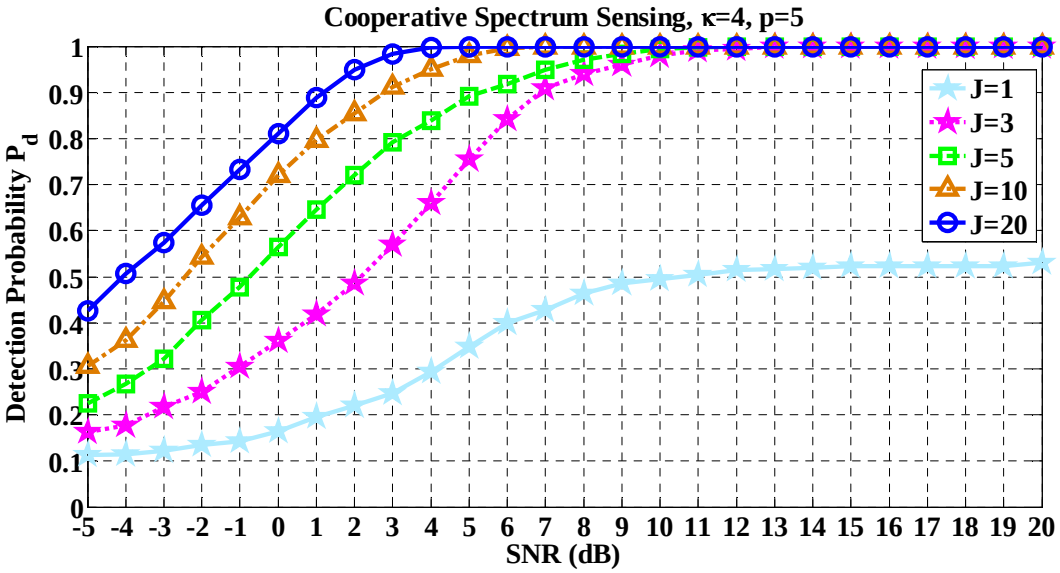

Figure 4.15: Global detection probability P_d vs. varying SNR values with different numbers of SUs, $\kappa = 4$ and $p = 5$ ($\Omega = 12.5\%$).

4.4.4 Real-world TVWS Signal Analysis

After the robust performance of the proposed sub-Nyquist wideband spectrum sensing schemes have been validated with simulated signals under individual and cooperative sensing setups, it is further tested over real-world TVWS signals collected by the RFeye sensing node installed in our lab as shown in Fig. 3.6.

To obtain the channel occupancy information over the real-world TVWS signals, a multicoset sampler is firstly applied to subsample the time domain signal, and then the signal support is recovered to estimate the active channel set. Compared with conventional energy detection, which needs to compute the received signal power at each channel and then compare the power against the predefined threshold from the historical statistics to distinguish between the channel occupied by PU signals and a spectrum hole, the proposed wideband spectrum sensing scheme does not require knowledge of the spectrum information either at the sampling stage or at reconstruction stage; thus the computation and implementation complexity is reduced. In addition, the blind signal support estimation directly obtains the positions of the active channels. Once the signal

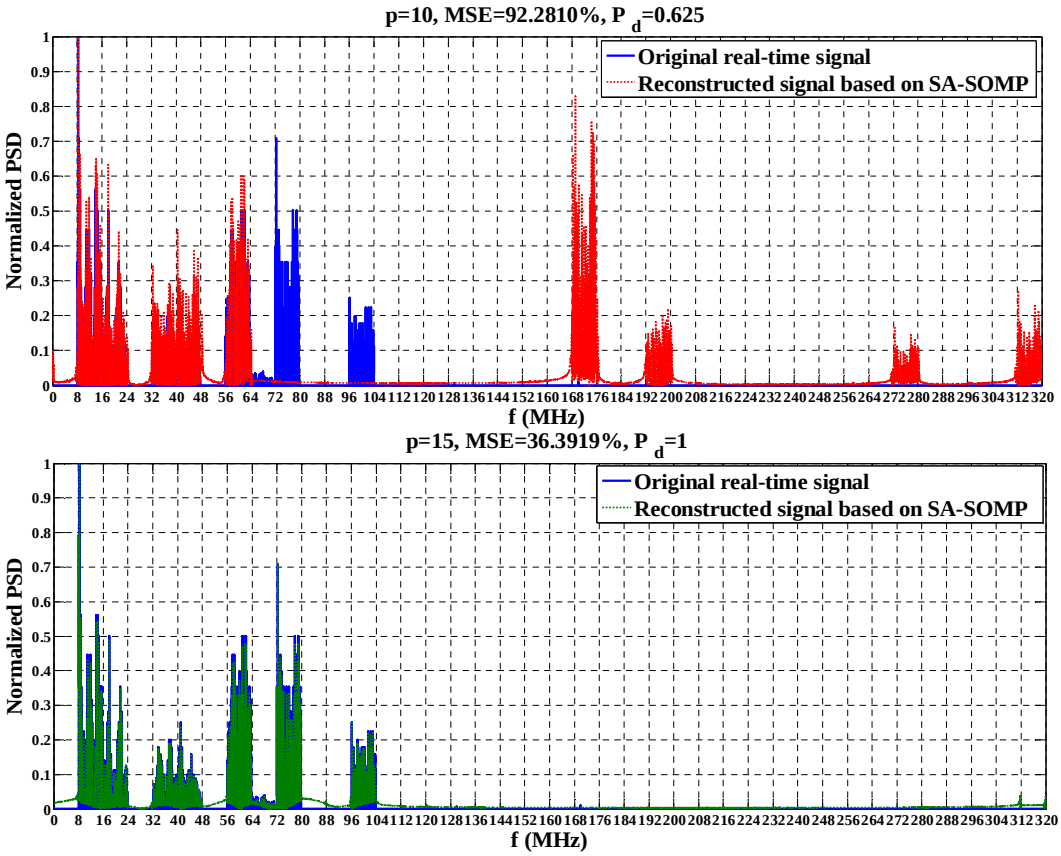

Figure 4.16: Normalized PSD of the reconstructed real-world TVWS signal under $p = 10$ and $p = 15$ at individual spectrum sensing.

support is recovered, reconstruction of the wideband signal has a closed-form solution, as presented in (4.25).

Fig. 4.16 shows the reconstructed real-world TVWS spectrum at an individual SU equipped with a multicoset sampler, for $p = 10$ and 15, respectively. It is observed that a smaller MSE of the reconstructed signal is achieved under a higher p, but at the cost of a higher sampling rate thus more sample processing. When $p = 10$, i.e., $\kappa < p < 2\kappa$, the individual wideband spectrum sensing scheme misses some occupied channels such that the detection probability P_d reduces to 0.625 and the reconstruction MSE gets higher as well.

Then, the proposed cooperative spectrum sensing scheme with $p = 10$ and $J = 3$ is considered. Due to the measurements sharing among SUs, the fusion centre gets an

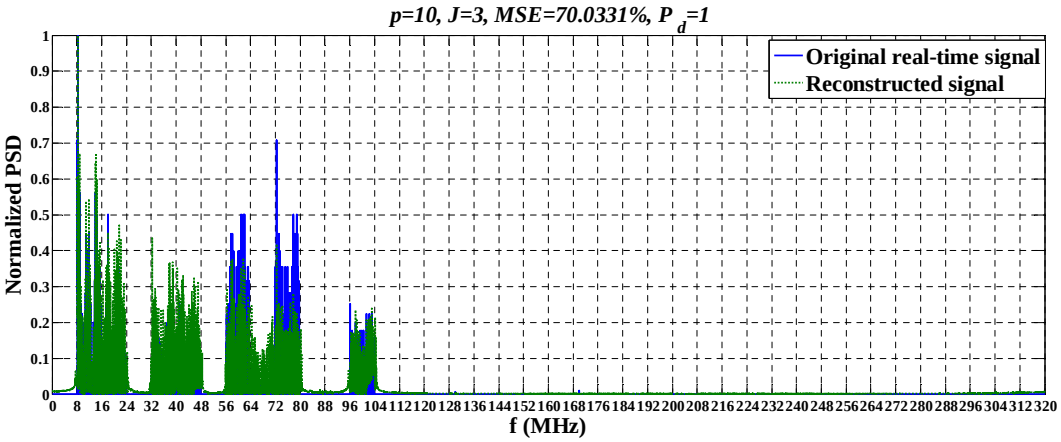

Figure 4.17: Normalized PSD of the reconstructed real-world TVWS signal under $p = 10$ at cooperative spectrum sensing of $J = 3$ SUs.

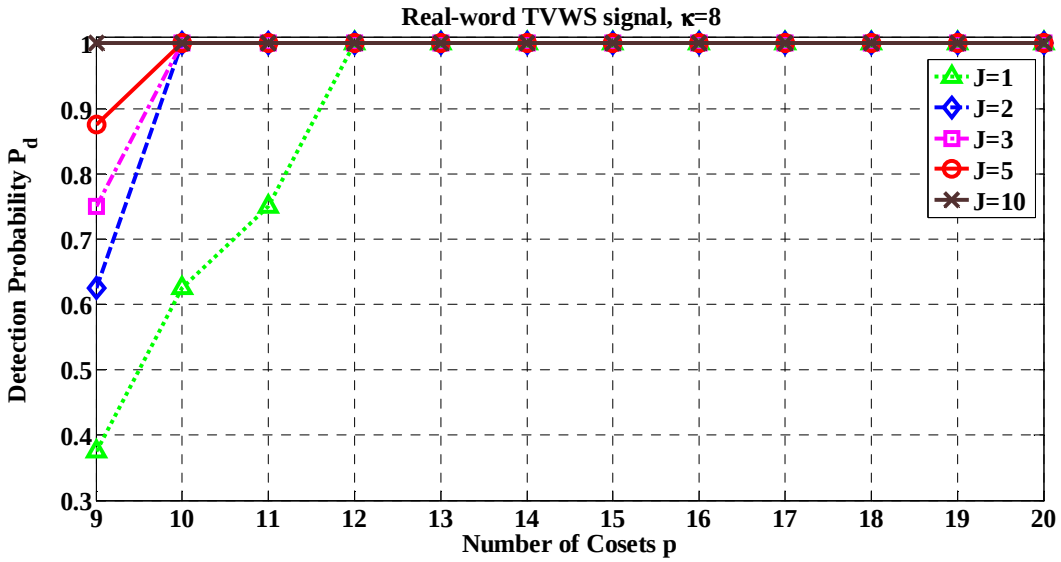

Figure 4.18: Detection probability P_d vs. number of cosets p for the real-world TVWS signal.

accurate signal support estimation such that the detection probability P_d increases to 1 and the reconstructed signal achieves a good approximation to the original signal, as shown in Fig. 4.17.

Fig. 4.18 illustrates the detection probability P_d against the sub-Nyquist sampling ratio Ω over the real-world TVWS signal. Similarly as shown in Fig. 4.15, the detection performance is improved as the number of SUs J increases. It is seen that a smaller number of cosets p proportional to the number of occupied channels κ suffices for the

reliable detection in the cooperative cognitive radio networks.

4.5 Summary

Wideband spectrum sensing is of critical importance to enable dynamic spectrum sharing. In this chapter, efficient multicoset sampling based wideband spectrum sensing schemes have been proposed for both individual and cooperative sensing cases to reduce energy consumption on wideband signal acquisition, processing, and transmission, with detection performance guarantee by exploiting the joint sparsity of the multiband signals. Based on a low-rate multi-channel architecture, sub-Nyquist sampling is implemented without complex front-end processing. The proposed wideband spectrum sensing schemes locate the active channels blindly without the prior knowledge of the spectral support for the received signal at either the sub-Nyquist sampling or reconstruction stage.

Compared with individual wideband spectrum sensing scheme based on MUSIC, the proposed scheme improves the detection accuracy in low SNR regimes. Exploiting the common signal support perceived at all SUs, the detection accuracy is further improved through cooperative spectrum sensing, in which measurements from multiple SUs are fused jointly to reach a final sensing decision. Based on low-dimensional measurements derived by subspace decomposition, the proposed cooperative spectrum sensing scheme gains better noise robustness while reduces both computation complexity and transmission overhead. Moreover, thanks to the measurement diversity across multiple SUs, reliable sensing results can be achieved at the minimal sampling rate specified by the Landau's theorem, such that the number of cosets p proportional to the signal sparsity κ is shown sufficient for reliable cooperative spectrum sensing.

The robust performance of the proposed wideband spectrum sensing scheme has also been validated over real-world TVWS signals recorded by the RFeye node at QMUL. In comparison with conventional sub-Nyquist wideband spectrum sensing schemes, numer-

ical analysis and experimental results show that the proposed scheme can achieve good detection performance as well as reduced computation and implementation complexity.

Chapter 5

Joint Sub-Nyquist Spectrum Sensing Scheme with Geolocation Database

To maximize spectrum access opportunities for white space devices, incorporating real-time spectrum sensing with geolocation database is a promising approach to enhance detection resolution with reduced computation complexity. In this chapter, a hybrid scheme of sub-Nyquist wideband spectrum sensing with geolocation database is proposed to achieve accurate detection of the surrounding spectrum with reduced number of required measurements and computation complexity. Two iterative algorithms are modified to incorporate a priori information from geolocation database, therefore enabling spectrum sensing to be performed only on a limited number of potentially vacant channels over TV White Space. Specifically, the related work and main contributions are firstly introduced in Section 5.1. Section 5.2 presents the system architecture and problem formulation of the proposed hybrid scheme. Section 5.3 describes the joint sparse recovery with geolocation database. Section 5.4 analyses and validates the proposed schemes. Finally, Section 5.5 concludes this chapter.

5.1 Introduction

5.1.1 Related Work

To enable dynamic spectrum access over white space, fast and accurate detection of the spectrum is crucial to ensure that there is no harmful interference caused to the surrounding licensed services, including Digital Terrestrial Televisions (DTT), Programme Making and Special Events (PMSE) users, e.g., wireless microphone systems, and other future incumbent users [28]. White space devices (WSDs) should either sense the presence of primary signals or make use of a geolocation database to determine which spectrum is unused in the vicinity [8, 10]. Current operational mechanism to discover available TV channels is using the geolocation database [34]. This is primarily because spectrum sensing is expensive in cost, energy consumption, and hardware complexity. In contrast, the geolocation approach does not require complex hardware and is easier to implement, where devices determine their locations and query a geolocation database that will return a list of available frequency channels and their associated maximum transmit powers at current location. However, geolocation database suffers from its inherent inefficiency. The geolocation approach uses propagation modelling to determine the available spectra, and hence, is very conservative in the channels it returns for a given location. Moreover, it can only protect registered systems, but PMSE users operate mostly on an unlicensed basis. For the concern of the speed of database update, the use of real-time spectrum sensing in addition to geolocation is proposed to resolve the issue for the efficient use of white space and harmonious coexistence with dynamic incumbent systems.

In [129] and [130], hybrid frameworks are proposed to incorporate the advantages of both geolocation database and spectrum sensing, in which different spectrum sensing modules are sequentially performed at each channel after its occupancy is initially determined by the geolocation database. However, for the received signal over a wide frequency range, sequentially scanning the channels one by one will introduce a long sensing period and thus may cause missed opportunities or interferences [48].

Directly acquiring the wideband signals to detect spectral opportunities is thus desirable to capture the instant spectrum changes [10]. To alleviate the high sampling rate, compressive sensing was introduced to implement wideband spectrum sensing [17]. In [116], a database assisted compressive wideband spectrum sensing algorithm is proposed to reduce the sensing costs by employing the information from geolocation database to construct a non-iteratively reweighted least square signal reconstruction. Specifically, the channel historical power information from geolocation database is utilised for the weight calculation to replace the iterative process of weights updating in the iteratively reweighted least square (IRLS) algorithm. However, the resolution and accuracy of channel power information from geolocation database would affect the reconstruction accuracy in such a non-iterative way. Moreover, if unregistered PU appears or dynamic change of the spectrum status occurs, the error in the prior information from geolocation database would severely degrade the recovery performance.

5.1.2 Contributions

Motivated by the above challenges, a low-complexity hybrid scheme of sub-Nyquist wideband spectrum sensing with geolocation database is explored in this chapter for the effective use of white spaces within the coexistence of dynamic incumbent systems, such as the wireless microphones that do not register in the database. Recent works show that the use of additional prior information on the support in compressive sensing has advantages in terms of number of required measurements and computational complexity during the reconstruction stage [131]. To relax the sensing sensitivity required on the sensor node, prior TV channel occupancy status from geolocation database is utilised in the sensing process. With the assists from geolocation database, part of the complexity of local wideband sensing is transferred to the core network, thus decreasing the processing complexity and energy consumption required on the spectrum sensing. To incorporate the channel status information from geolocation database, sub-Nyquist wideband spectrum sensing scheme based on multicoset sampling is exploited [132], in which

a low-dimensional measurement matrix is computed to locate the occupied channels through recovering its support based on the jointly sparse nature of multiband signals. Two reconstruction algorithms, greedy algorithm and ℓ_v-norm $(0 < v < 1)$ minimization, are employed in the recovery process. Theoretical analyses and experiment results show that the proposed hybrid scheme speeds up the sensing process with enhanced detection performance and smaller sampling rate, while the use of spectrum sensing can track the changes of spectrum occupancy state in real-time. This is specially important when the prior information from geolocation is not perfectly reliable, so the instant channel occupancy state provided by spectrum sensing reduces the risks of WSDs interfering with dynamic incumbent users.

5.2 System Architecture and Problem Formulation

5.2.1 System Architecture

Fig. 5.1 shows the block diagram of the proposed hybrid scheme. The aim of this framework is to enable the WSDs to use spectrum in the TV bands at a particular location and time on a shared basis subject to ensuring that there would be a low probability of harmful interference to other spectrum users in the band, such as digital TV broadcast signals, or dynamic incumbent systems, e.g., unregistered wireless microphones. WSDs' operation in TVWS will be controlled by the geolocation database, where WSDs measure their geographical location and query a geolocation database in order to get information on available frequencies at this location. The operational scenario with WSDs can be described as a communication between a master device and a slave device. Master WSD can establish a direct communication link with the geolocation database and request operational parameters for the transmission of any slave WSDs that are located within its coverage area.

For the efficient use of white spaces within the coexistence of dynamic incumbent

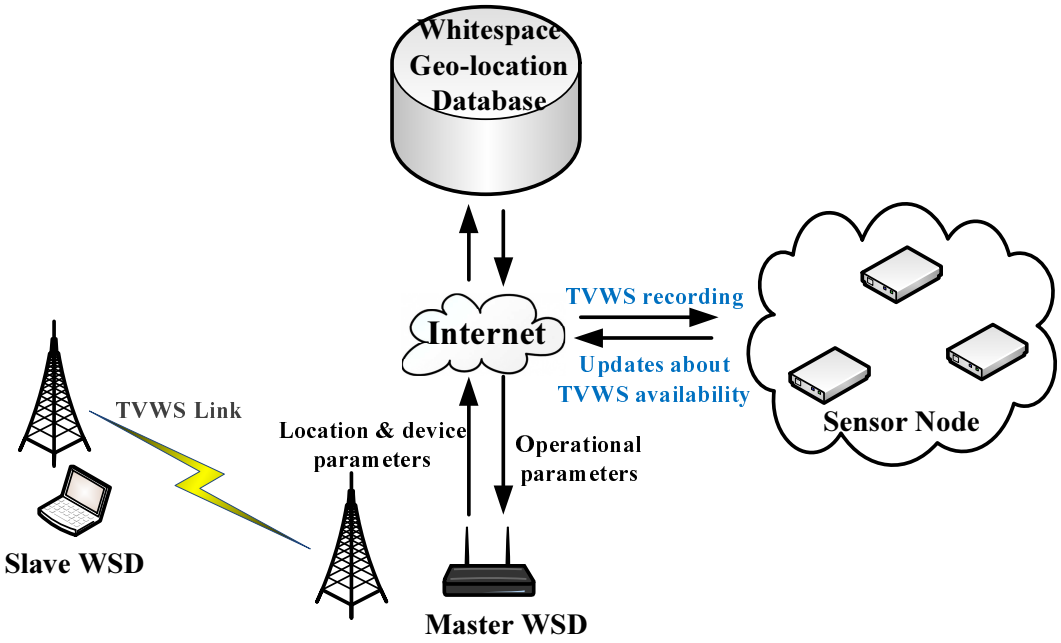

Figure 5.1: System architecture of the proposed hybrid scheme.

systems, a joint scheme of geolocation database and spectrum sensing is explored in this chapter. The rightmost side of Fig. 5.1 shows the diagram of the sensor network, which can be accessed and configured remotely. Spectrum sensing is implemented on the sensor nodes to scan the overall spectrum in real-time, and reports the dynamic changes of spectrum occupancy status to the geolocation database. Furthermore, in the context of spectrum sensing, some of the frequency bands are heavily used by the primary users such as local radio stations, local TV stations, etc., so the related information at the geolocation database will be stable due to TV broadcasting arrangement in the long run (e.g., years). Therefore, although the side-information from geolocation database is possibly with some errors due to the dynamic changes of the spectrum state, such information can be incorporated at the sensing terminals to reduce the sensing costs.

5.2.2 Problem Formulation

Exploiting the sparse nature of the wideband spectrum due to the under-utilisation in practice, sub-Nyquist sampling is employed to implement wideband spectrum sensing,

which acquires wideband signals using the sampling rate lower than the Nyquist rate and then detects spectral opportunities using these partial measurements [19]. To reduce the computation complexity, the channel status information from geolocation database, i.e., the locations of occupied channels, will be incorporated in the sensing framework. The purpose of this chapter is then to show how this prior information can be efficiently used in the sub-Nyquist wideband spectrum sensing.

The compressive measurement acquisition can be expressed by the following analytical model:

$$\boldsymbol{y} = \boldsymbol{\Phi}\boldsymbol{x} + \boldsymbol{\xi}, \tag{5.1}$$

where $\boldsymbol{\Phi} \in \mathbb{R}^{m \times N}$ is the sensing matrix to collect the compressive measurements $\boldsymbol{y}$ from $\boldsymbol{x}$, $m \in \mathbb{Z}$ (with $k < m < N$) refers to the dimension of $\boldsymbol{y}$, and $\boldsymbol{\xi}$ is the noise perturbation, whose magnitude is constrained by an upper bound δ, i.e., $||\boldsymbol{\xi}||_2 < \delta$.

Under certain assumptions, e.g., restricted isometry property (RIP) on $\boldsymbol{\Phi}$ [50], robust signal reconstruction with respect to (5.1) could be achieved as

$$\min_{\boldsymbol{x} \in \mathbb{R}^N} ||\boldsymbol{x}||_0 \quad \text{subject to } |||\boldsymbol{\Phi}\boldsymbol{x} - \boldsymbol{y}||_2^2 \leq \delta. \tag{5.2}$$

Recent works show that additional prior information on the signal can be employed in the sparse recovery framework to improve the recovery performance [133]. For instance, if incomplete or complete prior information on the support of the sparse domain is available, the sparse recovery framework can be modified to seek a signal that explains the measurements and whose support contains the smallest number of new additions to the known support T [131, 134, 135], so the sparsest solution is given by

$$\min ||(\boldsymbol{x})_{T^c}||_0 \ \text{ subject to } \ ||\boldsymbol{\Phi}\boldsymbol{x} - \boldsymbol{y}||_2^2 \leq \delta. \tag{5.3}$$

The minimization problem in (5.2) is aimed at finding the sparsest solution that explains the measurements. In (5.3), the problem is modified to minimize the number of nonzeros

in other positions only, i.e., those that do not belong to the known support T. An important property of (5.3) is that a solution $\bar{\boldsymbol{x}}$ is not strictly constrained to be nonzero in the locations specified by T, since the corresponding values are determined from the measurement constraints and the minimization of the objective function associated to the remaining positions [131]. Therefore, if there are some errors in the support set T, i.e., some positions in T actually do not belong to the support, the minimization problem in (5.3) can still reconstruct the actual signal, but more measurements may be required compared to the case when no errors are present in the known support T.

Suppose that the support of $\boldsymbol{x}$ is denoted as S, and $k := |S|$. The size of the known part of the support $t := |T|$, the size of unknown support $u := |U|$, and $U_e := T \setminus S$ is the error in the known part with the size $e := |U_e|$, so that $k = t + u - e$. The theoretical lower bound for exact reconstruction based on l_0-minimization can be expressed with the restricted orthogonality constant δ as [131]

$$\delta_{t+2u} < 1, \tag{5.4}$$

which is much weaker than that of the original sparse recovery $\delta_{2k} < 1$ [50] as the restricted orthogonality constant δ is nondecreasing, and $k \gg u$, $k \gg e$. Sufficient condition for exact reconstruction in terms of δ measures the theoretical minimum number of measurements needed. Therefore incorporating the prior known part of the support can reduce the number of measurements, so that the related sampling rate will be reduced for the power-limited devices.

To improve the recovery performance with reduced processing requirements, the information from geolocation database is incorporated in the proposed spectrum sensing scheme. By harnessing the benefits of both approaches, the hybrid framework is a promising solution for the efficient use of the white space with coexistence of dynamic incumbent systems, including digital TV broadcast signals and unregistered wireless microphones. Since the geolocation database stores available frequency channel lists and

their associated maximum transmit powers at current location and time, this chapter aims to study how to incorporate this channel occupancy status information in the sub-Nyquist wideband spectrum sensing to reduce the reconstruction complexity in terms of the sampling rate and computational costs.

The notation used in this chapter is as follows. The superscripts $(\cdot)^T$, $(\cdot)^H$ and $(\cdot)^\dagger$ denote transpose, Hermitian transpose and pseudo-inverse of a matrix ($\boldsymbol{X}^\dagger = (\boldsymbol{X}^H\boldsymbol{X})^{-1}\boldsymbol{X}^H$), respectively. $\boldsymbol{A}_{i,j}$ is the i-th entry of the matrix $\boldsymbol{A}$. $\boldsymbol{a}_i$ is the i-th column of the matrix $\boldsymbol{A}$. $\boldsymbol{A}[i]$ is the i-th row of the matrix $\boldsymbol{A}$. $\boldsymbol{A}_{\mathcal{T}}$ denotes the sub-matrix containing the columns of $\boldsymbol{A}$ with indices from $\mathcal{T}$. The notation, $[0, L-1] := [0, 1, ..., L-1]$. $\mathcal{T}^c$ denotes the complement of the set $\mathcal{T}$. $\mathcal{T}_1 \setminus \mathcal{T}_2 = \mathcal{T}_1 \cap \mathcal{T}_2^c$ denotes the set difference. And $|\mathcal{T}|$ denotes the size of set $\mathcal{T}$.

5.3 Joint Sparse Recovery Incorporated with Geolocation Database

The received signal $x(t)$ is assumed to be a continuous-time wideband signal. Since the wideband spectrum is normally under-utilised in reality, $x(t)$ bears a sparse property in the frequency domain such that all (or most) of its energy is concentrated in one or more disjoint frequency bands and its spectral measure is small relative to the overall signal bandwidth. Without loss of generality, the wideband spectrum to be monitored is evenly segmented into M narrowbands, each of them with bandwidth $\mathcal{B}_0$. The channels are indexed from 0 to $M-1$. Suppose there are up to κ active channels occupied during the sensing period with $\mathcal{S} = [\mathcal{S}_1, \mathcal{S}_2, ..., \mathcal{S}_\kappa]$ denoting the set containing the indices of the occupied channels. If the spectrum utilisation ratio is defined as α, then a sparse multiband signal is one satisfying $\alpha = \kappa/M < 1$. The task of wideband spectrum sensing is to find the presences and locations of the license transmissions or equivalently locating the active channel set $\mathcal{S}$.

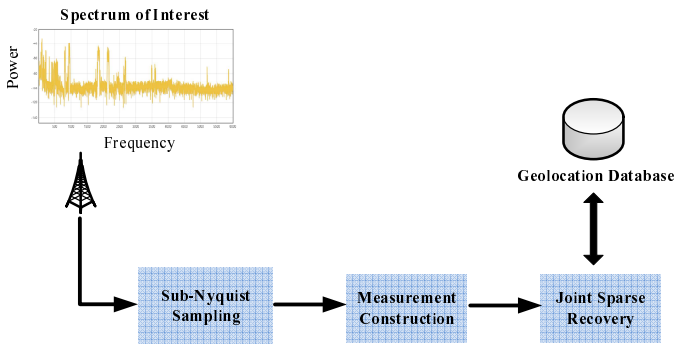

Figure 5.2: Whole flowchart of the proposed joint sub-Nyquist sensing scheme.

To reduce the energy consumption in high frequency signal processing, compressive multicoset sampling is adopted to reduce the signal sampling and acquisition costs with ease of implementation. From the practical standpoint, multicoset sampling can be realized by a time-interleaved ADC [121, 122], in which only a subset of channels are used. The whole procedure of the proposed scheme can be formulated into a three-step framework, as shown in Fig. 5.2:

1. Each sensor implements a multicoset sampler that *blindly* samples the signal at a rate lower than the Nyquist rate.

2. A low-dimensional measurement matrix is constructed from sub-Nyquist samples.

3. Based on the jointly sparse nature of the multiband signals, the occupied channels are located through joint sparse recovery, where prior channel status information from geolocation database will be incorporated to relax the computation complexity.

Given the number of channels M, multicoset sampling is executed by sampling the signal at the time instants $(mM + c_i)T$, where $i = 1, ..., p,\ m \in \mathbb{Z}$, and $1/T = f_s$ is the Nyquist sampling rate. Multicoset sampler can be realized by p parallel cosets, each of them taking uniform samples at time instants $\{mMT + c_iT\}$ by a decimated sampling rate $\frac{1}{MT} = f_s/M$ with a time offset of $\{c_iT\},\ i = 1, ..., p$. The average sub-Nyquist sampling ratio equals to $\alpha = p/M$. The measurement sequence of the i-th coset is

defined as

$$x_{c_i}[n] = \begin{cases} x(nT), & n = mM + c_i,\ m \in \mathbb{Z} \\ 0, & \text{otherwise.} \end{cases} \tag{5.5}$$

Applying Fourier transform to $x_{c_i}[n]$ gives the relationship between its spectrum $X_{c_i}(e^{j2\pi fT})$ and the unknown Fourier Transform of $x(t)$ [56]:

$$X_{c_i}(e^{j2\pi fT}) = \frac{1}{MT}\sum_{m=0}^{M-1} X_m(f)e^{j\frac{2\pi}{M}c_i m},\ \forall f \in [0, \mathcal{B}_0], \tag{5.6}$$

for every $1 \leq i \leq p$, where $X_m(f) = X(f + \frac{m}{MT})$ corresponds to the pieces of the original spectrum $X(f)$ in the m-th channel, which is shifted to the left by $\frac{m}{MT}$ units. As $x(t) = s(t)+n(t)$, the corresponding Fourier transform can be expressed as $X(f) = S(f)+N(f)$. We can rewrite (5.6) into the matrix form as

$$\mathbf{Y}(f) = \mathbf{A}\mathbf{X}(f) = \mathbf{A}[\mathbf{S}(f) + \mathbf{N}(f)],\ \forall f \in [0, \mathcal{B}_0], \tag{5.7}$$

where $\mathbf{Y}(f)$ is a vector of length p whose i-th element is $X_{c_i}(e^{j2\pi fT})$, $\mathbf{X}(f)$ is the unknown spectrum vectors of $x(t)$ in the M channels, i.e., $\mathbf{X}(f) = [X_0(f), X_1(f), ..., X_{M-1}(f)]^T$, and $\mathbf{A} \in \mathbb{C}^{p\times M}$ is a matrix with (i, j)-th element given by $\mathbf{A}_{i,j} = \frac{1}{MT}e^{j\frac{2\pi}{M}c_i(j-1)}$.

As stated in Chapter 4, reconstruction of $\boldsymbol{X}(f)$ in (5.7) is referred to as the multiple measurement vectors (MMV) problem, as $\boldsymbol{X}(f)$ is row-sparse, i.e., having nonzero entries in only a few rows. Extension of the single measurement vector (SMV) to the MMV problem is considered in [89], where the objective is to minimize the number of rows containing nonzero entries while satisfying the measurement constrain in (5.7). The problem can be formulated as

$$\min ||\mathcal{R}_{\ell_q}(\boldsymbol{X})||_0 \ \text{ subject to } \ \boldsymbol{Y} = \boldsymbol{A}\boldsymbol{X}, \tag{5.8}$$

where $\mathcal{R}_{\ell_q}(\boldsymbol{X})$ is a vector in $\mathbb{R}^M$ whose i-th entry is the ℓ_q vector norm of the i-th row

of $\boldsymbol{X}$, i.e.,

$$\begin{aligned} &\mathcal{R}_{\ell_q}(\boldsymbol{X}) = [v_1, v_2, ..., v_M]^T, \\ &\text{where } v_i = ||\boldsymbol{X}[i]||_q = (\textstyle\sum_{j=1}^{N} |x_{i,j}|^q)^{1/q}. \end{aligned} \tag{5.9}$$

As in the SMV problem, (5.8) is NP-hard but can be approximately solved by the following ℓ_1 minimization problem:

$$\min ||\mathcal{R}_{\ell_q}(\boldsymbol{X})||_1 \;\text{ subject to }\; \boldsymbol{Y} = \boldsymbol{A}\boldsymbol{X}. \tag{5.10}$$

Some existing convex relaxation and greedy algorithm for the sparse recovery problem have been proposed to extend to accommodate MMV problem [89, 93], which aims to solve $\boldsymbol{X}$ from the multiple-measurement vector $\boldsymbol{Y}$.

Since the parameter M in the multicoset sampler is set based on the number of channels in the spectrum of interest, the positions of nonzero rows of in (5.7) is equivalent to the active channel index set $\mathcal{S}$. As channel status information from geolocation database shows which part of channels are supposed to be occupied, we can incorporate this prior information on the indices of the corresponding rows with large norm in the recovery process, in order to enhance the recovery performance with fewer measurements under sub-Nyquist sampling. Based on the white space channel information from the geolocation database, the sensor node can get a response with details of available channels in the vicinity. Assuming that $\mathcal{T} \subset [0,\ M-1]$ is the prior knowledge of the occupied channel indices from geolocation database, its relation to the actual occupied channel set $\mathcal{S}$ can be expressed as:

$$\mathcal{S} = \mathcal{T} \cup \triangle \setminus \triangle_e, \tag{5.11}$$

where $\triangle := \mathcal{S} \setminus \mathcal{T}$ is newly occupied channel set, and $\triangle_e := T \setminus S$ is the newly released channel indices, i.e., the occupied channel indices recorded at geolocation database but actually released as vacant at current time.

Motivated by the above challenges, two iterative algorithms, greedy algorithm and iterative reweighted least square (IRLS) methods are modified in the MMV problem

to incorporate the information from geolocation database in the recovery process. The aforementioned methods construct an estimate of the signal at each iteration, thereby being more intuitive to incorporate $\mathcal{T}$ in the recursion as an initial condition.

5.3.1 Subspace-Augmented Joint Sparse Recovery with Prior Information

To reduce computation costs in the compact sensor node, the greedy algorithm SA-SOMP presented in Chapter 4 is extended to this joint sparse problem because of its lower complexity compared with other ℓ_1-minimization algorithms. To reduce the required number of measurements and the computational complexity, channel status information from geolocation database is incorporated in the reconstruction process to locate the instant occupied channels. The channel occupancy status from geolocation database gives a priori information about some of the occupied channels that should be selected as they may be used or reserved by the registered systems. This way, local spectrum sensing is performed only on a limited number of potentially vacant TV channels.

In the recovery process of SA-SOMP, the column of $\boldsymbol{A}$ that is most strongly correlated with the remaining part of the signal is chosen at each iteration. Then we subtract off its contribution from the measurement matrix $\boldsymbol{\chi}_s$ and iterate on the residual. Note that the indexes of the selected columns of $\boldsymbol{A}$ refers to the locations of nonzero rows of $\boldsymbol{\nu}_s$. As the parameter M in the multicoset sampler is set based on the number of channels in the received signal, the support of $\boldsymbol{\nu}_s$ is equivalent to the active channel set $\mathcal{S}$. Therefore, based on the information from the geolocation database, the initialization of the support recovery is modified to subtract off the contributions of these corresponding columns in the measurement matrix as they may be used or reserved by the registered licence systems. Thus, before starting the iteration, the residual is initialized as

$$\boldsymbol{r}_0 = \boldsymbol{\chi}_s - \boldsymbol{A}_{\mathcal{T}+1}(\boldsymbol{A}_{\mathcal{T}+1}^{\dagger}\boldsymbol{\chi}_s), \tag{5.12}$$

Algorithm 3 Joint sparse recovery in SA-SOMP with Prior Information

Require: $\boldsymbol{R} \in \mathbb{C}^{p\times p}$, $\boldsymbol{A} = [\boldsymbol{a}_1, ..., \boldsymbol{a}_M] \in \mathbb{C}^{p\times M}$, $\hat{\kappa}$, $\mathcal{T}$
Ensure: $\mathcal{S}$
1: $[\boldsymbol{U}_s, \boldsymbol{\Lambda}_s] \leftarrow \text{RREVD}(\boldsymbol{R}, \hat{\kappa})$, $\boldsymbol{\chi}_s = \boldsymbol{U}_s\sqrt{\boldsymbol{\Lambda}_s}$
2: $t = 0$, $\mathcal{S} = \mathcal{T} + 1$, $\boldsymbol{\nu}_0 = \boldsymbol{A}^{\dagger}_{\mathcal{T}+1}\boldsymbol{\chi}_s$, $\boldsymbol{r}_0 = \boldsymbol{\chi}_s - \boldsymbol{A}_{\mathcal{T}+1}\boldsymbol{\nu}_0$,
3: **while** $t \leq \hat{\kappa} - |\mathcal{T}|$ **do**
4: $t \leftarrow t + 1$
5: $m_t = \arg\max_m \parallel \boldsymbol{a}_m^{\mathbf{H}}\boldsymbol{r}_{t-1} \parallel_2$, $m \in 1, ..., M$
6: $\mathcal{S} \leftarrow \mathcal{S} \cup m_t$, $\boldsymbol{\nu}_t = \boldsymbol{A}^{\dagger}_{\mathcal{S}}\boldsymbol{\chi}_s$
7: $\boldsymbol{r}_t \leftarrow \boldsymbol{\chi}_s - \boldsymbol{A}_{\mathcal{S}}\boldsymbol{\nu}_t$
8: **end while**
9: **return** $\mathcal{S}$=$\mathcal{S}$-1

where $\mathcal{T} \subset [0, M-1]$ is added with 1 as the corresponding column indices of $\boldsymbol{A}$ start from 1. The entire procedure of the proposed joint sparse recovery augmented by geolocation database is summarized in Algorithm 3. A sparsity-based halting criterion is used in the recovery process, i.e., $t \leq \hat{\kappa} - |\mathcal{T}|$. Therefore, with the TV channel information $\mathcal{T}$ from geolocation database, the number of iterations will be reduced, so that the joint approach could speed up the sensing process.

5.3.2 Iterative Reweighted Support Detection with Prior Information

Besides the ℓ_1 norm, other functions of $\boldsymbol{X}(f)$ have also been proposed as objective functions. Among these algorithms, ℓ_v diversity measure $(0 < v < 1)$ has received great attention because of its improved performance as it provides a closer approximation to the ℓ_0-norm minimization. The objective function can be formulated as

$$J^{v,q}(\boldsymbol{X}) = ||\mathcal{R}_{\ell_q}(\boldsymbol{X})||_v^v = \sum_{i=1}^{M}(||\boldsymbol{X}[i]||_q)^v,\ 0 < v \leq 1,\ q \geq 1. \tag{5.13}$$

The ℓ_v norm minimization is nonconvex but can be solved through the transformation of the original problem into a sequence of convex problems using iterative reweighting [76]. In [136], a reweighted ℓ_2 algorithm is proposed to extend FOCal Underdetermined System Solver (FOCUSS) to the MMV problem to minimize the above objective, with $q = 2$,

referred to as MFOCUSS. More specifically, the objective function in (5.8) is modified as a weighted least square problem in Lagrangian form:

$$\min \ ||\boldsymbol{Y} - \boldsymbol{A}\boldsymbol{X}||_F^2 + \lambda \sum_{i=1}^{M} w_i (||\boldsymbol{X}[\boldsymbol{i}]||_2)^2, \tag{5.14}$$

where $||.||_F$ is the Frobenius norm, w_i is the weighting parameter, and λ is the Lagrange multiplier. The problem in (5.14) will be repeatedly solved by updating the weight w_i at each iteration using the solution from previous iteration: at each iteration, w_i will be set as

$$w_i^{(t)} = (||\boldsymbol{X}^{(t-1)}[i]||_2)^{v-2}. \tag{5.15}$$

where $w_i^{(t)},\ i = 1, ..., M$ is the value of the weighting vector to be used at the t-th iteration and $\boldsymbol{X}^{(t-1)}$ is the $(t-1)$-th iterate. After convergence, $\boldsymbol{X}^{(t-1)}$ will be sufficiently close to $\boldsymbol{X}^{(t)}$, so that $\sum_{i=1}^{M} w_i^{(t)} (||\boldsymbol{X}[\boldsymbol{i}]||_2)^2 = \sum_{i=1}^{M} ((||\boldsymbol{X}^{(t-1)}[i]||_2)^{v-2} (||\boldsymbol{X}[\boldsymbol{i}]||_2)^2$ will be close to $\sum_{i=1}^{M} ((||\boldsymbol{X}^{(t-1)}[i]||_2)^v$, which is the original ℓ_v norm problem in (5.13) with $q = 2$.

The weighting parameter $\boldsymbol{w}^{(t)}$ are computed from the row norms of the solution obtained in the previous iteration, so the corresponding rows with larger norm are likely to be de-emphasized as they are irrelevant in fitting the data and vice versa. In (5.15), as $0 < v < 1$, the weights will be chosen inversely proportional to the ℓ_2-norm of the rows. Since it gives a large weight to the small component, it will encourage a sparse solution in the minimization problem of (5.14).

As shown in the proposed hybrid system model in the Fig. 5.1, the white space response from geolocation database records the channel occupancy status, while the sensing network will monitor the whole spectrum to find the dynamic changes. As the i-th row in $\boldsymbol{X}(f)$ corresponds to the piece of the original spectrum in the subchannel, the occupied channel information from geolocation database indicates the indices of the corresponding rows with large norm. Similar as (5.3), the objective function in (5.14) can therefore be changed as the ℓ_v minimization over the remaining positions only, $i \notin \mathcal{T}$,

i.e.,

$$\min \ ||\boldsymbol{Y} - \boldsymbol{A}\boldsymbol{X}||_F^2 + \lambda \sum_{i \notin \mathcal{T}} w_i (||\boldsymbol{X}[\boldsymbol{i}]||_2)^2. \tag{5.16}$$

By defining

$$w_i = 0, \forall i \in \mathcal{T}, \tag{5.17}$$

the minimization in (5.14) is transformed in the form of (5.16).

Here, in order to add the prior channel occupancy information from geolocation database, the weighing strategy in the joint sparse reconstruction is modified as

$$w_i^{(t)} = \begin{cases} \tau(||\boldsymbol{X}^{(t-1)}[i]||_2)^{v-2}, & i \in \mathcal{T} \\ (||\boldsymbol{X}^{(t-1)}[i]||_2)^{v-2}, \ \text{otherwise}, \end{cases} \tag{5.18}$$

where τ is a specified small constant. For $\tau = 0$, the first expression in (5.18) reduces to 0 as required by (5.17).

Given an initial guess of the signal $\boldsymbol{X}^{(0)}$ (e.g., the least-squares solution), the iterative reweighting algorithm generates a sequence of iterations of as follows:

$$\boldsymbol{X}^{(t+1)} := \underset{\boldsymbol{X} \in \mathcal{C}^{M \times N}}{\arg\min} \ ||\boldsymbol{Y} - \boldsymbol{A}\boldsymbol{X}||_F^2 + \lambda \sum_{i=1}^{M} w_i (||\boldsymbol{X}[\boldsymbol{i}]||_2)^2. \tag{5.19}$$

The solution to (5.19) at the t-th iteration can be expressed as

$$\boldsymbol{X}^{(t+1)} = \boldsymbol{W}^{(t)} \boldsymbol{A}^T (\boldsymbol{A}\boldsymbol{W}^{(t)} \boldsymbol{A}^T + \lambda \boldsymbol{I})^{-1} \boldsymbol{Y}, \tag{5.20}$$

where $\boldsymbol{W}^{(t)} = \text{diag}\{[1/w_1^{(t)}, ..., 1/w_M^{(t)}]\}$. The initial weight is given by

$$w_i^{(0)} = \begin{cases} \tau, & i \in \mathcal{T} \\ 1, \ \text{otherwise}. \end{cases} \tag{5.21}$$

Algorithm 4 Iterative Reweighted Support Detection with Prior Information based on MFOCUSS

Require: $\boldsymbol{Y} \in \mathbb{C}^{p\times N}$, $\boldsymbol{A} = [\boldsymbol{a}_1, ..., \boldsymbol{a}_M] \in \mathbb{C}^{p\times M}$, $\mathcal{T}$, λ, $\hat{\kappa}$
Ensure: $\mathcal{S}$
1: Initialize $\boldsymbol{W}^{(0)}$ using (5.21) and $t = 0$
2: **while** halting criterion in (5.22) false **do**
3: Compute $\boldsymbol{X}^{(t+1)} = \boldsymbol{W}^{(t)}\boldsymbol{A}^T(\boldsymbol{A}\boldsymbol{W}^{(t)}\boldsymbol{A}^T + \lambda\boldsymbol{I})^{-1}\boldsymbol{Y}$
4: Weight $\boldsymbol{W}^{(t+1)}$ updates using (5.18)
5: $t = t + 1$
6: **end while**
7: Estimate support $\mathcal{S}$ by selecting the position of the first $\hat{\kappa}$ largest components in $\boldsymbol{W}^{(t+1)}$
8: **return** $\mathcal{S}$=$\mathcal{S}$-1

The algorithm is terminated once the convergence criterion has been satisfied, i.e.,

$$\frac{||\boldsymbol{X}^{(t+1)} - \boldsymbol{X}^{(t)}||_F}{||\boldsymbol{X}^{(t)}||_F} \leq \delta, \tag{5.22}$$

where δ is a user-selected parameter. Here, based on the sparsity guess of the support dimension $\hat{\kappa}$ from EFT [127], the estimated active channel set is determined by selecting the position of the first $\hat{\kappa}$ smallest components in the final weight $\boldsymbol{w}$. The entire procedure of the proposed joint sparse recovery based on MFOCUSS augmented by geolocation database is summarised in Algorithm 4.

5.4 Numerical Analysis

This section provides simulation results to evaluate the proposed wideband spectrum sensing scheme, in which the impact of different system parameters, such as the SNR, the sub-Nyquist sampling ratio, the spectrum occupancy ratio, and the detection performance with prior information from geolocation database, are investigated.

5.4.1 Spectrum Sensing Performance versus SNR and Sub-Nyquist Sampling Ratio

The joint sensing performance based on SA-SOMP and MFOCUSS is first evaluated in different conditions using the simulated signals with the number of occupied channels $\kappa = |\mathcal{S}| = 0.2M = 8$. So the channel occupancy ratio $\alpha = 20\%$. The active channel set $\mathcal{S}$ are generated uniformly at random from $[0, M-1]$, among which the prior known part $\mathcal{T}$ from geolocation database of size τ are randomly chosen from the elements of $\mathcal{S}$. The size of $\mathcal{T}$, referred as τ, is varied between 0 to κ. The case $t = 0$ corresponds to the sensing only case without assists from geolocation database. The case $t = \kappa$ means current channel occupancy states from geolocation database are reliable and no change occurs on the spectrum at current time.

Firstly, the received SNR is set as -5 dB and the number of cosets p is varied in the multicoset sampler from 10 to 40, corresponding to the sub-Nyquist sampling ratio $\Omega = p/M$ from 25% to 100%. As shown in the Fig. 5.3 and Fig. 5.4, the detection performance generally increases with the number of cosets p, and also improves as the percentage of the known part τ increases. With geolocation database, the resulting curves of both schemes are shifted to the left, showing that smaller sub-Nyquist sampling ratios (smaller number of cosets in implementation) are required in the joint sensing scheme to achieve the same detection probability compared with the sensing only. When $p = 15 < 2\kappa$ ($\Omega = 37.5\%$), joint sensing scheme based on SA-SOMP achieve 0.93 above detection probability when $\tau \geq 0.5\kappa$, while the sensing only has only 0.6 probability of correct detection. Compared with SA-SOMP, the joint sensing scheme based on MFOCUSS achieves better detection performance, as smaller number of cosets p is needed for the same detection probability. To achieve the desired detection probability of 0.9 [114], sensing only based on SA-SOMP needs around $p = 25$ cosets (sub-Nyquist sampling ratio $\Omega = 62.5\%$), and MFOCUSS needs around $p = 20$ cosets (sub-Nyquist sampling ratio $\Omega = 50\%$), while the joint sensing schemes need only $p = 15$ cosets. Moreover, joint sensing can update the lack of channel occupancy information in the geolocation

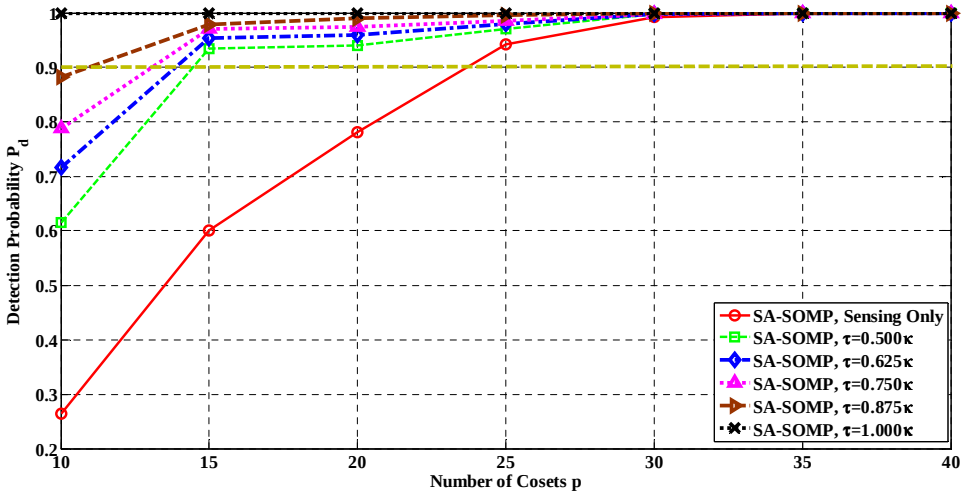

Figure 5.3: Detection probability P_d vs. number of cosets p with $\kappa = 8$ and SNR $= -5$ dB under different number of occupied channels known from geolocation database based on SA-SOMP.

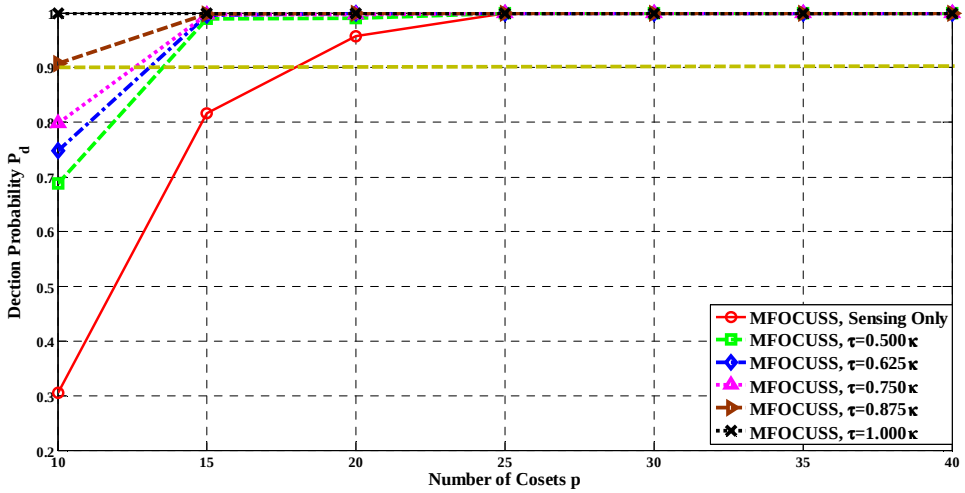

Figure 5.4: Detection probability P_d vs. number of cosets p with $\kappa = 8$ and SNR $= -5$ dB under different number of occupied channels known from geolocation database based on MFOCUSS.

database, thus eventually reaching the desired detection probability P_d.

Then the detection performance is evaluated with varying received SNR from -5 dB to 15 dB. Assume geolocation database provides 50% above occupied channel information. Multicoset sampler with $p = 15$ cosets is used to sample the received signals. As the results shown in the Fig. 5.5 and Fig. 5.6, the detection performance of the proposed joint sensing schemes are superior to that of the sensing only, especially more sensitive

to the low levels of the SNR.

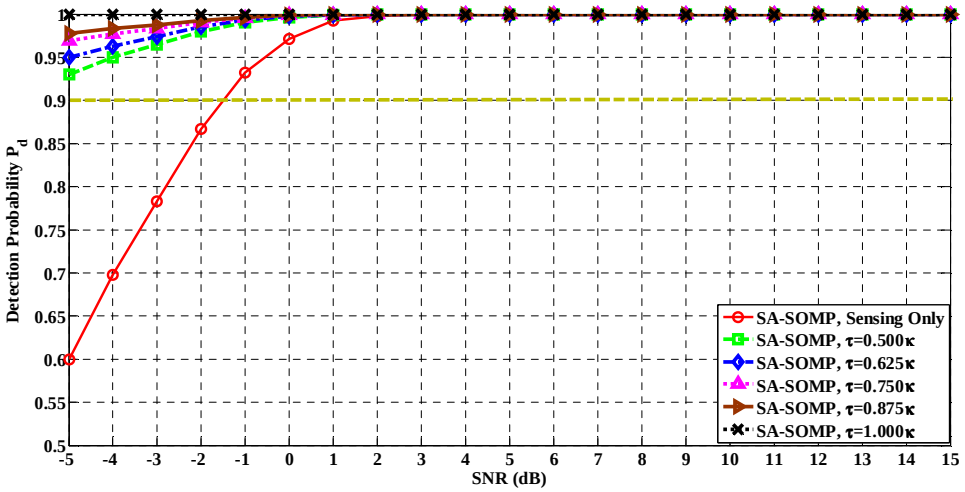

Figure 5.5: Detection probability P_d vs. SNR with $\kappa = 8$ and $p = 15$ under different number of occupied channels known from geolocation database based on SA-SOMP.

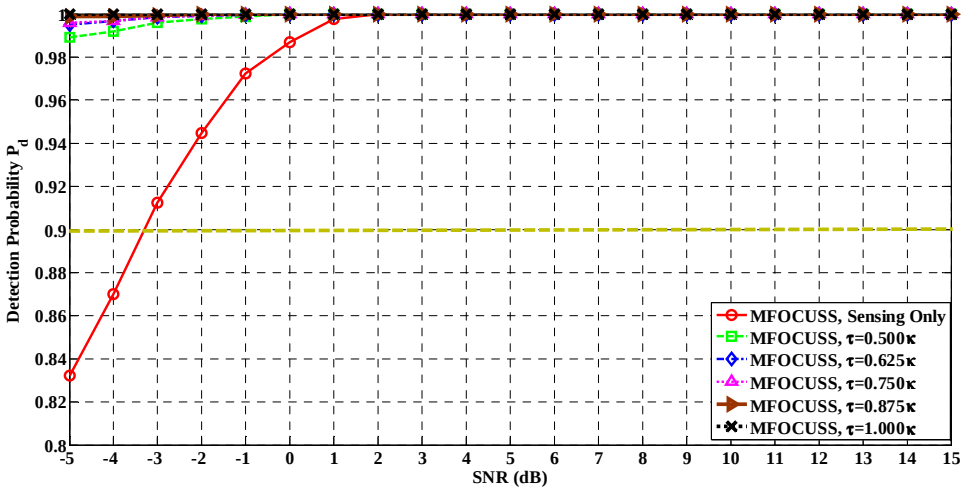

Figure 5.6: Detection probability P_d vs. SNR with $\kappa = 8$ and $p = 15$ under different number of occupied channels known from geolocation database based on MFOCUSS.

5.4.2 Average Iteration Numbers to Convergence

As shown in the Algorithm 3, a sparsity-based halting criterion is used in the recovery process based on SA-SOMP. Therefore, with the TV channel status information from

geolocation database, the number of iterations will be reduced to $\hat{\kappa} - \tau$, so that the joint approach would speed up the sensing process.

Fig. 5.7 shows the average number of iterations in the proposed scheme based on MFOCUSS to achieve the convergence criterion in (5.22). By employing the prior information from geolocation database, the number of iterations in the joint sensing scheme is reduced for all values of p. As τ increases, the corresponding curve is shifted to the bottom. This shows that the prior information on the channel occupancy states from geolocation database is appropriately used by the proposed MFOCUSS method through the weighting scheme given by (5.18). The use of the prior information allows a reduction in the number of iterations, therefore reducing the total computation time to convergence.

Comparing the number of iterations in MFOCUSS with that in SA-SOMP, it shows that a better detection performance is achieved in MFOCUSS at the cost of more number of iterations required in the recovery process. In addition, at each iteration, the computation complexity of SA-SOMP is $O(p^2M)$, while it is $O(pMN)$ in the MFOCUSS. Therefore, SA-SOMP provides a more computation-efficient solution for the proposed joint sparse recovery.

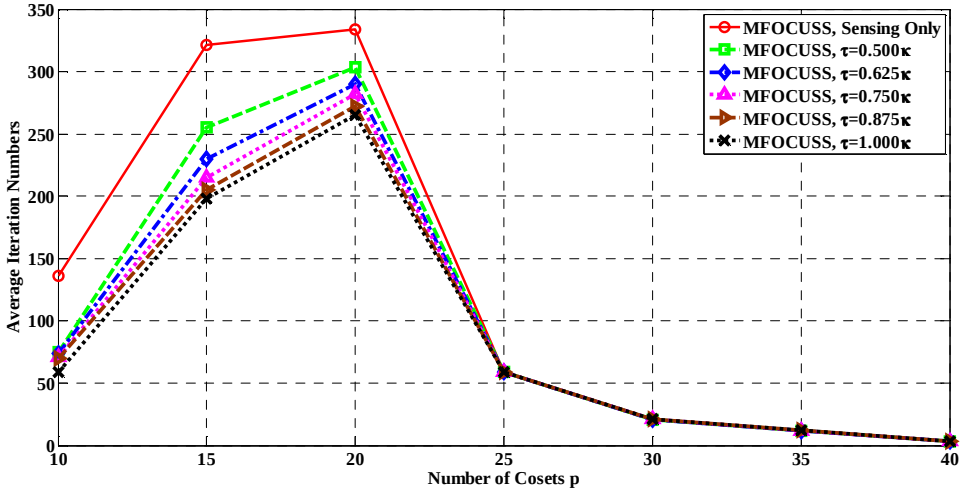

Figure 5.7: Average number of iterations based on MFOCUSS to achieve convergence.

5.4.3 Spectrum Sensing Performance with Partially Incorrect Prior Information

Fig. 5.3 and Fig. 5.4 follows that the prior information from geolocation database is correct for all given channels. As stated in Section 5.3, it may be the case that the information from geolocation database is not fully reliable, so some of the channel occupancy states are changed at current time. In this situation, the joint sensing scheme can still recover the actual signals, but more measurements are required compared to the case when no errors are present in $\mathcal{T}$.

In Fig. 5.8 and Fig. 5.9, the cases in which $\mathcal{T}$ contains some incorrect prior information are simulated, which means that apart from the c channels correctly belonging to the support, there are ω out of τ channels in $\mathcal{T}$ that do not belong to the current signal support. The simulation setting is same as that in Fig. 5.3 and Fig. 5.4, but with different combinations of c and ω in $\mathcal{T}$. As shown in the Fig. 5.8 and Fig. 5.9, the joint sensing scheme can still reconstruct the underlying signals and shows an improvement in detection performance with respect to the case with no prior information. The joint sensing scheme based on MFOCUSS achieves better detection performance than that of the SA-SOMP, where the incorrect elements in $\mathcal{T}$ are removed from the minimization problem.

5.5 Summary

In this chapter, a low-complexity hybrid scheme of sub-Nyquist wideband spectrum sensing with geolocation database is proposed for the effective use of white spaces within the coexistence of dynamic incumbent systems. The simulation results show that the prior channel statusu information from geolocation database leads to a reduction in the required sub-Nyquist sampling ratio to achieve the desired detection performance. Moreover, the reduction in the number of iterations and computation time for convergence

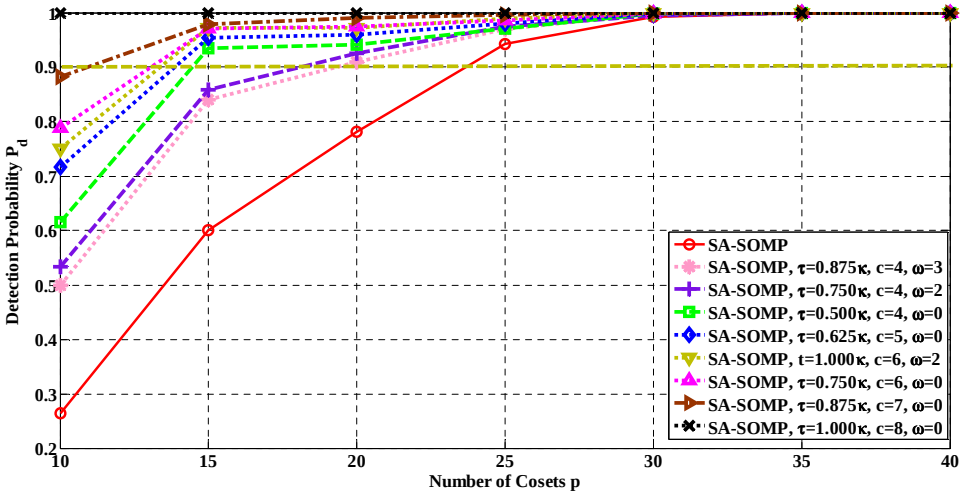

Figure 5.8: Detection probability P_d vs. number of cosets p with $\kappa = 8$ and SNR $= -5$ dB based on SA-SOMP under different number of occupied channels known from geolocation database with partially incorrect prior information.

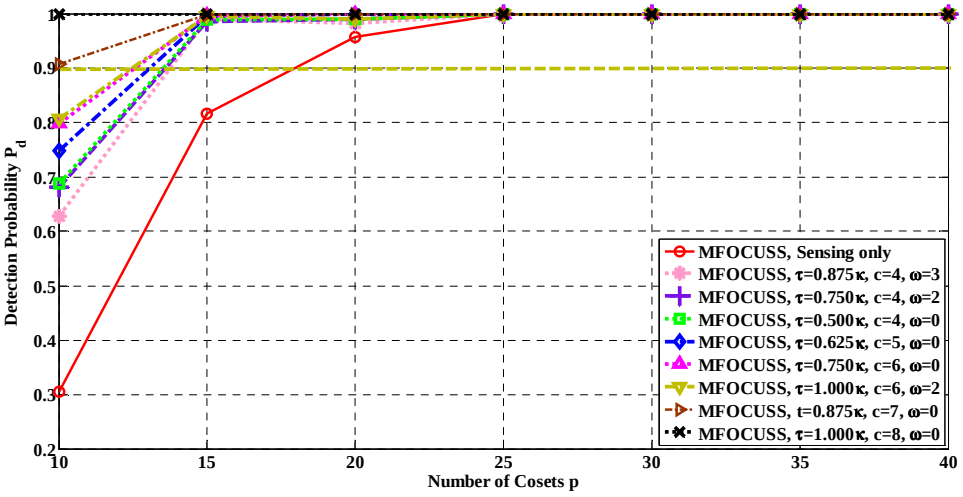

Figure 5.9: Detection probability P_d vs. number of cosets p with $\kappa = 8$ and SNR $= -5$ dB based on MFOCUSS under different number of occupied channels known from geolocation database with partially incorrect prior information.

is also verified when prior information is added in the recovery process. If the prior information is not perfectly reliable, there is still an improvement in detection performance compared with spectrum sensing only. Therefore by harnessing the information from geolocation database, the proposed sensing scheme can update the instant channel occupancy state to reduce the risks of interference to the existing incumbent users. This

makes it possible to apply the proposed joint sub-Nyquist scheme on compact devices to get accurate spectrum occupancy state with reduced processing requirements.

Chapter 6

Conclusions and future work

6.1 Summary

The ever growing demand for data, as well as advances in radio frequency (RF) technology, have promoted the use of wide bandwidth signals, for which the rates specified by the Shannon-Nyquist theorem impose challenges on both the signal acquisition hardware and digital signal processing. Wideband spectrum sensing is crucial to unlash the potentials of dynamic spectrum sharing. Compared with narrowband spectrum sensing, wideband sensing can sense multiple channels at the same time to increase the probability of finding unused spectrum. Sub-Nyquist sampling was motivated by the desire to sample wideband signals at rates far lower than the Nyquist rate, while still maintaining the essential information in the underlying signals. By invoking sub-Nyquist sampling techniques, the signal acquisition costs at secondary users (SUs) are significantly reduced, which is of great significance in dynamic spectrum sharing as the SUs are normally energy-constrained devices. In this thesis, the fundamental research has been carried out on the design of sub-Nyquist wideband spectrum sensing algorithms to improve detection performance in practical spectrum sharing networks.

In Chapter 3, to cope with the time-varying wideband spectrum after the secondary

market is opened for dynamic spectrum sharing, a sparsity independent sub-Nyquist wideband spectrum sensing is proposed that achieves wideband sensing independent of signal sparsity using low-speed ADCs based on sparse Fast Fourier Transform (sFFT). Based on the prior information on the number of channels and spectrum utilization, the received signals are pre-processed through a permutation and filtering scheme that reduces signal sparsity to implement sFFT on wideband spectrum sensing. As over TV white space (TVWS) the power spectral density is almost flat within each channel, the extracted subset of samples near the central frequency retains the corresponding channel occupancy state in each channel. The proposed scheme achieves a fast and accurate sub-Nyquist wideband spectrum sensing even when the signal is highly occupied by primary users (PUs).

In Chapter 4, efficient multicoset sampling based wideband spectrum sensing schemes have been proposed for both individual and cooperative sensing cases to reduce energy consumption on wideband signal acquisition, processing and transmission, with detection performance guarantee, by exploiting the joint sparsity of the multiband signals. Based on a low-rate multi-channel architecture, sub-Nyquist sampling is implemented without complex analog front-end processing. The proposed wideband spectrum sensing schemes locate the active channels blindly without the prior knowledge of the spectral support at either the sub-Nyquist sampling or reconstruction stage. Compared with individual wideband spectrum sensing scheme based on MUSIC, the proposed scheme improves the detection accuracy in low SNR regimes. Exploiting the common signal support perceived at all SUs, the detection accuracy is further improved through cooperative spectrum sensing, in which measurements from multiple SUs are fused jointly to reach a final sensing decision. Based on low-dimensional measurements derived by subspace decomposition, the proposed cooperative spectrum sensing scheme gains good noise robustness while reduces both computation complexity and transmission overhead. Moreover, thanks to the measurement diversity across multiple SUs, reliable sensing results can be achieved at the minimal sampling rate specified by the Landau's theorem,

such that the number of cosets p proportional to the signal sparsity κ is shown sufficient for reliable cooperative spectrum sensing.

Finally, in Chapter 5, to further reduce the computation complexity of wideband spectrum sensing, a low-complexity hybrid scheme of sub-Nyquist wideband spectrum sensing with geolocation database is proposed. Theoretical analyses show that the sufficient condition for exact reconstruction is reduced in the proposed joint sensing scheme. Detection performance of the proposed joint scheme is studied through the experiments on the simulated signals. The simulation results show that incorporating the prior information from geolocation database leads to a reduction in the required sub-Nyquist sampling ratio and the number of iterations to achieve the desired detection performance. Moreover, if the prior channel state information is not perfectly reliable, there is still an improvement in detection performance compared with sensing only. Therefore by harnessing the information from geolocation database, the proposed sensing scheme can update the instant channel occupancy state to reduce the risks of interference to the existing incumbent users with reduced processing requirements.

In a summary, in this thesis, sub-Nyquist wideband spectrum sensing schemes were developed for the efficient use of white spaces within the coexistence of dynamic incumbent systems. The performance of the proposed wideband spectrum sensing schemes has also been validated on real-world signals over TVWS, which demonstrated the effectiveness of applying sub-Nyquist sampling techniques in wideband spectrum sensing for improving the detection performance and energy efficiency.

6.2 Future work

In this section, we identify the following research challenges that need to be addressed in the future work.

6.2.1 Adaptive Wideband Spectrum Sensing

In most of the existing sub-Nyquist wideband spectrum sensing approaches, it is assumed that the sparsity of the signals to be acquired is known. However, in the context of dynamic spectrum sharing networks, the prior information about the spectrum occupancy ratio may not been known, which creates a great barrier to the usage of sub-Nyquist sampling in practical scenarios. Furthermore, the sparsity order of the wideband signals generally varies over the time and it may be difficult to estimate it in practice due to the dynamic spectrum utilization. Therefore, it's important to investigate adaptive sparsity order estimation to capture the spectrum usage in time-varying wireless environments, and subsequently to select appropriate sampling rate at the white space devices.

6.2.2 Performance Limits under Practical Imperfections

To date, most existing compressive wideband sensing techniques assume ideal operating conditions in terms of noise, channel, and hardware components. However, in practice, the presence of practical imperfections, such as noise uncertainty, dynamic channel environment, and transceiver hardware imperfections, may lead to significant performance degradation in real-time measurements. Therefore, it's an important future step to investigate the sub-Nyquist wideband sensing schemes under practical imperfections.

6.2.3 Real-time Compressive Wideband Spectrum Sensing Testbed

Among state-of-the-art sub-Nyquist wideband spectrum sensing techniques, few schemes were implemented on real testbeds. For this reason, the future research plan is to extend the work to test the wideband sensing algorithm on a practical platform. A suggested platform is the Universal Software Radio Peripheral (USRP), which is a software defined radio transceiver where real-time RF signals could be manipulated via a hosting com-

puter by using GNU radio or Matlab. So digital signal processing techniques could be implemented and real-time measurements could be collected. In this context, it's an important future topic to explore a practical implementation of sub-Nyquist wideband spectrum sensing to combine the theoretical sampling approaches with practical engineering aspects.

6.2.4 Short-and Long-Term White Space Measurement Analysis

It is a promising vision to utilize white spaces, i.e., vacant VHF and UHF TV channels, to satisfy wireless data demands. Due to the intrinsic randomness associated with the propagation in wireless environments, the assessment of the spectrum utilization characteristics in white spaces needs to be done by means of extensive measurements for accurate spectrum detection. Based on the fixed and portable RFeye nodes, short-term and long-term spectrum measurements can be conducted over large scales. Machine learning based measurement-driven analyses can then be carried out to better understand the features and variations in multiple locations and time periods by jointly exploring channel, location, and time correlations. These analyses will be useful to capture the white space characteristics and thus more efficiently apply the wideband spectrum sensing in practical scenarios.

References

[1] Y. Gao, Z. Qin, Z. Feng, Q. Zhang, O. Holland, and M. Dohler, "Scalable and Reliable IoT Enabled By Dynamic Spectrum Management for M2M in LTE-A," *IEEE Internet of Things Journal*, vol. 3, no. 6, pp. 1135–1145, Dec. 2016.

[2] R. N. Clarke, "Expanding Mobile Wireless Capacity: The Challenges presented by Technology and Economics," *Telecommun. Policy*, vol. 38, no. 8-9, pp. 693–708, Sep. 2014.

[3] J. Mitola and G. Maguire JR., "Cognitive Radio: Making Software Radios more Personal," *IEEE Pers. Commun.*, vol. 6, no. 4, pp. 13–18, Aug. 1999.

[4] T. M. Taher, R. B. Bacchus, K. J. Zdunek, and D. A. Roberson, "Long-term Spectral Occupancy Findings in Chicago," in *Proc. IEEE Int. Conf. on Dynamic Spectrum Access Netw. (DYSPAN)*, Aachen, Germany, May 2011, pp. 100–107.

[5] M. Lopez-Benitez, A. Umbert, and F. Casadevall, "Evaluation of Spectrum Occupancy in Spain for Cognitive Radio Applications," in *Proc. IEEE Veh. Technol. Conf. (VTC)*, Barcelona, Spain, Apr. 2009, pp. 1–5.

[6] K. Harrison, S. M. Mishra, and A. Sahai, "How Much White-Space Capacity Is There?" in *Proc. IEEE Int. Conf. on Dynamic Spectrum Access Netw. (DYSPAN)*, Singapore, Apr. 2010, pp. 1–10.

[7] K. Chatzikokolakis, P. Spapis, A. Kaloxylos, and N. Alonistioti, "Toward Spectrum Sharing: Opportunities and Technical Enablers," *IEEE Commun. Mag.*, vol. 53, no. 7, pp. 26–33, Jul. 2015.

[8] C. R. Stevenson, G. Chouinard, Z. Lei, W. Hu, S. J. Shellhammer, and W. Caldwell, "IEEE 802.22: The First Cognitive Radio Wireless Regional Area Network Standard," *IEEE Commun. Mag.*, vol. 47, no. 1, pp. 130–138, Jan. 2009.

[9] A. B. Flores, R. E. Guerra, E. W. Knightly, P. Ecclesine, and S. Pandey, "IEEE 802.11af: A Standard for TV White Space Spectrum Sharing," *IEEE Commun. Mag.*, vol. 51, no. 10, pp. 92–100, Oct. 2013.

[10] Office of Commun.. (Feb. 2015). *Implementing TV White Spaces*. [Online]. Available: http://stakeholders.ofcom.org.uk/binaries/consultations/

white-space-coexistence/statement/tvws-statement.pdf

[11] P. Kolodzy, "Spectrum Policy Task Force Report," *Federal Commun. Commission*, Nov. 2002, ET Docket No. 02-135.

[12] "Amendment of the Commission's Rules with Regard to Commercial Operations in the 3550-3650 MHz Band," *Federal Commun. Commission*, Sep. 2015, GN Docket No. 12-354.

[13] "In the Matter of Revision of Part 15 of the Commission's Rules to Permit Unlicensed National Information Infrastructure (U-NII) Devices in the 5 GHz Band: Notice of Proposed Rulemaking," *Federal Commun. Commission*, Feb. 2013., ET Docket No. 13-49.

[14] J. Wang, M. Ghosh, and K. Challapali, "Emerging Cognitive Radio Applications: A Survey," *IEEE Commun. Mag.*, vol. 49, no. 3, pp. 74–81, Mar. 2011.

[15] G. Ding, J. Wang, Q. Wu, Y.-D. Yao, F. Song, and T. A. Tsiftsis, "Cellular-Base-Station Assisted Device-to-Device Communications in TV White Space," *IEEE J. Sel. Areas Commun.*, vol. 34, no. 1, pp. 107–121, Jan. 2016.

[16] Z. Quan, S. Cui, A. H. Sayed, and H. V. Poor, "Optimal Multiband Joint Detection for Spectrum Sensing in Cognitive Radio Networks," *IEEE Trans. Signal Process.*, vol. 57, no. 3, pp. 1128–1140, Mar. 2009.

[17] Z. Tian and G. B. Giannakis, "Compressed Sensing for Wideband Cognitive Radios," in *Proc. IEEE Int. conf. on Acoust., Speech and Signal Process. (ICASSP)*, vol. 4, Honolulu, HI, Apr. 2007, pp. 1357–1360.

[18] H. J. Landau, "Necessary Density Conditions for Sampling and Interpolation of Certain Entire Functions," *Acta Mathematica*, vol. 117, no. 1, pp. 37-52, Jul. 1967.

[19] H. Sun, A. Nallanathan, C.-X. Wang, and Y. Chen, "Wideband Spectrum Sensing for Cognitive Radio Network: A Survey," *IEEE Trans. Wireless Commun.*, vol. 20, no. 2, pp. 74–81, Apr. 2013.

[20] H. Hassanieh, P. Indyk, D. Katabi, and E. Price, "Simple and practical algorithm for sparse Fourier transform," in *Proc. of the ACM-SIAM Symp. on Discrete Algorithms*, Kyoto, Japan, Jan. 2012, pp. 1183–1194.

[21] Z. Qin, Y. Gao, M. Plumbley, and C. Parini, "Wideband Spectrum Sensing on Real-time Signals at Sub-Nyquist Sampling Rates in Single and Cooperative Multiple Nodes," *IEEE Trans. Signal Process.*, vol. 64, no. 12, pp. 3106–3117, Jun. 2016.

[22] C.-P. Yen, Y. Tsai, and X. Wang, "Wideband Spectrum Sensing Based on Sub-Nyquist Sampling," *IEEE Trans. Signal Process.*, vol. 61, no. 12, pp. 3028–3040, Jun. 2013.

[23] F. Zeng, C. Li, and Z. Tian, "Distributed Compressive Spectrum Sensing in Cooperative Multihop Cognitive Networks," *IEEE J. Sel. Signal Process.*, vol. 5, no. 1, pp. 37–48, Feb. 2011.

[24] CRFS. (Oct. 2015). *RFeye Node 206.* [Online]. Available: https://uk.crfs.com/zh-hans/products/rfeyenode/node-20-6/

[25] Y.-C. Liang, K. C. Chen, G. Y. Li, and P. Mahonen, "Cognitive Radio Networking and Communications: An Overview," *IEEE Trans. Veh. Technol.*, vol. 60, no. 7, pp. 3386–3407, Sep. 2011.

[26] I. F. Akyildiz, W.-Y. Lee, M. C. Vuran, and S. Mohanty, "A Survey on Spectrum Management in Cognitive Radio Networks," *IEEE Commun. Mag.*, vol. 46, no. 4, pp. 40–48, Apr. 2008.

[27] "Second Memorandum Opinion and Order," *Federal Commun. Commission*, Sep. 2010, ET Docket No. 08-260.

[28] Office of Commun. (Jul. 2009). *Digital Dividend: Cognitive Access.* [Online]. Available: http://stakeholders.ofcom.org.uk/binaries/consultations/cognitive/statement/statement.pdf

[29] Y. Luo, L. Gao, and J. Huang, "Price and Inventory Competition in Oligopoly TV White Space Markets," *IEEE J. Sel. Areas Commun.*, vol. 33, no. 5, pp. 1002–1013, May 2015.

[30] Office of Commun. (Jul. 2016). *Designing the Broadband Universal Service Obligation: Call For Inputs.* [Online]. Available: https://www.ofcom.org.uk/__data/assets/pdf_file/0025/58336/broadband-uso.pdf.

[31] O. Holland *et al.*, "A Series of Trials in the UK as Part of the Ofcom TV White Spaces Pilot," in *Proc. Int. Workshop on Cognitive Cellular Syst. (CCS)*, Rhine

River, Germany, Sep. 2014, pp. 1–5.

[32] O. Holland, S. Ping, Y. Gao, Z. Qin, A. Aijaz, J. Chareau, P. Chawdhry, and H. Kokkinen, "To White Space or not to White Space: That is the Trial within the Ofcom TV White Spaces Pilot," in *Proc. IEEE Int. Conf. on Dynamic Spectrum Access Netw. (DYSPAN)*, Stockholm, Sweden, Sep. 2015, pp. 11–22.

[33] M. Fitch, M. Nekovee, S. Kawade, K. Briggs, and R. MacKenzie, "Wireless Service Provision in TV White Space with Cognitive Radio Technology: A Telecom Operator's Perspective and Experience," *IEEE Commun. Mag.*, vol. 49, no. 3, pp. 64–73, Mar. 2011.

[34] Office of Communications. (Nov. 2010). *Implementing Geolocation.* [Online]. Available: https://www.ofcom.org.uk/__data/assets/pdf_file/0035/46889/statement.pdf

[35] T. Yucek and H. Arslan, "A survey of Spectrum Sensing Algorithms for Cognitive Radio Applications," *IEEE Commun. Surveys Tutorials*, vol. 11, no. 1, pp. 116–130, Jan. 2009.

[36] G. Forney, "Maximum-likelihood sequence estimation of digital sequences in the presence of intersymbol interference," *IEEE Trans. Inf. Theory*, vol. 18, no. 3, pp. 363–378, May 1972.

[37] S. Verdu, "Minimum Probability of Error for Asynchronous Gaussian Multiple-access Channels," *IEEE Trans. Inf. Theory*, vol. 32, no. 1, pp. 85–96, Jan 1986.

[38] M. Derakhshani, T. Le-Ngoc, and M. Nasiri-Kenari, "Efficient Cooperative Cyclostationary Spectrum Sensing in Cognitive Radios at Low SNR Regimes," *IEEE Trans. Wireless Commun.*, vol. 10, no. 11, pp. 3754–3764, Nov. 2011.

[39] K. Kim, I. A. Akbar, K. K. Bae, J.-S. Um, C. M. Spooner, and J. H. Reed, "Cyclostationary Approaches to Signal Detection and Classification in Cognitive Radio," in *Proc. IEEE Int. Symp. on Dynamic Spectrum Access Networks (DySPAN)*, Dublin, Ireland, Apr. 2007, pp. 212–215.

[40] A. Tani and R. Fantacci, "A Low-Complexity Cyclostationary-Based Spectrum Sensing for UWB and WiMAX Coexistence With Noise Uncertainty," *IEEE Trans. Veh. Technol.*, vol. 59, no. 6, pp. 2940–2950, Jul. 2010.

[41] Y.-C. Liang, Y. Zeng, E. C. Peh, and A. T. Hoang, "Sensing-Throughput Tradeoff for Cognitive Radio Networks," *IEEE Trans. Wireless Commun.*, vol. 7, no. 4, pp. 1326–1337, Apr. 2008.

[42] A. Ebrahimzadeh, M. Najimi, S. Andargoli, and A. Fallahi, "Sensor Selection and Optimal Energy Detection Threshold for Efficient Cooperative Spectrum Sensing," *IEEE Trans. Veh. Technol.*, vol. 64, no. 4, pp. 1565–1577, Apr. 2015.

[43] R. Tandra and A. Sahai, "SNR Walls for Signal Detection," *IEEE J. Sel. Signal Process.*, vol. 2, no. 1, pp. 4–17, Feb. 2008.

[44] Z. Tian and G. B. Giannakis, "A Wavelet Approach to Wideband Spectrum Sensing for Cognitive Radios," in *Proc. Int. Conf. on Cognitive Radio Oriented Wireless Netw. and Commun. (CROWNCOM)*, Mykonos Island, Greece, Jun. 2006, pp. 1–5.

[45] Z. Sun and J. N. Laneman, "Performance Metrics, Sampling Schemes, and Detection Algorithms for Wideband Spectrum Sensing," *IEEE Trans. Signal Process.*, vol. 62, no. 19, pp. 5107–5118, Oct. 2014.

[46] Y. Pei, Y.-C. Liang, K. C. Teh, and K. H. Li, "Energy-Efficient Design of Sequential Channel Sensing in Cognitive Radio Networks: Optimal Sensing Strategy, Power Allocation, and Sensing Order," *IEEE J. Sel. Areas Commun.*, vol. 29, no. 8, pp. 1648–1659, Sep. 2011.

[47] R. Yu, Y. Zhang, L. Yi, S. Xie, L. Song, and M. Guizani, "Secondary Users Cooperation in Cognitive Radio Networks: Balancing Sensing Accuracy and Efficiency," *IEEE Wireless Commun.*, vol. 19, no. 2, pp. 30–37, Apr. 2012.

[48] S. Yoon, L. E. Li, S. C. Liew, R. R. Choudhury, I. Rhee, and K. Tan, "QuickSense: Fast and Energy-efficient Channel Sensing for Dynamic Spectrum Access Networks," in *Proc. IEEE Int. conf. on Computer Commun. (INFOCOM)*, Turin, Italy, Apr. 2013, pp. 2247–2255.

[49] B. Farhang-Boroujeny, "Filter Bank Spectrum Sensing for Cognitive Radios," *IEEE Trans. Signal Process.*, vol. 56, no. 5, pp. 1801–1811, May 2008.

[50] E. J. Candes and T. Tao, "Decoding by Linear Programming," *IEEE Trans. Inf. Theory*, vol. 51, no. 12, pp. 4203–4215, Dec. 2005.

[51] ——, "Near-Optimal Signal Recovery From Random Projections: Universal Encoding Strategies?" *IEEE Trans. Inf. Theory*, vol. 52, no. 12, pp. 5406–5425, Dec. 2006.

[52] E. J. Candes, J. Romberg, and T. Tao, "Stable Signal Recovery from Incomplete and Inaccurate Measurements," *Commun. Pure and Appl. Math.*, vol. 59, no. 8, pp. 1207–1223, Aug. 2006.

[53] E. J. Candes and J. Romberg, "Sparsity and Incoherence in Compressive Sampling," *Inverse Problems*, vol. 23, no. 3, pp. 969–985, Apr. 2007.

[54] J. A. Tropp, J. N. Laska, M. F. Duarte, J. K. Romberg, and R. G. Baraniuk, "Beyond Nyquist: Efficient Sampling of Sparse Bandlimited Signals," *IEEE Trans. Inf. Theory*, vol. 56, no. 1, pp. 520–544, Jan. 2010.

[55] M. Mishali and Y. C. Eldar, "From Theory to Practice: Sub-Nyquist Sampling of Sparse Wideband Analog Signals," *IEEE J. Sel. Signal Process.*, vol. 4, no. 2, pp. 375–391, Apr. 2010.

[56] P. Feng and Y. Bresler, "Spectrum-blind minimum-rate sampling and reconstruction of multiband signals," in *Proc. IEEE Int. conf. on Acoust., Speech and Signal Process. (ICASSP)*, vol. 3, Atlanta, GA, May 1996, pp. 1688–1691.

[57] R. Venkataramani and Y. Bresler, "Optimal Sub-Nyquist Nonuniform Sampling and Reconstruction for Multiband Signals," *IEEE Trans. Signal Process.*, vol. 49, no. 10, pp. 2301–2313, Oct. 2001.

[58] R. Schmidt, "Multiple Emitter Location and Signal Parameter Estimation," *IEEE Trans. on Antennas and Propag.*, vol. 34, no. 3, pp. 276–280, Mar. 1986.

[59] M. Rashidi, K. Haghighi, A. Owrang, and M. Viberg, "A Wideband Spectrum Sensing Method for Cognitive Radio Using Sub-Nyquist Sampling," in *Proc. IEEE Int. conf. on Digital Signal Process. and Signal Process. Educ. Workshop (DSP/SPE)*, Sedona, AZ, Jan. 2011, pp. 30–35.

[60] W.-J. Zeng, H. C. So, and L. Huang, "l_p-MUSIC: Robust Direction-of-Arrival Estimator for Impulsive Noise Environments," *IEEE Trans. Signal Process.*, vol. 61, no. 17, pp. 4296–4308, Sep. 2013.

[61] S. Muthukrishnan, *Data streams: Algorithms and applications.* Hanover, MA:

Now Publishers Inc., 2005.

[62] D. L. Donoho, "Compressed Sensing," *IEEE Trans. Inf. Theory*, vol. 52, no. 4, pp. 1289–1306, Apr. 2006.

[63] S. S. Chen, D. L. Donoho, and M. A. Saunders, "Atomic Decomposition by Basis Pursuit," *SIAM J. Sci. Comp.*, vol. 20, no. 1, pp. 33–61, Aug. 1998.

[64] E. J. Candes, M. B. Wakin, and S. P. Boyd, "Enhancing sparsity by reweighted ℓ_1 minimization," *J. of Fourier Anal. and Applicat.*, vol. 14, no. 5, pp. 877–905, Dec. 2008.

[65] D. L. Donoho and X. Huo, "Uncertainty Principles and Ideal Atomic Decomposition," *IEEE Trans. Inf. Theory*, vol. 47, no. 7, pp. 2845–2862, Nov. 2001.

[66] R. Tibshirani, "Regression Shrinkage and Selection via the Lasso," *J. of the Roy. Stat. Soc. Series B (Methodological)*, vol. 58, no. 1, pp. 267–288, 1996.

[67] N. P. Galatsanos and A. K. Katsaggelos, "Methods for Choosing the Regularization Parameter and Estimating the Noise Variance in Image Restoration and Their Relation," *IEEE Trans. on Image Process.*, vol. 1, no. 3, pp. 322–336, Jul. 1992.

[68] Y. C. Eldar, "Generalized SURE for Exponential Families: Applications to Regularization," *IEEE Trans. Signal Process.*, vol. 57, no. 2, pp. 471–481, Feb. 2009.

[69] J. A. Tropp and A. C. Gilbert, "Signal Recovery From Random Measurements Via Orthogonal Matching Pursuit," *IEEE Trans. Inf. Theory*, vol. 53, no. 12, pp. 4655–4666, Dec. 2007.

[70] D. L. Donoho, Y. Tsaig, I. Drori, and J. L. Starck, "Sparse Solution of Underdetermined Systems of Linear Equations by Stagewise Orthogonal Matching Pursuit," *IEEE Trans. Inf. Theory*, vol. 58, no. 2, pp. 1094–1121, Feb. 2012.

[71] D. Needell and J. A. Tropp, "Cosamp: Iterative Signal Recovery From Incomplete and Inaccurate Samples," *Appl. and Comput. Harmonic Anal.*, vol. 26, no. 3, pp. 301–321, May 2009.

[72] T. Blumensath and M. E. Davies, "Iterative Hard Thresholding for Compressed Sensing," *Appl. and Comput. Harmonic Anal.*, vol. 27, no. 3, pp. 265–274, Nov. 2009.

[73] M. Wang, W. Xu, and A. Tang, "On the Performance of Sparse Recovery via-

$l_p$minimization," *IEEE Trans. Inf. Theory*, vol. 57, no. 11, pp. 7255–7278, Nov. 2011.

[74] I. Daubechies, R. DeVore, and M. Fornasier, "Iteratively reweighted least squares minimization for sparse recovery," *Commun. Pure Appl. Math.*, vol. 63, no. 1, pp. 1–38, Jan. 2010.

[75] D. P. Wipf and B. D. Rao, "Sparse Bayesian learning for basis selection," *IEEE Trans. Signal Process.*, vol. 52, no. 8, pp. 2153–2164, Aug. 2004.

[76] D. Wipf and S. Nagarajan, "Iterative Reweighted ℓ_1 and ℓ_2 Methods for Finding Sparse Solutions," *IEEE J. Sel. Signal Process.*, vol. 4, no. 2, pp. 317–329, Apr. 2010.

[77] D. P. Wipf, B. D. Rao, and S. Nagarajan, "Latent Variable Bayesian Models for Promoting Sparsity," *IEEE Trans. Inf. Theory*, vol. 57, no. 9, pp. 6236–6255, Sep. 2011.

[78] Z. Zhang and B. D. Rao, "Sparse Signal Recovery With Temporally Correlated Source Vectors Using Sparse Bayesian Learning," *IEEE J. Sel. Signal Process.*, vol. 5, no. 5, pp. 912–926, Sep. 2011.

[79] S. Ji, Y. Xue, and L. Carin, "Bayesian Compressive Sensing," *IEEE Trans. Signal Process.*, vol. 56, no. 6, pp. 2346–2356, Jun. 2008.

[80] W. Chen, D. Wipf, Y. Wang, Y. Liu, and I. J. Wassell, "Simultaneous Bayesian Sparse Approximation With Structured Sparse Models," *IEEE Trans. Signal Process.*, vol. 64, no. 23, pp. 6145–6159, Dec. 2016.

[81] Z. Quan, S. Cui, H. V. Poor, and A. H. Sayed, "Collaborative Wideband Sensing for Cognitive Radios," *IEEE Signal Process. Mag.*, vol. 25, no. 6, pp. 60–73, Nov. 2008.

[82] H. Sun, A. Nallanathan, S. Cui, and C. X. Wang, "Cooperative Wideband Spectrum Sensing Over Fading Channels," *IEEE Trans. Veh. Technol.*, vol. 65, no. 3, pp. 1382–1394, Mar. 2016.

[83] Z. Tian, "Compressed Wideband Sensing in Cooperative Cognitive Radio Networks," in *Proc. IEEE Global Commun. Conf. (GLOBECOM)*, New Orleans, LA, Nov. 2008, pp. 1–5.

[84] J. A. Bazerque and G. B. Giannakis, "Distributed Spectrum Sensing for Cognitive Radio Networks by Exploiting Sparsity," *IEEE Trans. Signal Process.*, vol. 58, no. 3, pp. 1847–1862, Mar. 2010.

[85] Z. Li, F. R. Yu, and M. Huang, "A Distributed Consensus-Based Cooperative Spectrum-Sensing Scheme in Cognitive Radios," *IEEE Trans. Veh. Technol.*, vol. 59, no. 1, pp. 383–393, Jan. 2010.

[86] L. Xiao, S. Boyd, and S. Kim, "Distributed Average Consensus with Least-mean-square Deviation," *J. Parallel Distrib. Comput.*, vol. 67, no. 1, pp. 33–46, Jan. 2007.

[87] J. Meng, W. Yin, H. Li, E. Hossain, and Z. Han, "Collaborative Spectrum Sensing from Sparse Observations in Cognitive Radio Networks," *IEEE J. Sel. Areas Commun.*, vol. 29, no. 2, pp. 327–337, Feb. 2011.

[88] Q. Ling, Z. Wen, and W. Yin, "Decentralized Jointly Sparse Optimization by Reweighted ℓ_q Minimization," *IEEE Trans. Signal Process.*, vol. 61, no. 5, pp. 1165–1170, Mar. 2013.

[89] J. Chen and X. Huo, "Theoretical Results on Sparse Representations of Multiple-Measurement Vectors," *IEEE Trans. Signal Process.*, vol. 54, no. 12, pp. 4634–4643, Dec. 2006.

[90] M. Fornasier and H. Rauhut, "Recovery Algorithms for Vector-valued Data with Joint Sparsity Constraints," *Society for Industrial and Appl. Math. J. on Numerical Analysis*, vol. 46, no. 2, pp. 577–613, Feb. 2008.

[91] Y. C. Eldar and M. Mishali, "Robust Recovery of Signals From a Structured Union of Subspaces," *IEEE Trans. Inf. Theory*, vol. 55, no. 11, pp. 5302–5316, Nov. 2009.

[92] M. E. Davies and Y. C. Eldar, "Rank Awareness in Joint Sparse Recovery," *IEEE Trans. Inf. Theory*, vol. 58, no. 2, pp. 1135–1146, Feb. 2012.

[93] J. A. Tropp, A. C. Gilbert, and M. J. Strauss, "Simultaneous Sparse Approximation via Greedy Pursuit," in *Proc. IEEE Int. conf. on Acoust., Speech and Signal Process. (ICASSP)*, vol. 5, Philadelphia, PA, Mar. 2005, pp. v/721–v/724.

[94] M. F. Duarte, S. Sarvotham, D. Baron, M. B. Wakin, and R. G. Baraniuk, "Dis-

tributed Compressed Sensing of Jointly Sparse Signals," in *Asilomar Conf. on Signals, Syst. and Comput.*, Oct. 2005, pp. 1537–1541.

[95] D. Cohen, A. Akiva, B. Avraham, and Y. C. Eldar, "Centralized Cooperative Spectrum Sensing from Sub-Nyquist Samples for Cognitive Radios," in *Proc. IEEE Int. Conf. on Commun. (ICC)*, London, UK, Jun. 2015, pp. 7486–7491.

[96] E. J. Candes and T. Tao, "The Power of Convex Relaxation: Near-Optimal Matrix Completion," *IEEE Trans. Inf. Theory*, vol. 56, no. 5, pp. 2053–2080, May 2010.

[97] E. J. Candes and Y. Plan, "Matrix Completion With Noise," *Proceedings of the IEEE*, vol. 98, no. 6, pp. 925–936, Jun. 2010.

[98] E. J. Candes and B. Recht, "Exact Low-rank Matrix Completion via Convex Optimization," in *Proc. Annual Allerton Conf. on Commun., Control, and Comput.*, Sep. 2008, pp. 806–812.

[99] J.-F. Cai, E. J. Candes, and Z. Shen, "A Singular Value Thresholding Algorithm for Matrix Completion," *SIAM J. Optim.*, vol. 20, no. 4, pp. 1956–1982, Mar. 2010.

[100] S. Ma, D. Goldfarb, and L. Chen, "Fixed Point and Bregman Iterative Method for Matrix Rank Minimization," *J. Math. Programming*, vol. 128, no. 1-2, pp. 321–353, Jun. 2011.

[101] K.-C. Toh and S. Yun, "An Accelerated Proximal Gradient Algorithm for Nuclear Norm Regularized Least Squares Problems," *Pacific J. Optimization*, vol. 6, no. 3, pp. 615–640, Sep. 2010.

[102] P. Paysarvi-Hoseini and N. C. Beaulieu, "On the Benefits of Multichannel/Wideband Spectrum Sensing with Non-Uniform Channel Sensing Durations for Cognitive Radio Networks," *IEEE Trans. Commun.*, vol. 60, no. 9, pp. 2434–2443, Sep. 2012.

[103] W. Chen and I. J. Wassell, "Optimized Node Selection for Compressive Sleeping Wireless Sensor Networks," *IEEE Trans. Veh. Technol.*, vol. 65, no. 2, pp. 827–836, Feb. 2016.

[104] X. Zhang, Y. Ma, and Y. Gao, "Adaptively Regularized Compressive Spectrum Sensing From Real-time Signals to Real-time Processing," in *Proc. IEEE Global*

Commun. Conf. (GLOBECOM), Washington, D.C., Dec. 2016, pp. 1–6.

[105] B. Sun, Q. Chen, X. Xu, Y. He, and J. Jiang, "Permuted and Filtered Spectrum Compressive Sensing," *IEEE Signal Process. Lett.*, vol. 20, no. 7, pp. 685–688, Jul. 2013.

[106] J. Jiang, H. Sun, D. Baglee, and H. V. Poor, "Achieving Autonomous Compressive Spectrum Sensing for Cognitive Radios," *IEEE Trans. Veh. Technol.*, vol. 65, no. 3, pp. 1281–1291, Mar. 2016.

[107] Z. Zhang, Z. Han, H. Li, D. Yang, and C. Pei, "Belief Propagation Based Cooperative Compressed Spectrum Sensing in Wideband Cognitive Radio Networks," *IEEE Trans. Wireless Commun.*, vol. 10, no. 9, pp. 3020–3031, Sep. 2011.

[108] Z. Zeinalkhani and A. H. Banihashemi, "Iterative Recovery Algorithms for Compressed Sensing of Wideband Block Sparse Spectrums," in *Proc. IEEE Int. Conference on Commun. (ICC)*, Ottawa, Canada, Jun. 2012, pp. 1630–1634.

[109] X. Ying, J. Zhang, L. Yan, G. Zhang, M. Chen, and R. Chandra, "Exploring Indoor White Spaces in Metropolises," in *Proc. Int. Conf. on Mobile Computing and Networking (MobiCom)*, Miami, FL, Oct. 2013, pp. 255–266.

[110] J. Ribeiro *et al.*, "Testbed for Combination of Local Sensing with Geolocation Database in Real Environments," *IEEE Wireless Commun.*, vol. 19, no. 4, pp. 59–66, Aug. 2012.

[111] H. Hassanieh, L. Shi, O. Abari, E. Hamed, and D. Katabi, "GHz-wide Sensing and Decoding Using the Sparse Fourier Transform," in *Proc. IEEE Int. Conf. on Computer Commun. (INFOCOM)*, Toronto, CA, Apr. 2014, pp. 2256–2264.

[112] W. Kester, *Mixed-signal and DSP Design Techniques*, 1st ed. Oxford: Newnes, 2003.

[113] G. B. Arfken, H. J. Weber, and F. E. Harris, *Mathematical Methods for Physicists*, 7th ed. San Diego: Academic Press, 2001.

[114] "IEEE Standard for Wireless Regional Area Networks Part 22: Cognitive Wireless RAN MAC and PHY specifications: Policies and procedures for operation in the TV Bands," *IEEE Std. 802.22-2011*, pp. 1–680, Jul. 2011.

[115] M. Frigo and S. G. Johnson. (Apr. 2007) FFTW 3.2.3. [Online]. Available:

http://www.fftw.org/

[116] Z. Qin, Y. Gao, and C. G. Parini, "Data-Assisted Low Complexity Compressive Spectrum Sensing on Real-Time Signals Under Sub-Nyquist Rate," *IEEE Trans. Wireless Commun.*, vol. 15, no. 2, pp. 1174–1185, Feb. 2016.

[117] Y. Ma, Y. Gao, and C. G. Parini, "Sub-Nyquist Rate Wideband Spectrum Sensing over TV White Space for M2M Communications," in *Proc. IEEE Int. conf. on World of Wireless, Mobile and Multimedia Netw. (WoWMoM)*, Boston, MA, Jun. 2015, pp. 1–6.

[118] M. A. Lexa, M. E. Davies, J. S. Thompson, and J. Nikolic, "Compressive power spectral density estimation," in *Proc. IEEE Int. conf. on Acoust., Speech and Signal Process. (ICASSP)*, May 2011, pp. 3884–3887.

[119] M. Mishali and Y. C. Eldar, "Blind Multiband Signal Reconstruction: Compressed Sensing for Analog Signals," *IEEE Trans. Signal Process.*, vol. 57, no. 3, pp. 993–1009, Mar. 2009.

[120] T. Wimalajeewa and P. K. Varshney, "OMP Based Joint Sparsity Pattern Recovery Under Communication Constraints," *IEEE Signal Process. Lett.*, vol. 62, no. 19, pp. 5059–5072, Oct. 2014.

[121] S. M. Louwsma, A. J. M. van Tuijl, M. Vertregt, and B. Nauta, "A 1.35 GS/s, 10 b, 175 mW Time-Interleaved AD Converter in 0.13 μm CMOS," *IEEE J. of Solid-State Circuits*, vol. 43, no. 4, pp. 778–786, Apr. 2008.

[122] K. Poulton, R. Neff, B. Setterberg, B. Wuppermann, T. Kopley, R. Jewett, J. Pernillo, C. Tan, and A. Montijo, "A 20 GS/s 8 b ADC with a 1 MB memory in 0.18 μm CMOS," in *Proc. IEEE Int. Solid-State Circuits Conf.*, vol. 1, Feb. 2003, pp. 318–496.

[123] E. J. Candes, J. Romberg, and T. Tao, "Robust Uncertainty Principles: Exact Signal Reconstruction from Highly Incomplete Frequency Information," *IEEE Trans. Inf. Theory*, vol. 52, no. 2, pp. 489–509, Feb. 2006.

[124] Y. Zeng and Y.-C. Liang, "Eigenvalue-based Spectrum Sensing Algorithms for Cognitive Radio," *IEEE Trans. Commun.*, vol. 57, no. 6, pp. 1784–1793, Jun. 2009.

[125] P. Vallet, X. Mestre, and P. Loubaton, "Performance Analysis of an Improved MUSIC DoA Estimator," *IEEE Trans. Signal Process.*, vol. 63, no. 23, pp. 6407–6422, Dec. 2015.

[126] B. Nielson and D. R. Cox, *Asymptotic Techniques for Use in Statistics*, 1st ed. London; New York: Chapman and Hall/CRC, 1989.

[127] A. Quinlan, J.-P. Barbot, P. Larzabal, and M. Haardt, "Model Order Selection for Short Data: An Exponential Fitting Test (EFT)," *EURASIP J. Adv. Signal Process.*, vol. 2007, Oct. 2006, Art. ID 71953.

[128] Y. C. Eldar, P. Kuppinger, and H. Bolcskei, "Block-Sparse Signals: Uncertainty Relations and Efficient Recovery," *IEEE Trans. Signal Process.*, vol. 58, no. 6, pp. 3042–3054, Jun. 2010.

[129] R. Dionisio, J. Ribeiro, P. Marques, and J. Rodriguez, "Combination of a Geolocation Database Access with Infrastructure Sensing in TV Bands," *EURASIP J. Wireless Commun. Netw.*, vol. 2014, no. 1, pp. 1–14, Dec. 2014.

[130] N. Wang, Y. Gao, and B. Evans, "Database-Augmented Spectrum Sensing Algorithm for Cognitive Radio," in *Proc. IEEE Int. Conf. on Commun. (ICC)*, London, UK, Jun. 2015, pp. 7468–7473.

[131] N. Vaswani and W. Lu, "Modified-CS: Modifying Compressive Sensing for Problems With Partially Known Support," *IEEE Trans. Signal Process.*, vol. 58, no. 9, pp. 4595–4607, Sep. 2010.

[132] Y. Ma, Y. Gao, Y.-C. Liang, and S. Cui, "Reliable and Efficient Sub-Nyquist Wideband Spectrum Sensing in Cooperative Cognitive Radio Networks," *IEEE J. Sel. Areas Commun.*, vol. 34, no. 10, pp. 2750–2762, Oct. 2016.

[133] C. J. Miosso, R. von Borries, and J. H. Pierluissi, "Compressive Sensing With Prior Information: Requirements and Probabilities of Reconstruction in l_1-Minimization," *IEEE Trans. Signal Process.*, vol. 61, no. 9, pp. 2150–2164, May 2013.

[134] W. Yin, Z. Wen, S. Li, J. Meng, and Z. Han, "Dynamic Compressive Spectrum Sensing for Cognitive Radio Networks," in *Proc. IEEE Conf. on Information Sciences and Systems*, Mar. 2011, pp. 1–6.

[135] L. Liu, Z. Han, Z. Wu, and L. Qian, "Collaborative Compressive Sensing Based

Dynamic Spectrum Sensing and Mobile Primary User Localization in Cognitive Radio Networks," in *Proc. IEEE Global Commun. Conf. (GLOBECOM)*, Dec. 2011, pp. 1–5.

[136] S. F. Cotter, B. D. Rao, K. Engan, and K. Kreutz-Delgado, "Sparse Solutions to Linear Inverse Problems with Multiple Measurement Vectors," *IEEE Trans. Signal Process.*, vol. 53, no. 7, pp. 2477–2488, Jul. 2005.